University of Pretoria etd – Combrinck, M (2006)

Chapter 4

4 AUTOMATED INTEGRATED ANALYSIS OF TDEM DATA

"Nature is not a competition. It doesn't really matter, when you go out, if you don't identify anything. What matters is the feeling in the heart." (Richard Adams, B. 1920, British Writer)

"Exploring the unknown defines the essence of humanity." (The author)

4.1 An integrated analysis algorithm

A software supported approach was developed for the:

- More effective visualization of the field data for rapid anomaly detection
- Automatic calculation and visualization of decay curve characteristics
- The use of the S-layer transform for the creation of conductivity-thickness cross section for the outline of finite conductors.

An automation of some strategies as outlined in chapter 3 was implemented in a C++ algorithm. Data analysis is performed on a time basis (i.e. decay curves) and not on a spatial basis (i.e. profile plots). Furthermore, the S-layer transform part of the algorithm assumes centre of the loop (sounding) data only. The algorithm does an automatic analysis, discussed below, of each measured decay curve. The only user input required is to specify system parameters and regression analysis limits, although default values for these are given.

4.2 Visualization of the field data for rapid anomaly detection

Even though the ultimate gaol of TEM interpretation is to end up with a conductivity-depth section or conductor location and properties, it is always good to have the original data readily available as well. This often helps to clarify ambiguities in interpretations or models, e.g. the presence of a small, three-dimensional feature visible on raw data profiles would imply possible failure of layered interpretations in that region. Noise is also identified with more confidence on original data than after processing or transforms. TEM data can, however, be quite challenging to present in a complete manner without losing detail. Two factors contributing to this are the logarithmic span of data (with the small,

late time values often being more significant) and the fact that the half space (or background) response often dominates that of the target.

A very simple approach was followed to minimize the effects of these two factors. Data at every station are presented as a fraction of an average response calculated over the complete data set. The reasoning behind this is that background (half space or layered earth) should contribute the most to measured values over a large data set (as conductor responses are considered "anomalous" to this background). Adding all these responses together and calculating an average value at each time channel leads to the average response expected in a specific survey area. The fraction responses ($\partial B_z/\partial t$ divided by average) at every station then show deviations of a station from the average or background response. The advantage of this type of data presentation above standard profiles is that it can be displayed as colour contoured pseudo-sections giving the same priority to all time channels and very successfully enhancing anomalous regions. An example of this procedure on synthetic data is shown in figure 4.1. The success of this procedure is of course dependent on a relatively similar background response over a given survey area, although fairly good results have been obtained in the case history discussed in chapter 5, which was conducted over a complex geological area. The same presentation of data (although independently developed) was also found in a paper by Eaton and Hohmann (1987). In their case, however, the conductor to half space response was considered as a signal to noise ratio and was examined for different survey geometries.

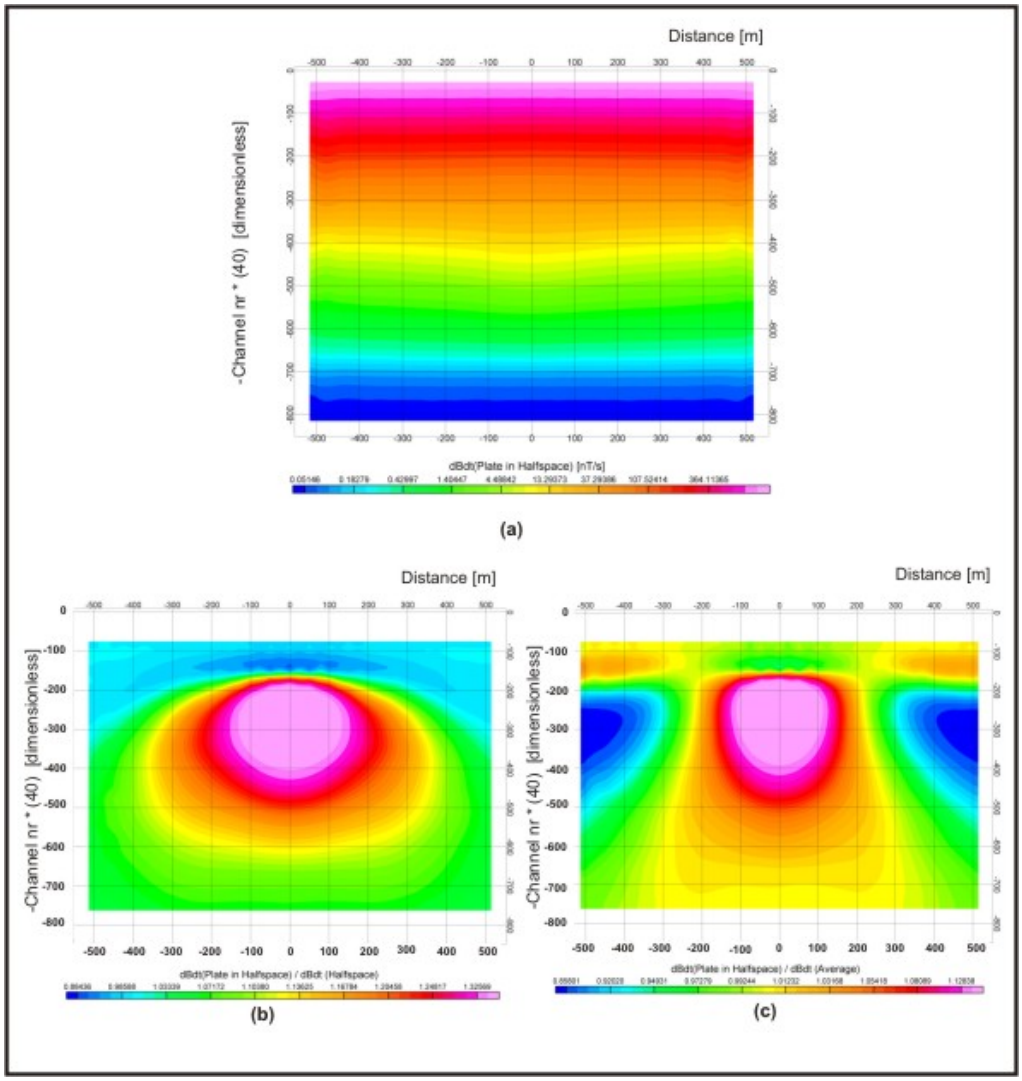

Figure 4-1 In (a) the raw data are presented in a contoured log-scale. In (b) the data were normalised using the half space value used in the forward model. In (c) the data were normalised as discussed above.

4.3 Decay curve analysis

The decay curve analysis is implemented in three steps.

- Decay curves analyzed for layered earth (i.e. power law) behaviour.
- Decay curves analyzed for exponential decay indicating confined conductors.
- Decay curves analyzed for sign changes not related to noise.

4.3.1 Layered earth behaviour

The objectives of this analysis are:

- to determine whether there is any straight line behaviour in the logarithmic domain of a sounding data set;
- to determine the largest number of channels (and channel numbers) on which the behaviour can be found;
- to test whether these slopes are close to either -2.5 or -4 and consequently
- to classify the sounding as half space or S-layer type.

Firstly, the time channels and corresponding absolute $\partial B_z/\partial t$ values are transformed to the logarithmic domain. The next step is to determine which channels (if any) approximate straight line behaviour the best. The "best fit" is based on the correlation coefficient (R^2); the closer it is to one, the closer the data display power law decay behaviour. All possible combinations of channels are tested starting with the user-specified minimum number of channels, the default being four. The least squares fit for channels one to four is therefore calculated, followed by two to five, three to six, etc. Then the number of channels is increased by one and the whole process repeated, i.e. channels one to five are analysed, followed by two to six, etc. This process continues until the number of data points evaluated is equal to the number of points in the data set and only one least squares fit is done, e.g. channels one to twenty. For every combination of channels the results are tested to determine the "best fit". The "best fit" combination will have a R^2 value that falls within a specified range; it will have the slope closest to either -2.5 or -4; and if there are two combinations having the same properties thus far priority is given to the value corresponding to the largest number of channels and latest times (figure 4.2).

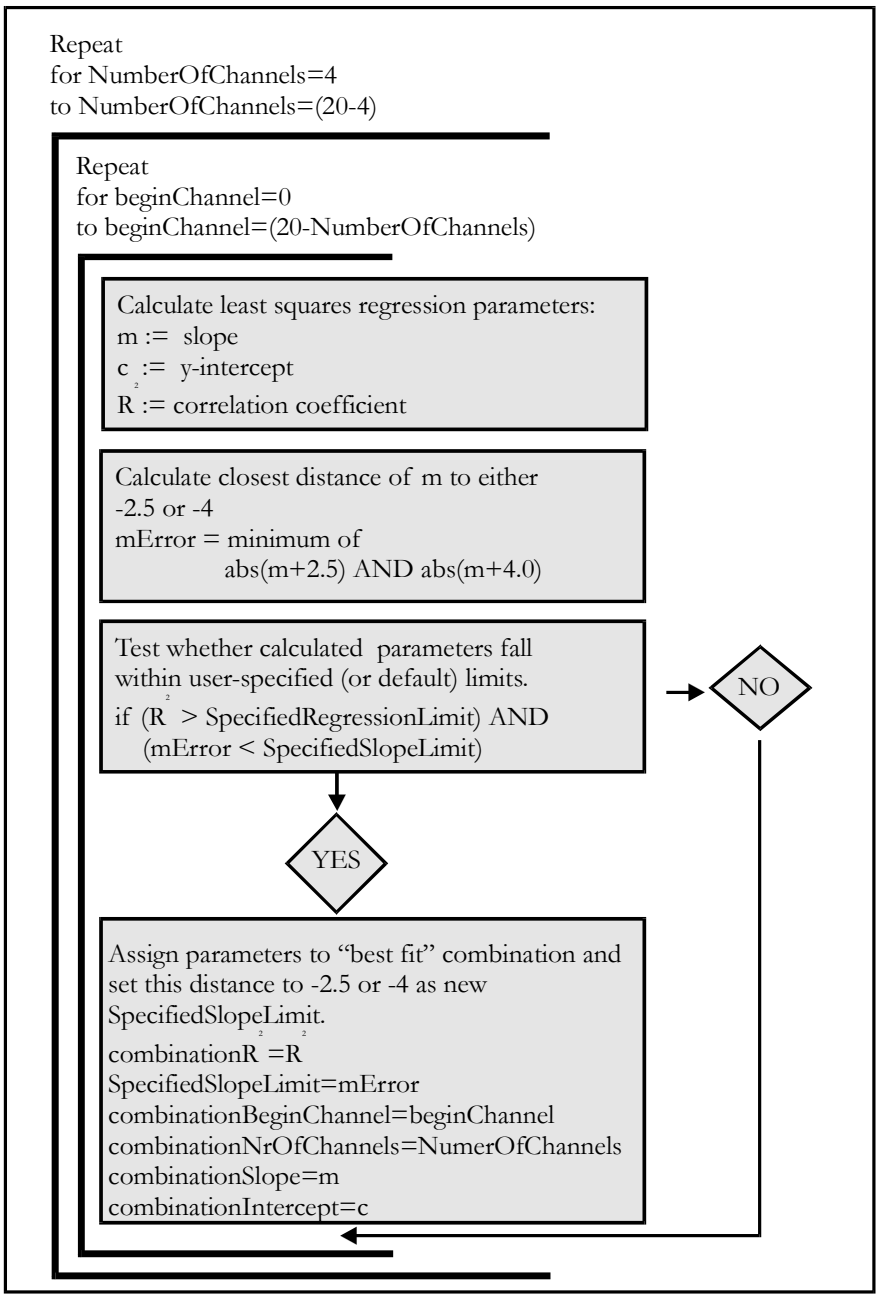

Figure 4-2 Flow diagram for decay curve slope analysis.

Based on the decay curve analysis function every sounding is classified as exhibiting half space behaviour, S-layer behaviour or neither of these.

4.3.2 Confined conductor behaviour

Analysing soundings for behaviour typical of confined conductors is done very similar to the layered earth case. Once again, all stations and all channel combinations are analysed with higher priority to more channels and later times. The main difference is that straight line behaviour is now looked for in the semi-logarithmic environment, i.e. only the $\partial B_z/\partial t$ values are transformed to the logarithmic domain. Furthermore, there are no predefined

slope values that need to be tested for and any regression fit within the specified R^2 limit is accepted as a possible conductor. The channels exhibiting the exponential decay are stored as well as the decay constant which is calculated as the inverse of the "best fit" slope.

4.3.3 IP effect or severe lateral variation in subsurface conductivity

The test for sign change of the $\partial B_z/\partial t$ component is done because with the central loop sounding configuration it implies a deviation from a layered, quasi-static subsurface. Sign changes can be ascribed to an IP (induced polarization) effect or significant lateral variations in the subsurface conductivity distribution, including two- or three-dimensional geological units. Having negative values of $\partial B_z/\partial t$ in a data set does not necessarily imply a sign change and it is important to distinguish between a well sampled, repeatable sign change and (normally late time) erratic noise. This was done by requiring at least two points of a specific sign to be followed by four points of opposite sign before a sign change is flagged in the data.

4.3.4 Results, output and presentation

The process of decay curve analysis as described here is extremely quick and takes less than a second for 1600 stations on a Pentium IV PC. The parameters determined through these functions are written to the output ASCII file and can be presented in GEOSOFT as symbols on plan or pseudo-section format. A very useful presentation for first anomaly isolation was also found through contouring the calculated decay constants (see Chapter 5). This immediately allowed areas of anomalous conductivities to be isolated in plan view. It is important to remember that all these procedures will indicate positions of anomalous data points and not yet positions of conductors themselves.

4.4 Numerical calculation of the S-layer differential transform

4.4.1 Defining the S-layer transform

The S-layer differential transform was discussed briefly in paragraph 3.4.3. It was chosen as the preferred imaging algorithm to include in the Sounding Interpretation program for the following reasons,

- Speed
- No need for an initial model
- Although it is based on the same imaging principles as the CDI transform it is easier to implement with fewer empirical factors that need to be included
- The late time approximation used in the algorithm is very applicable to the impulse response, central-loop configuration this work is based on
- For the specific case of a conductive host rock environment the S-layer differential transform shows good resolving capabilities
- As mentioned by Tartaras et. al. (2000) the main drawback of this method is the fact that it requires a numerical differentiation scheme which tends to introduce noise in the interpretation results. The implementation of a robust, yet accurate numerical differentiation scheme based on the specific properties of TEM data therefore receives high precedence. Further enhancements include a noise filter based on data points satisfying the theoretical conditions for the S-layer transform.

The S-layer differential transformation results in two equations that have to be solved for every time channel obtained at every station. Originally derived by Sidorov and Tikshaev (1969) these are summarised by Tartaras et. al. (2000) as:

$$S = \frac{16\pi^{1/3}}{(3M\Sigma n)^{1/3}\,\mu_0^{4/3}} \frac{\left(|V|^{5/3}\right)}{\left(|V|'^{4/3}\right)} \tag{4.1}$$

$$d = \frac{1}{\mu_0 S}\left(-\frac{4|V|}{|V|'} - t\right) \tag{4.2}$$

where

S = cumulative conductance [S]

d = depth [m]

M = magnetic dipole moment of transmitter [Am^2]

$\sum$ = receiver area [m^2]

n = number of turns of receiver coil

t = time [s]

$|V|$ = electromotive force of ideal receiver loop [V] $= -\sum n\left(\partial B_z / \partial t\right)$

$|V|'$ = time derivative of measured voltage $|V|$ [V/s].

The time derivative of the measured voltage ($|V|'$) is the parameter that has to be determined through numerical differentiation. This value is used to calculate both cumulative conductance (S) and depth (d) of an equivalent S-layer for each time channel and noise generated by differentiation will consequently be introduced into both these numbers. However, in order to find the earth parameter of interest, conductivity (σ), another numerical differentiation has to be performed as,

$$\sigma(d) = \frac{\partial S}{\partial d} \quad [\text{Siemens.m}^{-1}] \tag{4.3}$$

which follows from the definition of cumulative conductance. Thus, not only is a new set of errors generated in this step, but all errors from the first differentiation are carried over and enlarged by this second differentiation.

The following features are investigated:

- three numerical differentiation techniques are analysed in terms of the specific nature of TDEM data, as described above
- the most appropriate use of smoothing filters
- the effects of the re-sampling of data points to equal time intervals.

4.4.2 Numerical differentiation of TEM data

In the late time, TDEM responses measured over a one-dimensional subsurface can be described as a power-law function, equation 4.4, with k=2.5 for a half space and k=4 for a thin conductive layer (S-layer). This creates the possibilities of using standard polynomial approximations, but in the logarithmic and semi logarithmic domains. Consider the following power-law decay:

$$V(t) = At^{-k} \tag{4.4}$$

$A =$ constant

k = decay constant

If the natural logarithm of this function is taken on both sides, it becomes,

$$\ln(V(t)) = \ln A - k\ln(t) \tag{4.5}$$

Substituting ln(V(t)) with y(x), ln(t) with x and –k with m, we end up with the equation of a straight line (and a polynomial function) in the logarithmic domain.

If there is a two- or three-dimensional conductor present it will contribute to the late-time response in the form of an exponential function as shown in equation 4.6.

$$V(t) = Ae^{-kt} \tag{4.6}$$

A = constant

k = decay constant

If the natural logarithm of this function is taken on both sides, it becomes,

$$\left.\begin{aligned} \ln(V(t)) &= \ln(Ae^{-kt}) \\ \ln(V(t)) &= \ln A - kt \end{aligned}\right\} \tag{4.7}$$

Equation 4.7 is again a linear function in the semi-logarithmic domain. This behaviour only becomes dominant on TDEM sounding data if the conductor is much more conductive than the surrounding host rock or when the host rock response has been removed from the data through subtraction or deconvolution. Raw field data (as on which the S-layer differential transform is normally applied) would mostly exhibit predominantly power-law decay, although it will be distorted slightly in the presence of conductive layers or finite conductors. In the logarithmic domain TDEM data appear as functions deviating from a general linear trend and can be locally approximated by second or third order polynomials. Finding a relationship between the derivative of a function and the derivative of the same function in the logarithmic or semi-logarithmic domains would enable us to

apply polynomial-based differentiation techniques to data in the domain where they can be approximated best by polynomial functions. These very specific properties of being logarithmically sampled and exhibiting power-law or exponential decays make TEM data distinctly unsuitable for the most common numerical differentiation schemes such as the Lagrange formulas (Burden and Faires, 1993) which are based on functions exhibiting polynomial behaviour.

4.4.2.1 Analytical relationship between derivative transforms in the various domains

The objective is to find an analytical relationship between the derivative of a function in the linear domain (V'(t)) and the derivatives calculated in the semi-logarithmic (g'(t)) and logarithmic domains (h'(ln(t))) respectively. The strategy is simply to apply the chain rule of differentiation to functions presenting the data in the different domains.

Semi-logarithmic domain

In the semi-logarithmic domain the natural logarithms of the V values are taken and treated as a function of (linear) time. It is presented by the function $g(t)=\ln(V(t))$.

$$g(t) = \ln V(t)$$
$$\therefore V'(t) = V(t) \cdot g'(t) \qquad (4.8)$$

Logarithmic domain

In the logarithmic domain the natural logarithms of both the V values and times are taken and the function $h(\ln(t))=g(t)=\ln(V(t))$ is plotted against $\ln(t)$. A substitution of variables is made to simplify the derivation.

$$h[\ln(t)] = \ln[V(t)]$$
$$h[\ln(t)] = \ln\left[V\left(e^{\ln(t)}\right)\right]$$

Now, let $x = \ln(t)$ and $t = e^x$.

Then

$$h(x) = \ln\left[V\left(e^x\right)\right]$$
$$h'(x) = D_x\left\{\ln\left[V\left(e^x\right)\right]\right\}$$
$$h'(x) = \frac{1}{V\left(e^x\right)} \cdot V'\left(e^x\right) \cdot e^x$$
$$h'(x) \cdot V\left(e^x\right) \cdot \frac{1}{e^x} = V'\left(e^x\right)$$
$$\therefore V'(t) = h'(\ln(t)) \cdot V(t) \cdot \frac{1}{t} \qquad (4.9)$$

The formulas for transforming the derivatives are straightforward, trivial to apply, and analytically correct (i.e. no truncation error is induced in the transformation process). This enables us to choose the best domain for performing numerical differentiation based on the nature of data and available differentiation schemes.

Synthetic TEM data for a 10 ohm.m half space are used to illustrate this point. The Lagrange 3-point formula was applied to the example data set in the three different domains and transformed back to the linear domain using the appropriate formulas. The results were compared to the analytical derivative of the data and the percentage errors are shown in Figure 4-3. The advantage of differentiating in the logarithmic domain is very clear. Also indicated on this graph are derivative values obtained from a two-point power-law formula in the linear domain. These values are exactly equal to the Lagrange 3-point formula applied in the logarithmic domain. This formula was derived by fitting a power-law function to two points and taking the derivative of this interpolating function in exactly the same way as the Lagrange formulas are derived from polynomials.

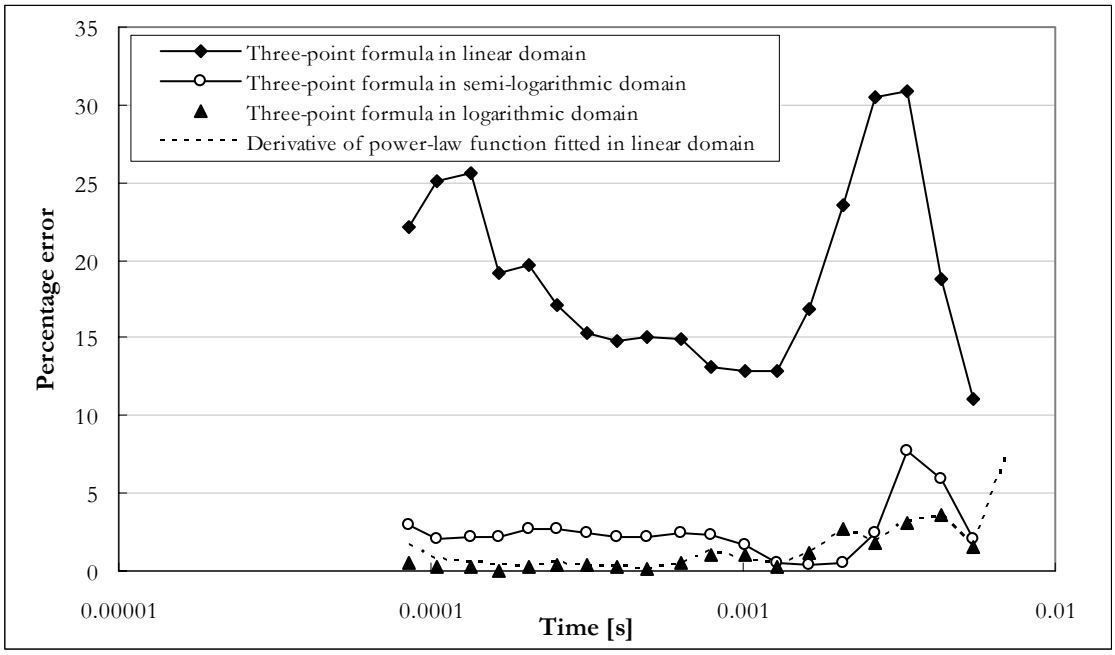

Figure 4-3 Percentage errors for differentiation in different domains of TDEM data for a 10 Ohm.m half space.

4.4.2.2 Description of three polynomial based numerical differentiation techniques

The specific numerical differentiation implemented by Tartaras et. al. (2000) is described only as "… a numerical differentiation scheme that computes a first order derivative for the provided TDEM data using polynomial interpolation." This is unfortunately not clear

enough to reconstruct with confidence and an exact comparison of this method with the other methods is not included in this study. Tartaras et. al. (2000) also applied smoothing of data "… prior to and following differentiation". This is a common technique applied to reduce noise but ultimately alters data.

Numerical differentiation is an unstable method, because although the accuracy of the formulas increases with smaller values of "h" (distance between successive nodes), this also causes the round-off error to increase. Divisions by small numbers tend to exaggerate round-off errors and should be avoided if possible. A better way of increasing the accuracy is to use formulas derived from higher order polynomials with the same inter-node distance "*h*", e.g. the three-point and five-point Lagrange polynomial-based formulas (Burden and Faires, 1993).

Three different strategies for differentiation are compared in this study.

4.4.2.2.1 Lagrange three-point formula

The Lagrange three-point numerical differentiation formula is described in most text books on numerical analysis and a detailed derivation can be found in Burden and Faires (1993). In short, derivative values of discretely sampled data points are approximated by the analytical derivative of a second order Lagrange polynomial fitted through three consecutive data points, i.e.

$$\begin{aligned} f'(x) &\approx D_x\left[\frac{(x-x_i)(x-x_{i+1})}{(x_{i-1}-x_i)(x_{i-1}-x_{i+1})}f(x_{i-1})+\frac{(x-x_{i-1})(x-x_{i+1})}{(x_i-x_{i-1})(x_i-x_{i+1})}f(x_i)\right. \\ &\quad \left.+\frac{(x-x_{i-1})(x-x_i)}{(x_{i+1}-x_{i-1})(x_{i+1}-x_i)}f(x_{i+1})\right] \\ &= D_x\left[L_{i-1}(x)f(x_{i-1})+L_i(x)f(x_i)+L_{i+1}(x)f(x_{i+1})\right], \text{ for } x\in\{x_{i-1};x_i;x_{i+1}\}. \end{aligned} \tag{4.10}$$

Effectively the method reduces to a sum of weighted function values and for the special case of calculating $f'(x_i)$ (the derivative at the centre point) for equally spaced data points it reduces to

$$f'(x_i) \approx \frac{1}{h}\left(-\frac{1}{2}\cdot f(x_{i-1})+0\cdot f(x_i)+\frac{1}{2}\cdot f(x_{i+1})\right) \tag{4.11}$$

where $h=(x_i-x_{i-1})$.

End points of equally spaced values have weights of *(-1.5; 2; -0.5)* and (*0.5; -2; 1.5*) for first and last points respectively while the weights for unequally spaced data points have to be calculated for every point using equation 4.10. Errors (and noise) in the calculated derivative are dependent on sampling interval, errors in data values (small errors in data are

enhanced in derivative calculations), computer round-off effects and how accurately the causative function can be approximated locally by a second order polynomial.

4.4.2.2.2 Derivative of cubic spline interpolated function (referred to as "cubic spline derivative method")

The Lagrange three-point method will give analytically correct results for functions of order one or two. The most intuitive way to extend the approximation for a wider range of functions is to increase the degree of the Lagrange approximating polynomial. However, this does not always improve the final result as is illustrated by Burden and Faires (1993) in Figure 4-4.

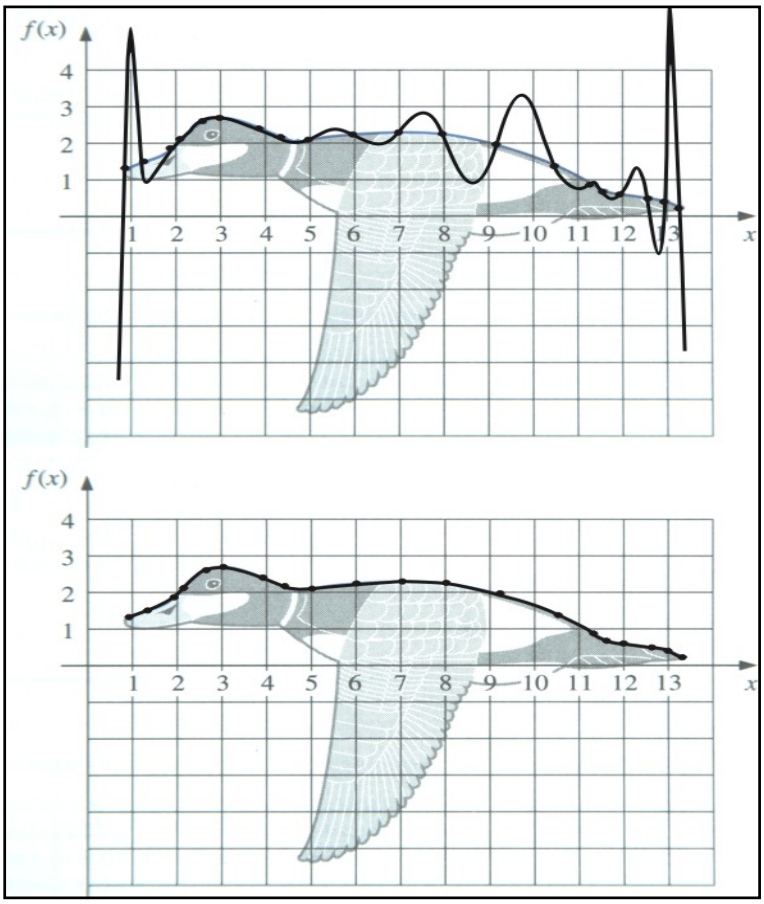

Figure 4-4 A Lagrange interpolating polynomial fitted to the data points outlining the back of a duck (top) and a cubic spline curve fitted to the same data points (bottom). (From Burden and Faires, 1993, Figures 3.11 and 3.12)

Lagrange interpolation requires that the approximated function values on the measured positions be exactly equal to the discrete data points. This introduces unwanted oscillations which are especially detrimental to any consecutive derivative calculations. An alternative is to fit higher order functions using the least squares errors approach.

However, low order polynomials will result in loss of high frequency information and high degree polynomials still suffer from unwanted oscillations.

TEM is based on diffusion of electrical currents into the earth and this is a smooth process, never oscillating in nature, and therefore not suited to this type of interpolation. Furthermore, although TEM data locally approximate polynomial functions in the logarithmic domain they cannot in general be represented by the same order polynomial on all time channels. A better strategy to follow is piecewise polynomial approximation. One method to interpolate data under these conditions is known as the cubic spline method that involves fitting third order polynomials to each consecutive pair of data points, requiring the function values to be equal to the measured data values as well as continuity of the first and second order derivatives ensuring smoothness of the function. As with the Lagrange three-point formula, an approximation to the derivative of the sampled function is obtained by taking the analytical derivative of the third order cubic spline polynomials at every point. The cubic spline method is computationally more intensive than the Lagrange three-point formula but it can also be used to resample data to equally spaced intervals (which simplifies smoothing of data) if required. The free (or natural) boundary conditions were invoked in this study (assume that the second derivatives of the end points are zero) as the information required for clamped boundary points are not available.

4.4.2.2.3 Differentiation as the inverse of integration

In contrast to numerical differentiation, numerical integration (its inverse) is a stable method and not particularly sensitive to noise. The same relationship holds for the downward (unstable) and upward (stable) continuation filters used in processing of potential field data. Cooper (2004) introduced the "inverse of upward continuation" as a more stable downward continuation filter. The same principle can now be extended to the problem at hand and differentiation can be substituted by a stable "inverse of integration" filter. This can be formulated as follows. Define $f(x_i)$ as the n data points to be differentiated, $f'(x_i)$ as the required derivative values and $\mathbf{A}$ an operator of integration. Then

$$\mathbf{A} \cdot f'(x_i) = f(x_i), \qquad i = 0 \ldots n. \tag{4.12}$$

For the case where **A** is singular, not square or a non-linear operator, equation 4.12 must be solved with a method such as generalised least squares inversion or other equivalent techniques (Cooper, 2004). Disadvantages of solving systems of equations in this way are:

- need for a good initial model
- no guarantee for convergence
- no guarantee for uniqueness of the solution
- mathematical intensity

However, if **A** can be formulated as a non-singular, square and linear matrix, equation 4.12 becomes a system of linear equations with the same number of unknowns as equations (implying the existence of an inverse operator and a unique solution) which can be solved by multiplying both sides with $\mathbf{A}^{-1}$.

$$f'(x_i) = \mathbf{A}^{-1} \cdot f(x_i), \qquad i = 0...n. \tag{4.13}$$

In this case equation 4.12 can also be solved by applying Gaussian elimination with backward substitution. Depending on whether **A** and $\mathbf{A}^{-1}$ will be calculated only once (for a fixed number of equally spaced data points) or whether it will have to be recalculated (for unequally spaced data points). For 20 data points it will require 3060 multiplications/divisions and 2850 additions/subtractions to solve equation 4.12 using Gauss elimination with backward substitution. The equivalent numbers for calculating $\mathbf{A}^{-1}$ are 10 660 and 10 070. Thereafter 400 multiplications/divisions and 380 additions/ subtractions are required to solve for the $f'(x_i)$.

Construction of the integration matrix

Integration and differentiation can be done very simply in the frequency domain by respective division or multiplication with the factor ($i\omega$) where ω is angular frequency and $i = \sqrt{-1}$. However, the process of Fourier transformation on discrete data points adds noise to data and time (or spatial) domain calculations, although more complex and time-consuming, are preferred in order to obtain cleaner data.

The first point that has to be addressed in any integration procedure is that of the integration constant, formulated as

$$\int f'(x)dx = f(x) + c, \tag{4.14}$$

where c can take on any value (implying an infinite number of solutions). An easy solution is to use definite integrals instead, so that

$$\int_a^b f'(x)dx = f(b) - f(a). \tag{4.15}$$

From equation 4.12, the system of equations that has to be solved now reduces to a general form as shown in equation 4.16.

$$\begin{bmatrix} a_{11} & a_{12} & . & . & a_{1n} \\ a_{21} & . & . & . & . \\ . & . & . & . & . \\ . & . & . & . & . \\ a_{n1} & . & . & . & a_{nn} \end{bmatrix} \begin{bmatrix} f'(x_1) \\ . \\ . \\ . \\ f'(x_n) \end{bmatrix} = \begin{bmatrix} f(x_b) - f(x_a) \\ . \\ . \\ . \\ f(x_n) - f(x_{n-1}) \end{bmatrix}. \tag{4.16}$$

The elements of **A** (a_{ii}) must now be defined so as to produce numerical integration of the $f'(x_i)$. Simpson's rule is a standard and very effective method suitable for polynomial functions. For equally spaced points it is given by

$$\int_{x_{i-1}}^{x_{i+1}} f'(x)dx = f(x_{i+1}) - f(x_{i-1}) \approx \frac{h}{3}\left[f'(x_{i-1}) + 4 \cdot f'(x_i) + f'(x_{i+1})\right], \tag{4.17}$$

where

$$h = (x_{i+1} - x_i) = (x_i - x_{i-1}).$$

This formula will generate *n-2* equations. In order to have a square matrix and unique solutions we need two more independent equations. This is done by deriving two end-point Simpson's rule formulas. The midpoint Simpson's rule is derived by fitting a second order polynomial through three consecutive points and integrating this polynomial from the first to the third point. The same strategy is followed for the end points except that we integrate from the first to the second point at the start of the sequence and from the second to the third point at the end. This results in the following two equations.

$$\int_{x_1}^{x_2} f'(x)dx = f(x_2) - f(x_1) \approx \frac{h}{3}\left[\frac{5}{4} f'(x_1) + 2 \cdot f'(x_2) - \frac{1}{4} f'(x_2)\right], \tag{4.18}$$

and

$$\int_{x_{n-1}}^{x_n} f'(x)dx = f(x_n) - f(x_{n-1}) \approx \frac{h}{3}\left[-\frac{1}{4} f'(x_{n-2}) + 2 \cdot f'(x_{n-1}) + \frac{5}{4} f'(x_n)\right], \tag{4.19}$$

where

$$h = (x_{i+1} - x_i).$$

For equally spaced points, equation 4.16 can thus be rewritten as

$$\frac{h}{3}\begin{bmatrix} 5/4 & 2 & -1/4 & 0 & . & . & 0 \\ 1 & 4 & 1 & 0 & . & . & 0 \\ 0 & 1 & 4 & 1 & 0 & . & 0 \\ 0 & 0 & 1 & 4 & 1 & . & 0 \\ 0 & . & . & . & . & . & 0 \\ 0 & . & . & 0 & 1 & 4 & 1 \\ 0 & . & . & 0 & -1/4 & 2 & 5/4 \end{bmatrix}\begin{bmatrix} f'(x_1) \\ f'(x_2) \\ . \\ . \\ . \\ f'(x_{n-1}) \\ f'(x_n) \end{bmatrix} = \begin{bmatrix} f(x_2)-f(x_1) \\ f(x_3)-f(x_1) \\ f(x_4)-f(x_2) \\ \dots \\ f(x_{n-1})-f(x_{n-3}) \\ f(x_n)-f(x_{n-2}) \\ f(x_n)-f(x_{n-1}) \end{bmatrix} \tag{4.20}$$

or

$$\begin{bmatrix} 2\,1/2 & 4 & -1/2 & 0 & . & . & 0 \\ 1 & 4 & 1 & 0 & . & . & 0 \\ 0 & 1 & 4 & 1 & 0 & . & 0 \\ 0 & 0 & 1 & 4 & 1 & . & 0 \\ 0 & . & . & . & . & . & 0 \\ 0 & . & . & 0 & 1 & 4 & 1 \\ 0 & . & . & 0 & -1/2 & 4 & 2\,1/2 \end{bmatrix}\begin{bmatrix} f'(x_1) \\ f'(x_2) \\ . \\ . \\ . \\ f'(x_{n-1}) \\ f'(x_n) \end{bmatrix} = \frac{3}{h}\begin{bmatrix} 2\left[f(x_2)-f(x_1)\right] \\ f(x_3)-f(x_1) \\ f(x_4)-f(x_2) \\ \dots \\ f(x_{n-1})-f(x_{n-3}) \\ f(x_n)-f(x_{n-2}) \\ 2\left[f(x_n)-f(x_{n-1})\right] \end{bmatrix}. \tag{4.21}$$

The matrix **A** is square and symmetrical with the highest values on the diagonal as pivot elements except for the first and last rows. The inverse of this matrix, $\mathbf{A}^{-1}$, depends on the number of data points, n, and can be calculated using any standard algorithm. In the general case where data points are unequally spaced the weights (a_{ii}) are different for every data set and both the matrix and its inverse have to be recalculated for every sounding. The derivation of Simpson's rule for unequally spaced points is given in APPENDIX A.

4.4.2.3 Smoothing and re-sampling of data points

Before testing of the three integration methods discussed above, one need to consider the process and effect of smoothing of the data at various stages of the differentiation process. Smoothing of data before and after numerical differentiation is an accepted method of reducing the noise in data (Tartaras et. al., 2000). However, any smoothing applied to the data, will change the data and will influence the final interpretation. In the S-layer differential transform algorithm there are four possible opportunities to smooth data and the question arises which of these will optimise the algorithm with minimum alteration of the data.

The last factor taken into consideration is the spacing of data points. The time channels at which data are measured are almost equally spaced in the logarithmic domain. The calculated depths (to which the second differentiation has to be performed) will have intervals dependent on the conductivity of the subsurface. The advantage of re-sampling

data to equal intervals is that the weights (and inverse matrices) used for differentiation and smoothing only has to be calculated once. Applying the transform to unequally spaced data points means less tampering with the original data but it is much more time intensive. The method use for smoothing is the three-point moving average filter for equally spaced points and a weighted extension for unequally spaced points (equation 4.22).

$$f(x_2)_{Weighted\ Moving\ Average} = \frac{2\cdot(x_3 - x_2)}{(x_3 - x_1)}\cdot f(x_1) + f(x_2) + \frac{2\cdot(x_2 - x_1)}{(x_3 - x_1)}\cdot f(x_3) \qquad (4.22)$$

4.4.3 Comparison of differentiation methods applied to synthetic data

4.4.3.1 First order numerical differentiations compared to the analytical derivative of a function

A TDEM decay curve is simulated by an analytical function (equation 4.23), defined as the sum of exponential and power law terms. (There are no analytical formulations of complete layered earth TEM responses in closed form, therefore an "equivalent" analytical function is used.)

$$\begin{aligned} f(x) = {} & 0.000001\cdot t^{-5/2} + 0.00000000001\cdot t^{-4} + 0.00000001\cdot t^{-3} \\ & + 2000\cdot e^{-2500t} + 12000\cdot e^{-8000t} + 10\cdot e^{-400t} \end{aligned} \qquad (4.23)$$

The first order analytical derivative of this function is compared to the following numerical scenarios:

- All three numerical differentiation algorithms are applied to unequally spaced data points and without smoothing of the data. The results are shown in figure 4.5(a).
- The same as (1) but with smoothing of the function before the derivatives were calculated. The results are shown in figure 4.5(b).
- The same as (1), but with the unequally spaced data points re-sampled to equally spaced data points using the cubic spline interpolation method. Figure 4.5(c) shows the results without smoothing of the data, as in Figure 4.5(a).
- The results in Figure 4.5(d) is the equally spaced data points equivalent of 4.5(b).
- A summary of the average errors (absolute values) for every alternative is given in Figure 4.6.

From these comparisons the following are concluded:

The inversion method gives the smallest average error, followed by the cubic spline and three point methods.

For unsmoothed data the equally spaced points slightly outperform the unequally spaced points, but the reverse is true for smoothed data.

Smoothing of data seems to be the largest contributing factor to errors in noise-free data.

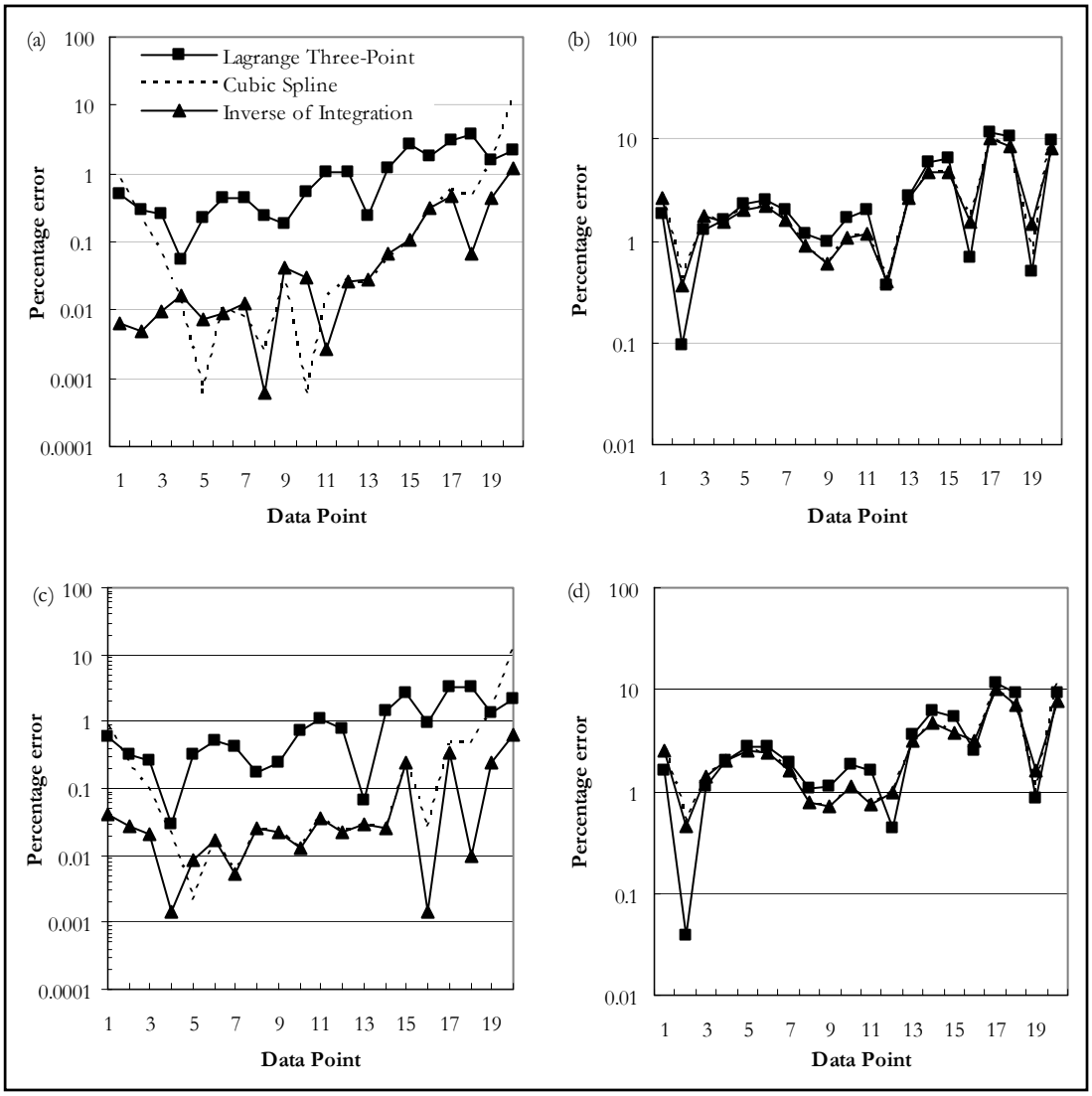

Figure 4-5: Comparison of differentiation methods applied to (a) unequally spaced points without smoothing of data, (b) unequally spaced points with smoothing of data, (c) equally spaced points without smoothing of data and (d) equally spaced points with smoothing.

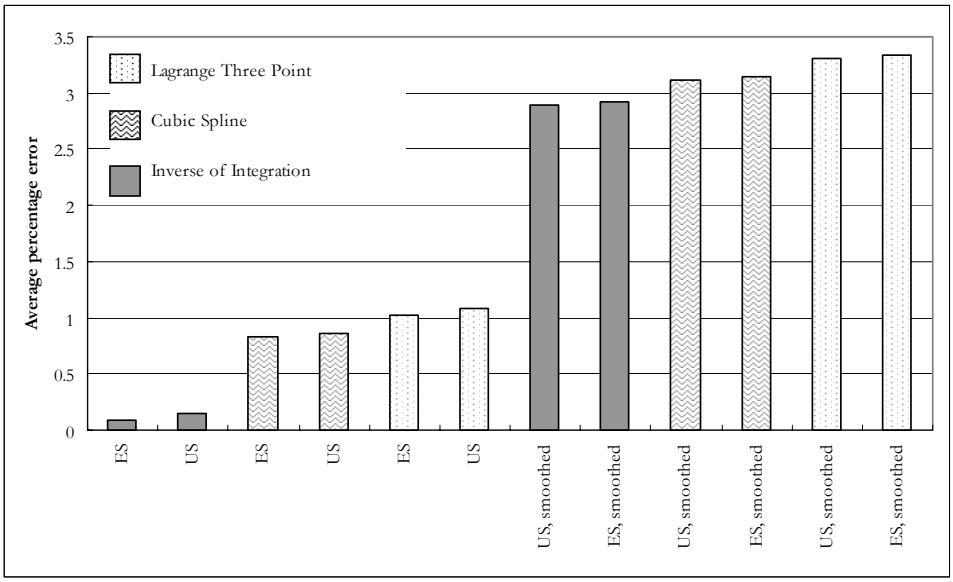

Figure 4-6: A summary (in ascending order) of the average error over twenty data points for each of the alternatives in Figure 4.5. (ES: equal spacing, US: unequal spacing)

4.4.3.2 S-layer differential transform applied to forward modelled data

A set of data was calculated for a three-layer earth using MARCO software developed by AMIRA. The model and data are shown in Figure 4-7.

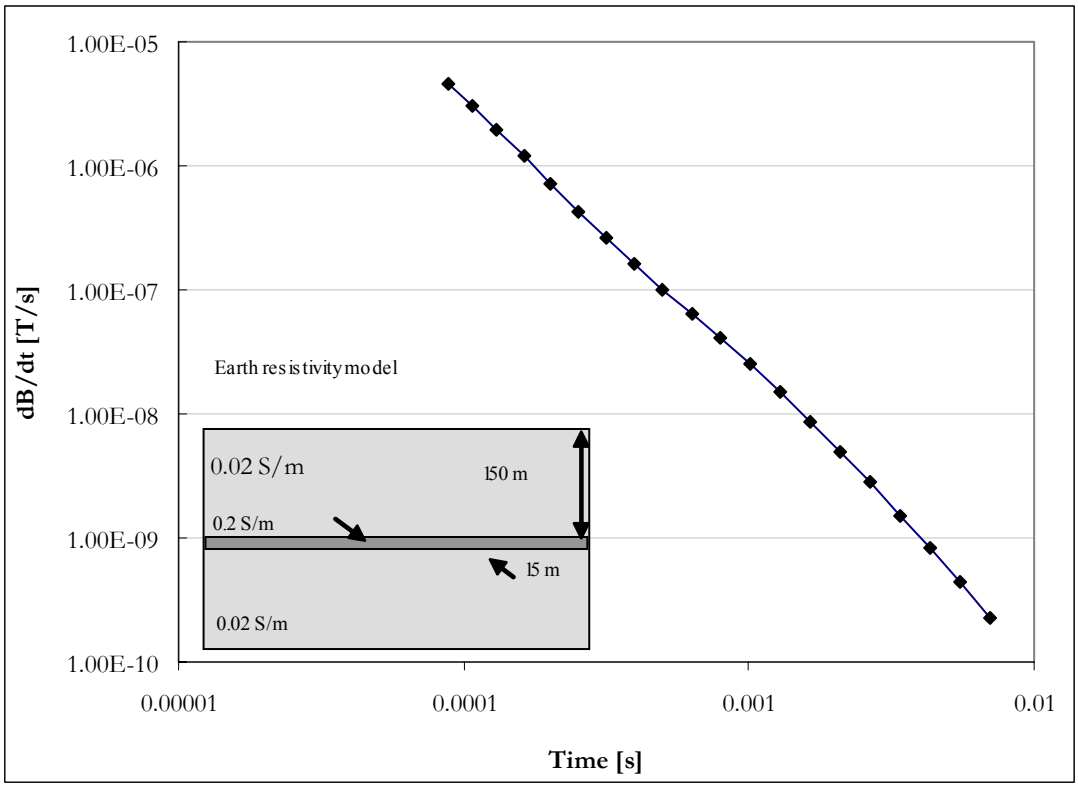

Figure 4-7: Synthetic data and model for three-layer earth.

The numerical calculation of the S-layer transform was done using the following steps:

1. Input $|V|$ values $\left(= \frac{\partial B_z}{\partial t} \text{ if normalised to receiver area of } 1\text{m}^2 \right)$
2. Calculate $|V|'$, i.e. $\frac{\partial^2 B_z}{\partial t^2}$
3. Calculate S from equation 4.1
4. Calculate d from equation 4.2
5. Calculate $\frac{\partial S}{\partial d} = \sigma$

Numerical differentiations are performed in steps 2 and 5. Smoothing filters are applied at various stages in the algorithm cumulating up to the strategy proposed by Tartaras et. al. (2000) which is smoothing before and after each differentiation. Figure 4-8 top shows the results of three variations:

- smoothing of $|V|$ before step 1
- smoothing of $|V|$ before step 1 and S after step 3
- smoothing of $|V|$ before step 1, S after step 3 and σ after step 5.

As can be expected the successive smoothing slightly lowers the maximum amplitude and widens the response curve. However, it is critical *not* to smooth $|V|'$ (figure 4.8 bottom), which introduces extensive noise. This is due to the ratios of $|V|$ and $|V|'$ used to calculate S and d.

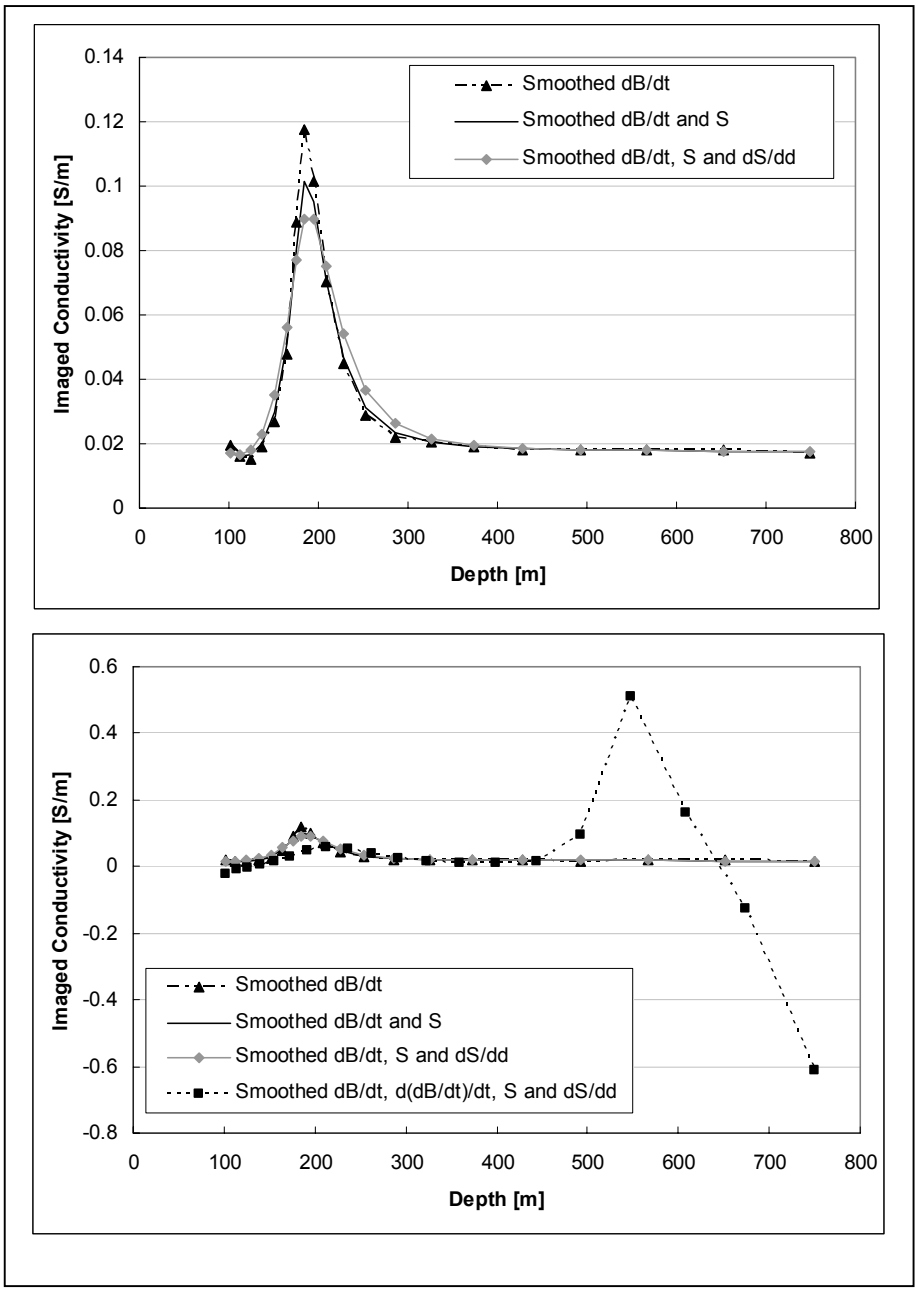

Figure 4-8: Effects of smoothing at different points in S-layer transform algorithm.

Figure 4-9 shows the output of the S-layer transform (imaged conductivity versus depth) for twelve different combinations of differentiation method, smoothing and spacing of data. (Smoothing of data here implies smoothing $|V|$, S and σ.) Both smoothing and resampling of data reduces the maxima of responses leading to an underestimation of the conductivity contrast.

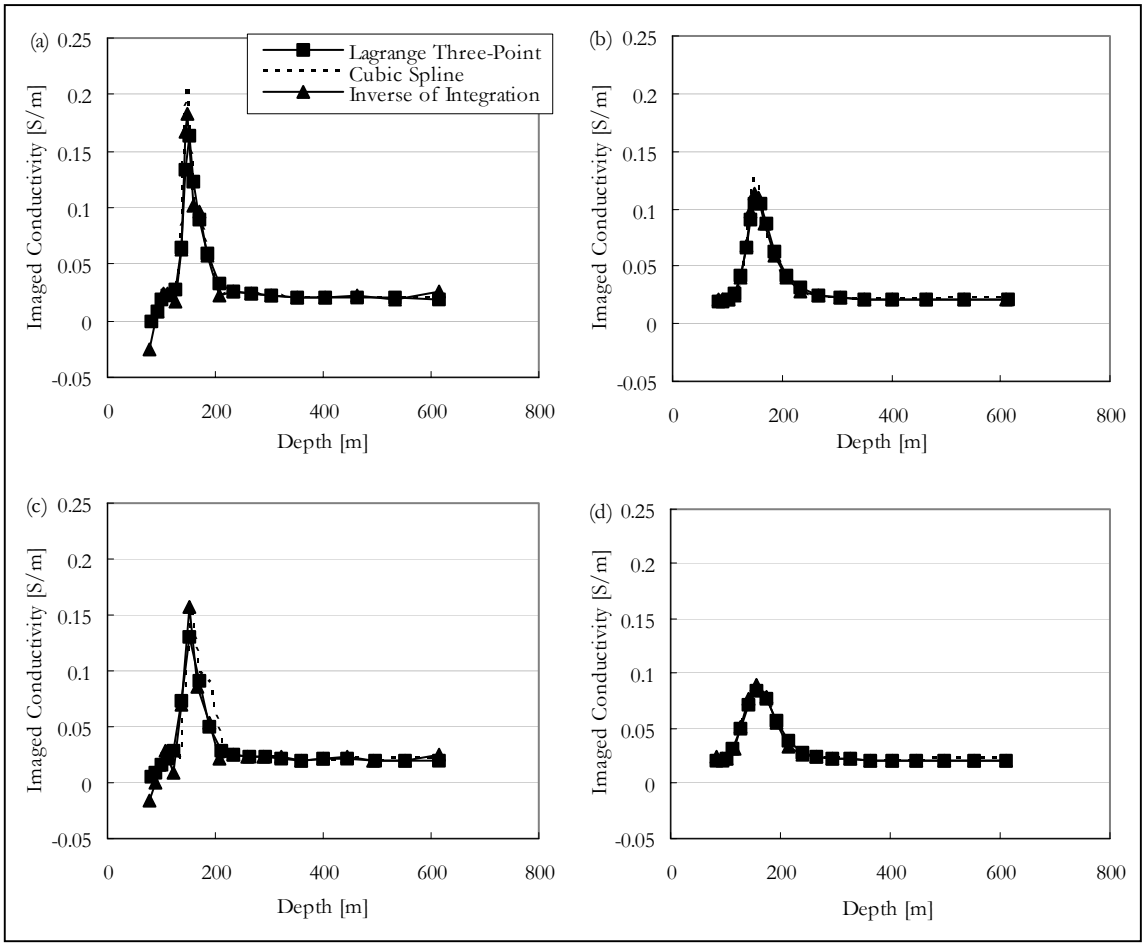

Figure 4-9: Comparison of S-layer differential transform results for the three numerical differentiation methods applied on (a) unequally spaced data points without smoothing of data, (b) unequally spaced data points with smoothing of data, (c) equally spaced data without smoothing and (d) equally spaced data with smoothing.

1.4.4 Comparison of differentiation methods on field data

Four soundings are chosen from a field data set to represent both clean and noisy data (Figure 4-10) and all twelve processing combinations are applied to these soundings. The data were acquired with a Geonics Protem system in the central loop sounding configuration utilising a 100mX100m transmitter loop, 15A current, 25Hz base frequency and effective receiver area of 100m^2. Figures 4-11 to 4-16 summarise the results with (a) unequally spaced data points without smoothing of data, (b) unequally spaced data points with smoothing of data, (c) equally spaced data points without smoothing of data and (d) equally spaced data points with smoothing every time.

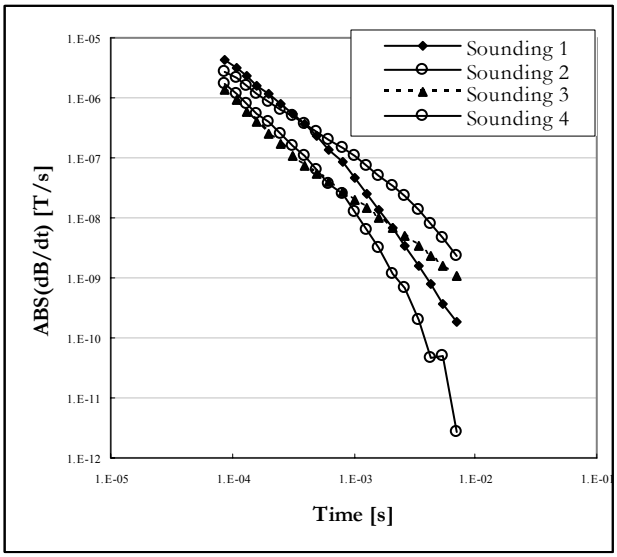

Figure 4-10: Four field data soundings; 1 to 4 are very smooth and considered to be clean data, while 5 & 6 contains noise.

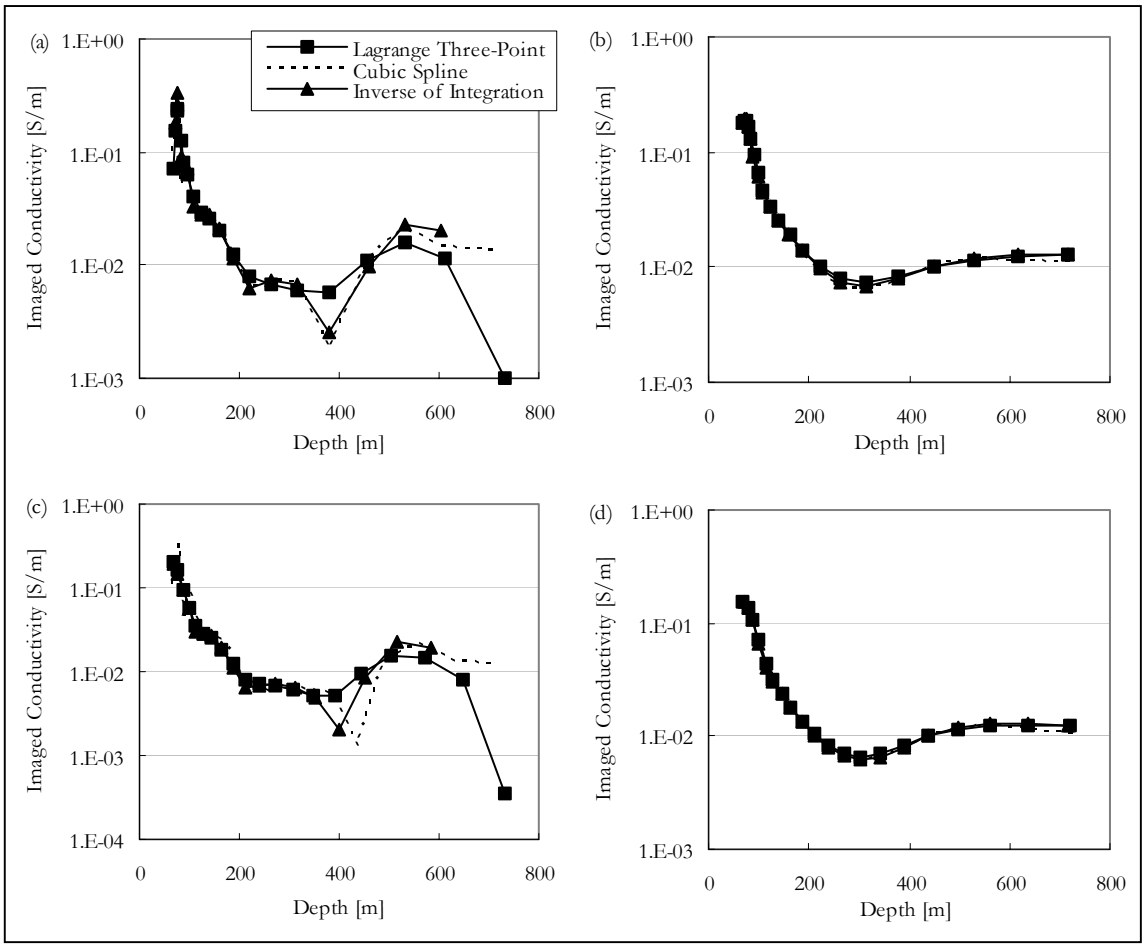

Figure 4-11: S-layer differential transform results for Sounding 1.

Sounding 1 (Figure 4-11) would be considered "noise-free" in that none of the data points would probably be masked (ignored) in manual interpretation of the data. However, comparing the smoothed and unsmoothed results it is clear that it does contain some noise which can be filtered out successfully with the weighted moving average filter. The unequally spaced points are less sensitive to the noise and after smoothing there is no noticeable difference between the three different methods of differentiation. (With field data it is not possible to calculate percentage errors and smoothness of conductivity-depth curves are used as an indication of accuracy based on the smoothly dissipative nature of TEM currents.)

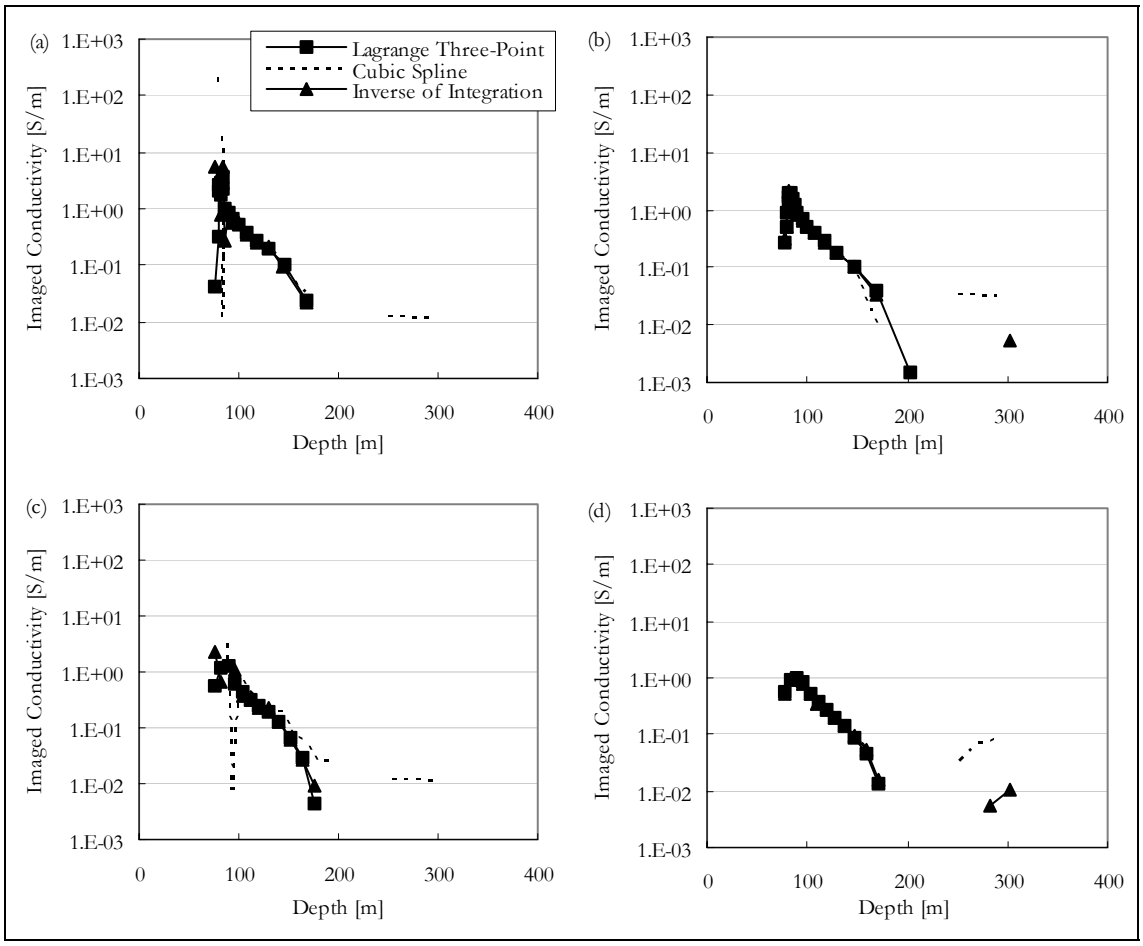

Figure 4-12: S-layer differential transform results for Sounding 2.

Sounding 2 contains slightly more noise (Figure 4-12). The most noticeable effect is that the re-sampling to equally spaced data points causes the method to fail. (This is mostly due to re-sampling of the cumulative conductance (S) curve which is differentiated in step 5 of the algorithm. This curve, although smooth, sometimes forms a relation rather than a

function, implying more than one S value for each depth and this is not accounted for in re-sampling with the cubic spline method.)

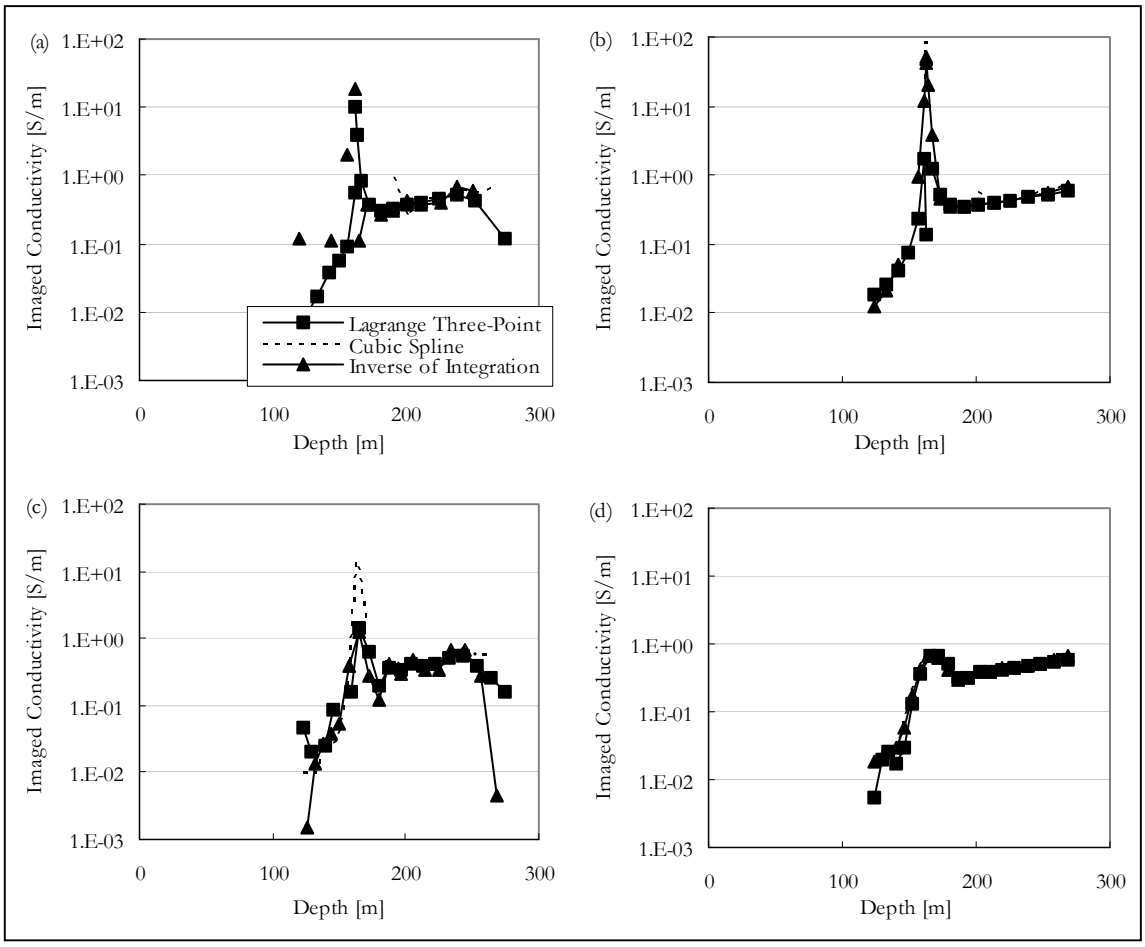

Figure 4-13: S-layer differential transform results for Sounding 3.

For Sounding 3 (Figure 4-13) the same pattern holds. Here the advantage of smoothing is very clear, especially on the "inverse of integration" method. In Sounding 4 (Figure 4-14) even the unequally spaced, smoothed data become noisy with gaps (indicating negative conductivities having no physical meaning). This is once again due to the cumulative conductance curve not increasing monotonically, although the measured data is smooth the algorithm might fail in this case as the assumption of cumulative conductance on which the S-layer transform is based, is violated.

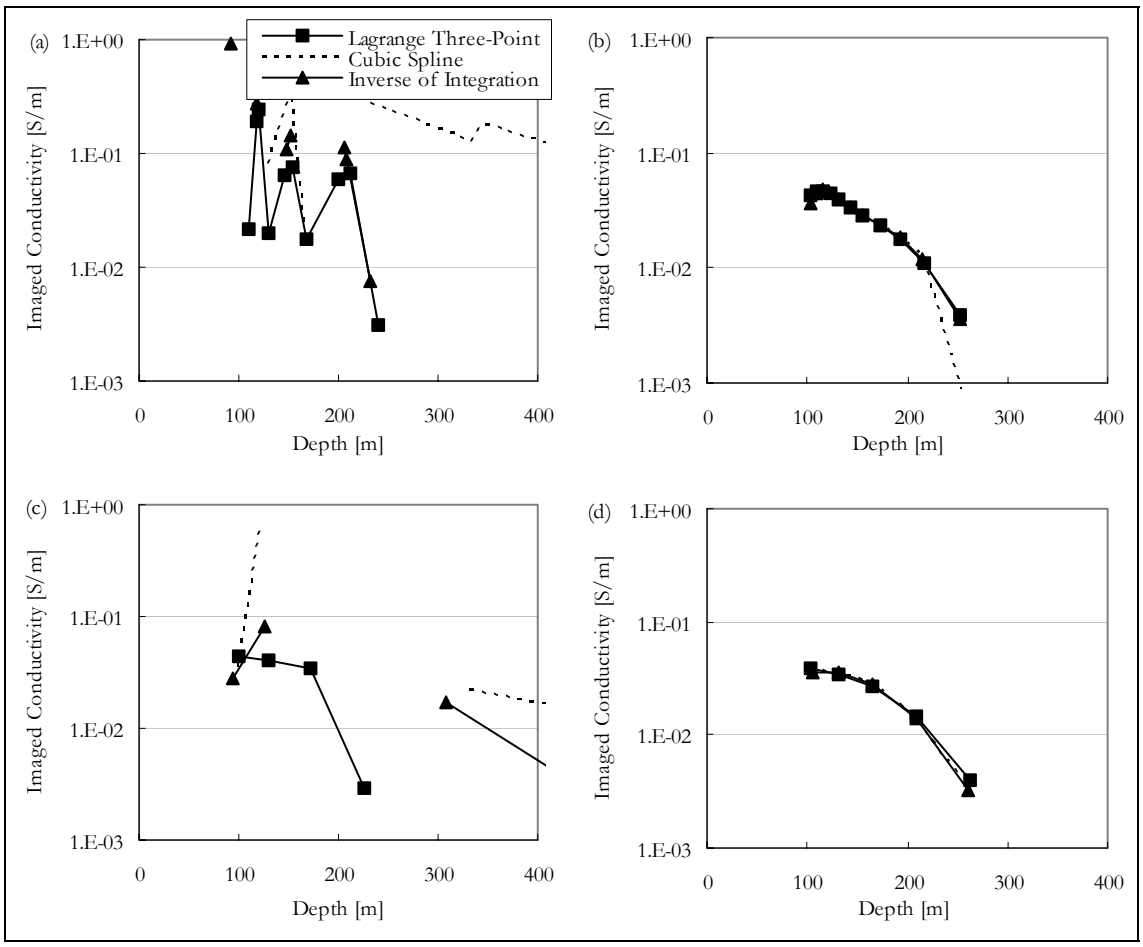

Figure 4-14: S-layer differential transform results for Sounding 4.

4.4.5 Concluding remarks on numerical differentiation

The S-layer differential transform (and other imaging techniques) are useful tools in automated interpretation of TDEM data because it is fast and do not require a starting model. It is not as accurate as inversion methods but remains useful in providing starting models for these more time consuming procedures. As numerical differentiation is very unstable, it is important to take great care when applying this operator in the S-layer transform. When working with field data, data have to be smoothed but with cognizance of the influence on the final result. Even though time-effectiveness can be increased in using algorithms for equally spaced data points it produces very poor results when applied to the S-layer transform. As for the method of differentiation, the "inverse of integration" performed best on synthetic data but it is arguable whether the 0.4% increase in accuracy is worth the additional effort compared to the Lagrange three-point formula. However, the

S-layer transform remains very fast (less than five seconds on a PC for 1500 soundings) no matter which differentiation method is chosen. Finally, only good quality data can be expected to give good quality results and if a truly automated process is required a filter passing only relatively noise-free data should be applied before the S-layer differential transform is applied

.

4.5 The S-layer correction factor

4.5.1 Defining a S-layer correction factor

The S-layer algorithm applied to the synthetic examples above, necessitated the implementation of a scale factor in order to obtain the correct depths and conductivity values. This factor is determined empirically as follows.

Half space responses were calculated using the late time approximation (Kaufman and Keller, 1983) as well as a numerical implementation of the solution valid for all times (W. J. Botha, unpublished). The S-layer transform is applied to these voltages in order to obtain depths and conductivities (resistivities for comparison). These resistivity values are compared to the original input values. Resistivities used were 10 ohm.m, 50 ohm.m, 100 ohm.m, 500 ohm.m, 1000 ohm.m and 5000 ohm.m with comparative results shown in Fig 4.15. In the figure, the open diamonds are the values obtained from the S-layer transform applied to the full expression, the filled diamonds those obtained from using the asymptotic values, while the solid line indicate the original resistivity value.

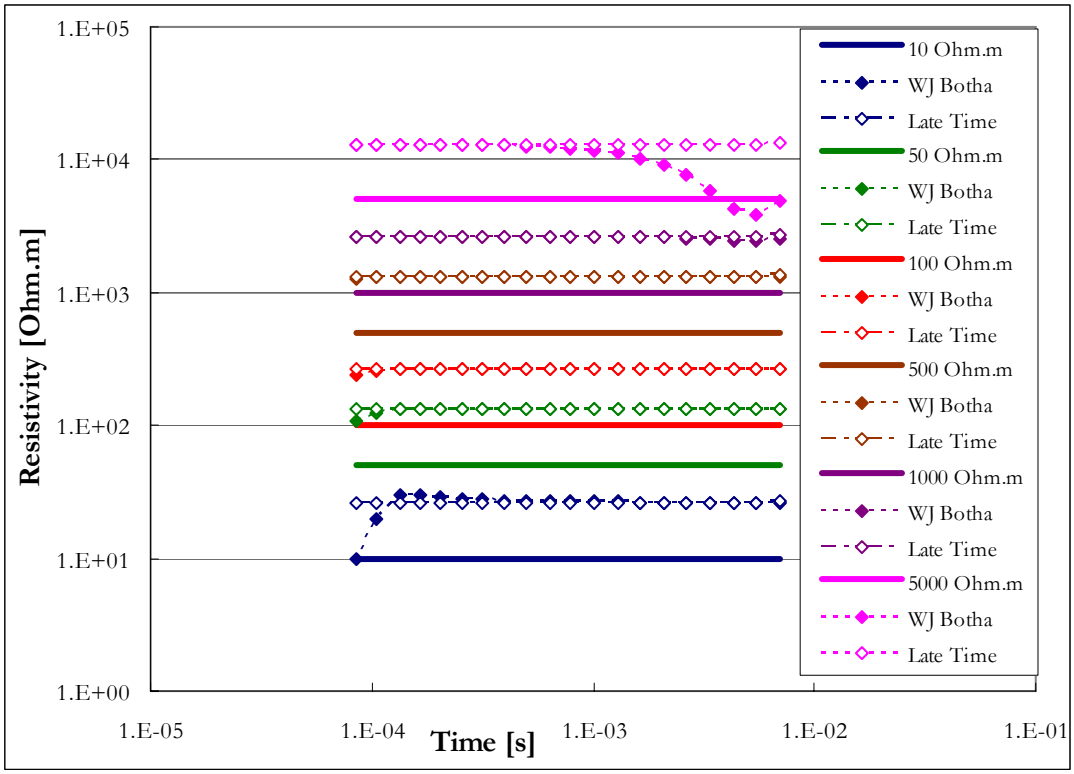

Figure 4-15: Half space resistivities compared to resistivities from S-Layer differential transform.

The 10 ohm.m full solution shows distortions in the first time channels when the late time has not been reached. Distortions are also visible on the late channels of the 5000 ohm.m data. The correlation of the full solution data to the late time approximation results is as expected – in times adhering to the late time approximations the values are equal. From the figure it is immediately obvious that the resistivities produced by the S-Layer transform are consistently higher than that of the input values.

It was found that the ratio of the resistivities calculated from the S-layer transform divided by the modelled resistivity yielded a constant of 2.6192. Since the conductivities (1/resistivities) are calculated in the algorithm as the derivative of conductance (S) to depth (d), this "error" could be produced either in the calculation of S or d, since depth (d) is a function of S (eq. 4.2). Correction factors can be applied in either the S or d formulae and will yield "correct" (i.e. equal to half space) conductivities as long as the following relationships hold.

$$\left(\frac{\partial S}{\partial d}\right)_{SCALED} = \left(\frac{\partial S}{\partial d}\right) / 2.6192$$

$$= \left(\frac{\partial (S \cdot S_{factor})}{\partial (d \cdot \frac{d_{factor}}{S_{factor}})}\right)$$

So that,

$$2.6192 = \frac{S_{factor}}{\left(\frac{d_{factor}}{S_{factor}}\right)}$$

$$= \frac{S^2{}_{factor}}{d_{factor}}$$

There are of course an infinite number of correction factors that will satisfy this requirement (Figure 4.16) and an urgent need arouse to explain the origin of this discrepancy. Three possibilities are investigated based on comparison with synthetic data from models which have all shown that depths are overestimated by the transform. Only correction factors which will decrease calculated depths are therefore discussed (the red line on Fig 4.16 indicates the possible depth correction factors ranging from almost zero to one). The following possibilities for the observed error were considered.

- A possible error in equation 4.1.
- A possible error in equation 4.2.
- An error in the physical assumptions made during the S-layer transform.

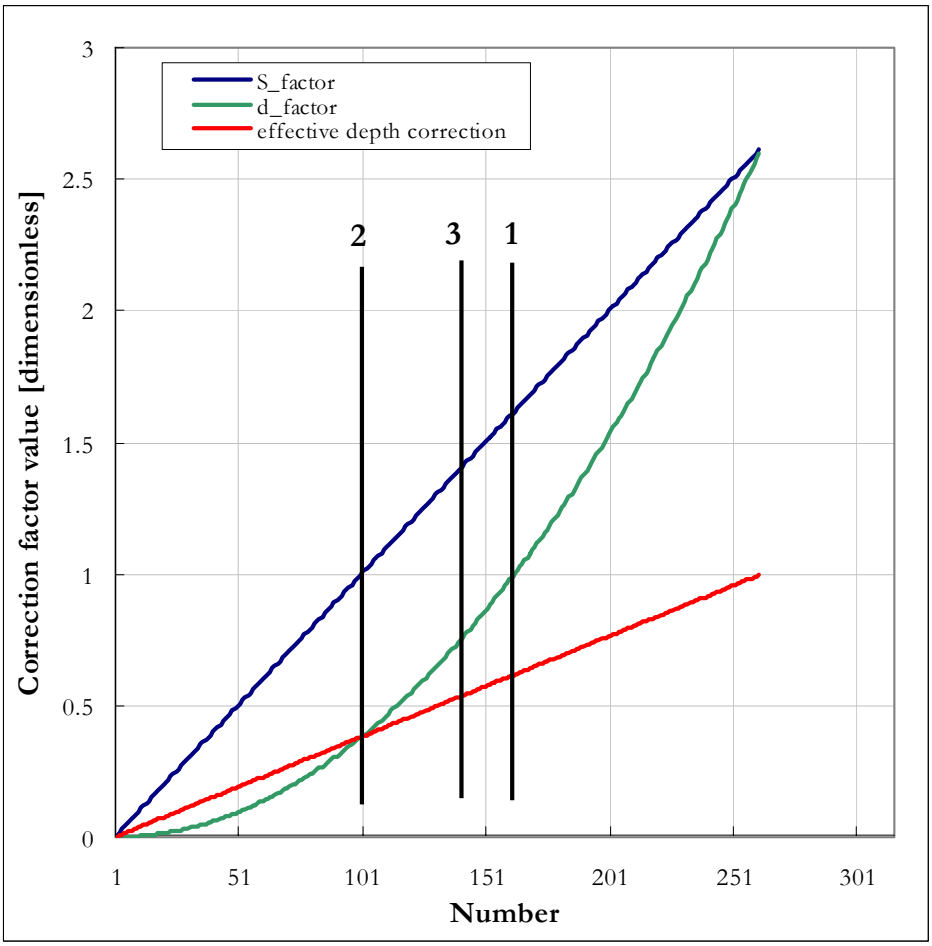

Figure 4-16: Values for S and d corrections giving correct resistivity values and the effective depth correction resulting from each pair. (from Excel: summary of depth conversion factor models)

4.5.1.1 Correction factor: Possibility 1

The assumption made here is that somehow an error is introduced in Eq. 4.1 only and that only this needs to be corrected for. This implies that (vertical line 1, Figure 4.16):

$$d_{FACTOR} = 1$$

$$S_{FATOR} = \sqrt{2.6192}$$

this leads to a depth correction *multiplication factor* of 0.6185.

4.5.1.2 Correction factor: Possibility 2

Now the assumption is made that an error is introduced in Eq. 4.2 only and that only this needs to be corrected for. This implies that (vertical line 2, Figure 4.16)

$$d_{FACTOR} = \frac{1}{2.6192} = 0.3818$$

$$S_{FATOR} = 1$$

this leads to a depth correction multiplication factor of 0.3818.

4.5.1.3 Correction factor: Possibility 3

The third possibility is that the equations used in the transform are indeed mathematically sound but that the physical assumptions regarding current distributions made in the S-layer transform lead to poor approximations of the models used. In figure 2.1 it was shown that the equivalent current filament that was successfully used by Nabighian to calculate the half space response, did not spaciously coincide with the actual maxima of the current distribution in the sub surface. It was decided to test this same discrepancy on the S-layer transform. In other words, it is assumed that the equivalent filament for the S-layer behaviour, as with the equivalent filament for the half space behaviour, does not coincide with the electric field maxima in the subsurface. In order to test this theory the cumulative conductance was calculated, as is done by the S-layer transform, for the electric field maxima and equivalent current filaments (smoke-rings) respectively. The depth expressions given in equation 4.24(a), (After Nabighian and Macnae, 1991) was used in equation 4.24(b) to calculate the cumulative conductances for a 30 ohm.m half space shown in figure 4.17.

$$d_{Electric\ Field\ Maximum} = \sqrt{\frac{2t}{\sigma\mu_0}}$$

$$d_{Equivalent\ Current\ Filament} = 4\sqrt{\frac{t}{\pi\sigma\mu_0}}. \qquad 4.24(a)$$

$$S(d_{i+1}) = S(d_i) + \sigma \cdot [d_{i+1} - d_i]. \qquad 4.24(b)$$

As can be expected, the cumulative conductance curves are straight lines with slopes $\left(\frac{\partial S}{\partial d}\right)$ equal to the conductivity (Fig 4.17). It can be seen that although both curves will give correct conductivity values the S and d values vary distinctly.

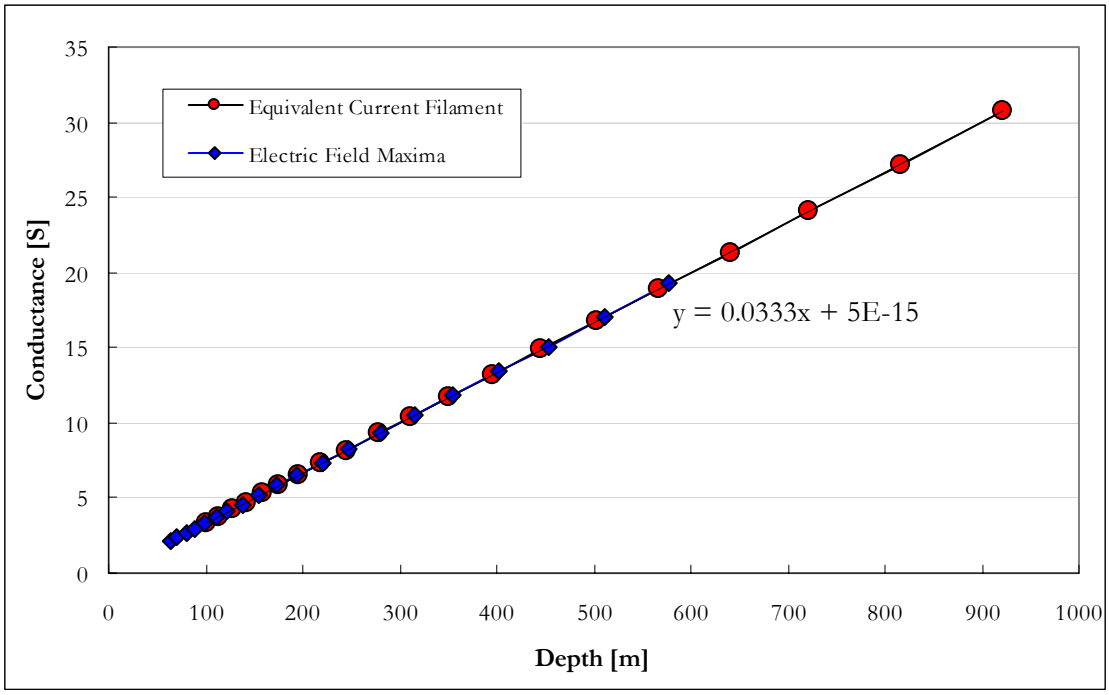

Figure 4-17: Cumulative conductance curves for late time halfsapce approximations.

Looking specifically at depths, the equivalent current filament depths range from 99 m to 920 m, while the electric field maxima map between 63 m and 577 m. The S-layer transform is also based on using current filaments to approximate a whole earth response and is it reasonable to expect that the S-layer transform will give similar errors in the depth to current maxima results.

In Figure 4.18 the cumulative conductance curve (green) of the S-layer differential transform is compared with the curves from Figure 4.17. It shows the same approximate depth range as that of the single equivalent current filament but with conductance values much lower than expected (resulting in underestimation of conductivity values). Based on these graphs the third set of correction factors is proposed which will transform the S-layer transform values to coincide with the maxima of the electric field. The corrected conductance curve is shown in pink (Figure 4.18).

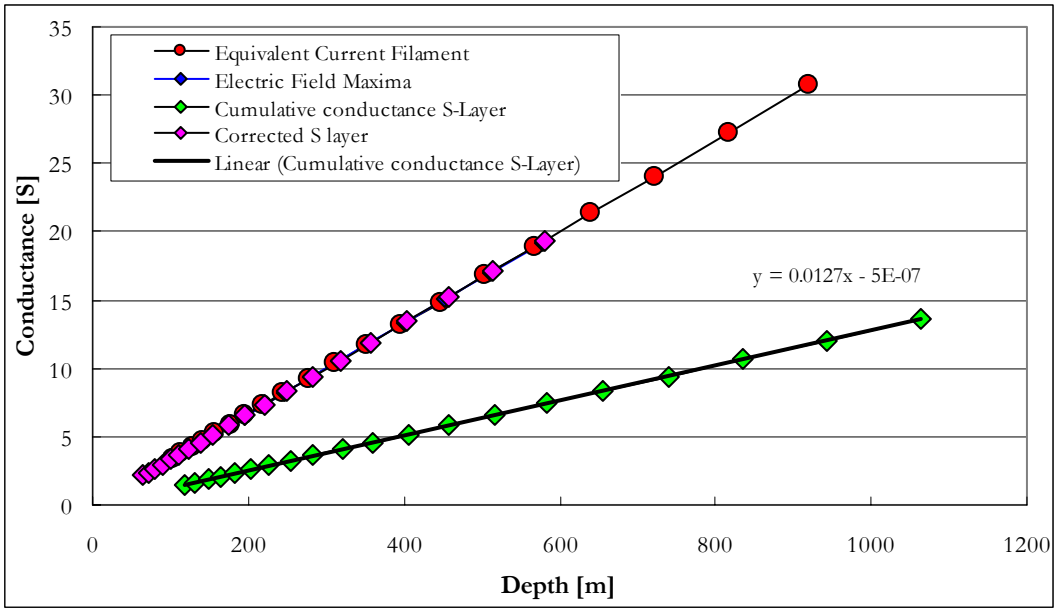

Figure 4-18: Cumulative conductance curves for late time half space and S-layer approximations.

Though the 'smoke ring' idea was developed by representing the half space response by a single current filament, expanding outward and downward, the S-layer transform likewise uses a single filament to present the S-layer behaviour. It was consequently assumed that the factor that relates the filament depth to the electrical field maxima in the half space behaviour will be the same in the S-layer approach. This factor of 0.7807 was then used to calculate a correction factor for S, given below.

$d_{FACTOR} = 0.7807$

$S_{FATOR} = 1.43$

leading to a depth correction multiplication factor of 0.5460.

1.5.2 Correction factor: Application to synthetic data

The three possibilities for a correction factor are compared on five synthetic data sets in this section. All synthetic data were generated with MARCO software assuming the following system parameters:

Tx loop:	50m X 50m
Tx current:	5 A
Rx loop:	1 m^2
Time channels in seconds:	

Ch. 1-5	Ch. 6-10	Ch. 11-15	Ch. 16-20
8.8E-05	0.000251	0.000799	0.002648
0.000107	0.000314	0.001014	0.003373
0.000131	0.000396	0.001287	0.004297
0.000162	0.000499	0.001636	0.005475
0.000201	0.000631	0.002081	0.006978

Apart from the S-layer differential transform results (one for each of the 3 correction scenario's) solutions are also shown in Figures 4-19 to 4-23 that were obtained with TEMIX software layered earth inversion (two and three layers) and Occam's smooth model inversion (10 layers). All layered earth inversions have an error of less than 1%. For the two-layer earth (Model 1) the second choice of the correction factor (blue) is the closest to the input model although correction factor 3 (black) correlates best with the smooth layered earth inversion (green).

MODEL 1: Two-layer earth

Layer	Thickness	Resistivity (conductivity)
1	100 m	50 ohm.m (0.02 S/m)
2	infinite	5 ohm.m (0.2 S/m)

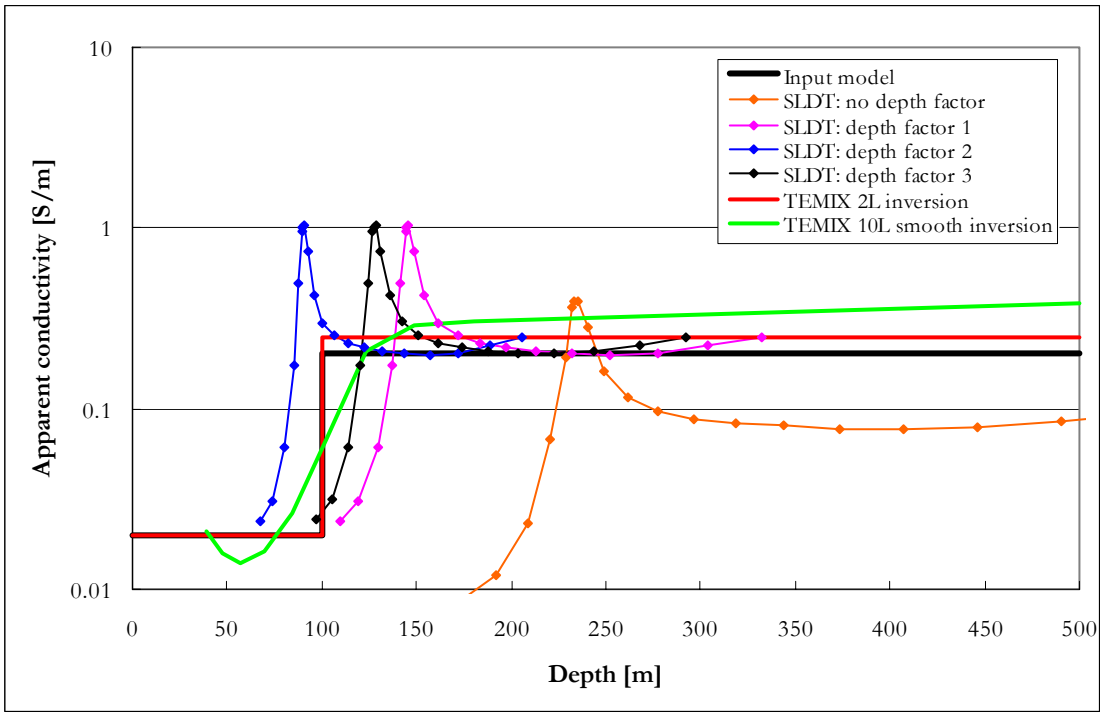

Figure 4-19: Comparison of S-layer differential transform (SLDT) solutions using different depth factors and layered earth inversions of synthetic data for a two layer earth.

MODEL 2: Three-layer earth (thin conductive layer)

Layer	Thickness	Resistivity (conductivity)
1	150 m	50 ohm.m (0.02 S/m)
2	15 m	5 ohm.m (0.2 S/m)
3	infinite	50 ohm.m (0.02 S/m)

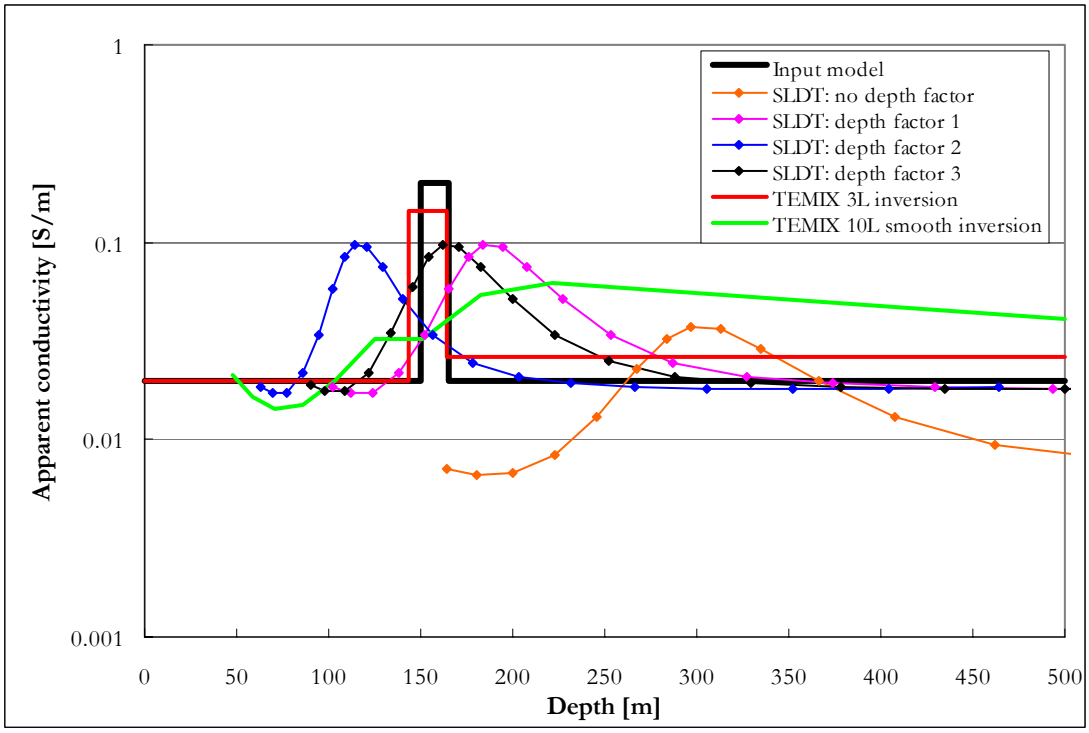

Figure 4-20: Comparison of S-layer differential transform (SLDT) solutions using different depth factors and layered earth inversions of synthetic data for a three layer earth (thin conductive layer).

In the case of a thin conductive layer correction factor 3 is the most accurate of the SLDT's (S-layer differential transform) and also outperforms the smooth layer inversion (Figure 4-20).

MODEL 3: Three-layer earth (thick conductive layer)

Layer	Thickness	Resistivity (conductivity)
1	150 m	50 ohm.m (0.02 S/m)
2	50 m	5 ohm.m (0.2 S/m)
3	inf	50 ohm.m (0.02 S/m)

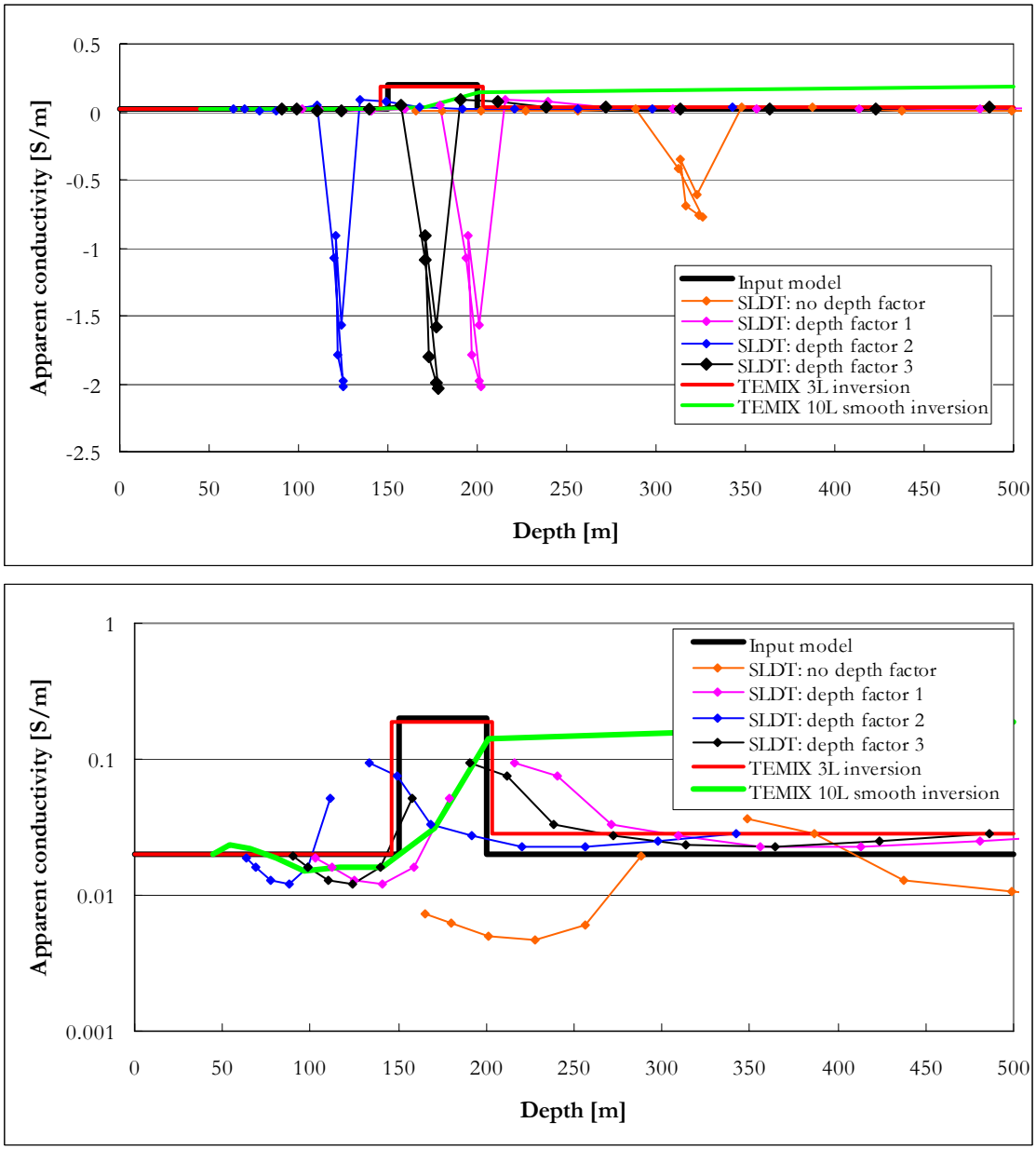

Figure 4-21: Comparison of S-layer differential transform (SLDT) solutions using different depth factors and layered earth inversions of synthetic data for a three layer earth (thick conductive layer). Top: negative values included; Bottom: no negative values.

The thick conductive layer (Model 3) shows an apparent failure of the SLDT algorithm with decreasing depths calculated at increasing times, resulting in negative apparent conductivities (Figure 4-21). This is explained by the "reflecting smoke ring" concept where high conductance features start acting as a secondary source and additional currents are generated diffusing both upward and downward from this point. However, at some stage the primary diffusive pattern outlives the secondary event and the expected increase

in cumulative conductance with time can be mapped again (Figure 4-2 bottom). This behaviour is investigated in more detail in the next section.

MODEL 4: Conductive plate in half space

Half space resistivity (conductivity)	50 ohm.m (0.02 S/m)
Plate resistivity (conductivity)	5 ohm.m (0.2 S/m)
Plate dimensions (horizontal)	200m X 200m
Plate thickness (vertical)	20m
Plate depth to top	150m

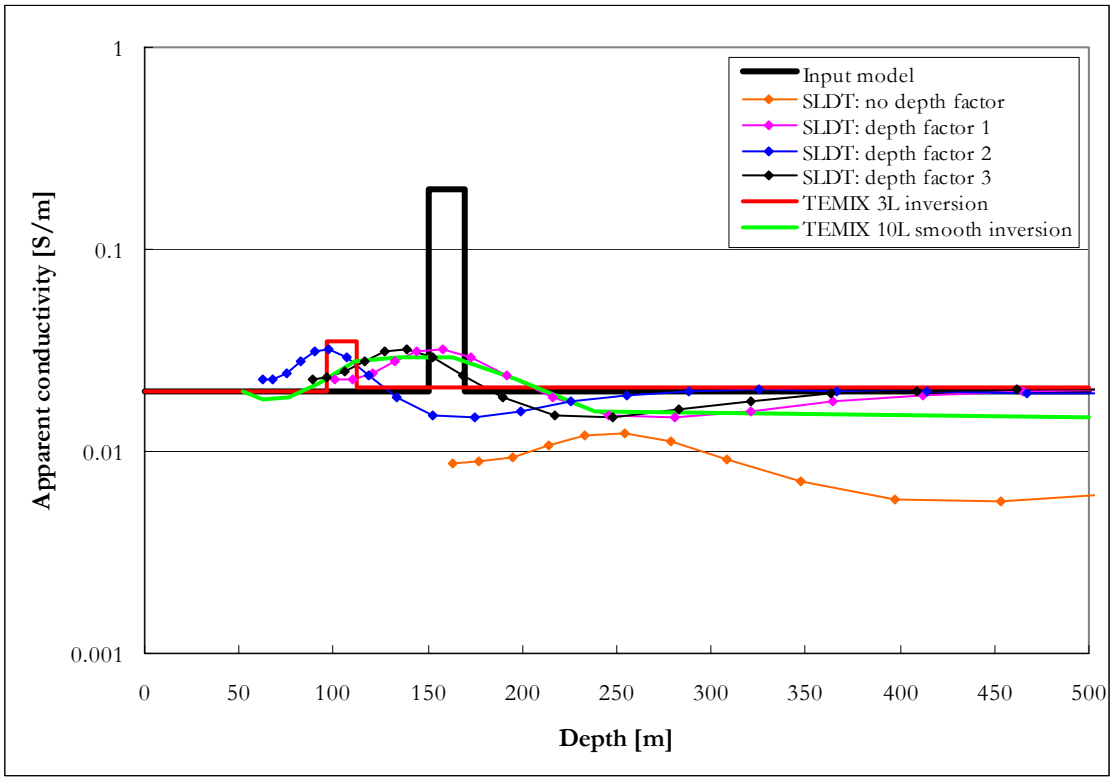

Figure 4-22: Comparison of S-layer differential transform (SLDT) solutions using different depth factors and layered earth inversions of synthetic data for a thin conductive plate in a resistive half space.

The thin conductive plate is underestimated in depth and conductivity by all the methods employed (except the SLDT no correction which still overestimates depth). The SLDT correction factor 3 correlates best with the smooth inversion and is closer to the input

model than the three layer inversion. This is to be expected as the basic assumption of an infinite layer (in horizontal extent) is violated.

MODEL 5: Conductive prism in half space

Half space resistivity (conductivity)	50 ohm.m (0.02 S/m)
Prism resistivity (conductivity)	5 ohm.m (0.2 S/m)
Prism dimensions (horizontal)	200m X 200m
Prism thickness (vertical)	200m
Prism depth to top	150m

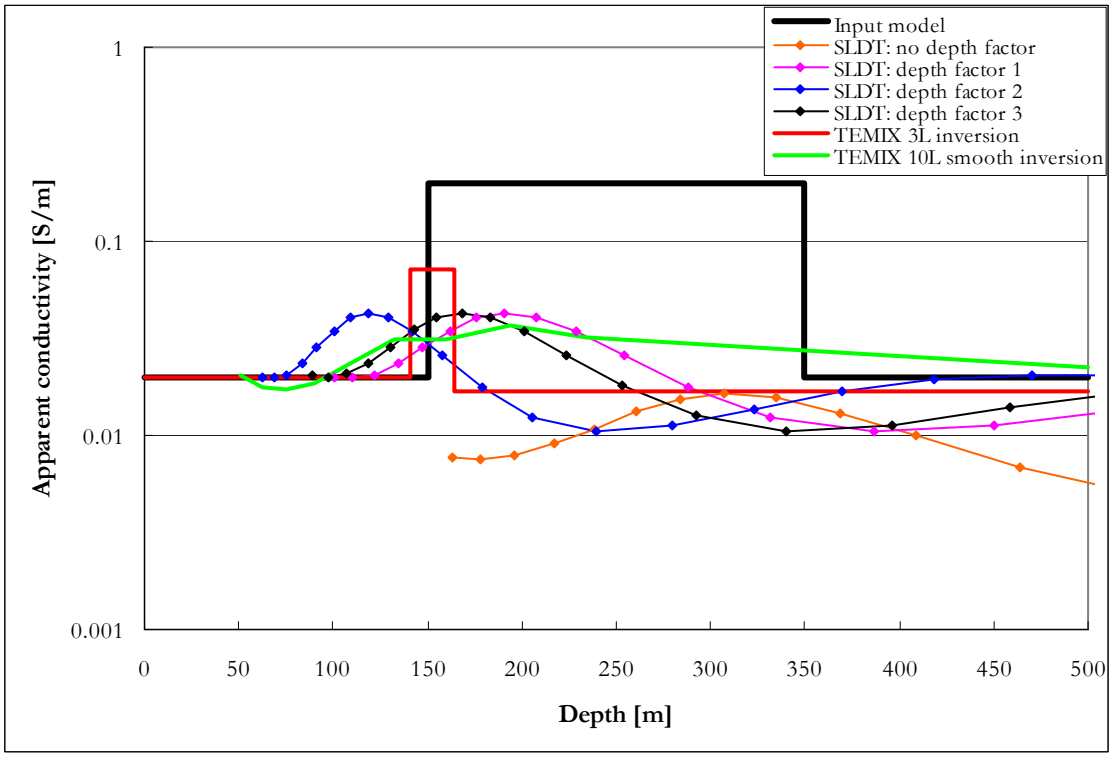

Figure 4-23: Comparison of S-layer differential transform (SLDT) solutions using different depth factors and layered earth inversions of synthetic data for a conductive prism in a resistive half space.

The depth to top of a conductive prism is well defined by the layered earth inversion as well as the correction factor 3 results.

In conclusion, the third scenario for correction correlates best with the actual model depths on synthetic data and was implemented in the software.

4.5.3 Behaviour of the S-layer transform when applied to synthetic data

In order to test (and develop a better understanding of the method) the conductivity-depth results of the improved S-layer transform a number of synthetic models are presented with their corresponding transformed results. Both the cumulative conductance [S] and conductivity [σ] curves are given for each model. The influence of noise added to the data is also investigated. The software used for the forward models is MARCO developed by AMIRA. The following system parameters were used for modelling:

Receiver area: 1 m^2

Receiver time channels: 0.08813 ms (Ch. 1) to 6.978 ms (Ch. 20) logarithmically spaced, i.e. the H range of the Geonics EM37.

Transmitter loop: 50 m X 50 m

Transmitter turn-off time: 40 μs

Transmitter current: 1 A

Configuration: Central loop sounding

4.5.3.1 Half space with conductivity of 0.02 S/m (50 ohm.m)

Figures 4-24 and 4-25 show the results from the S-layer transform for the case of a 50 ohm.m half space. The cumulative conductance curve (Figure 4-24) rises smoothly and the imaged conductivity versus depth levels out close to the expected value of 0.02 S/m when the late time approximation as validated.

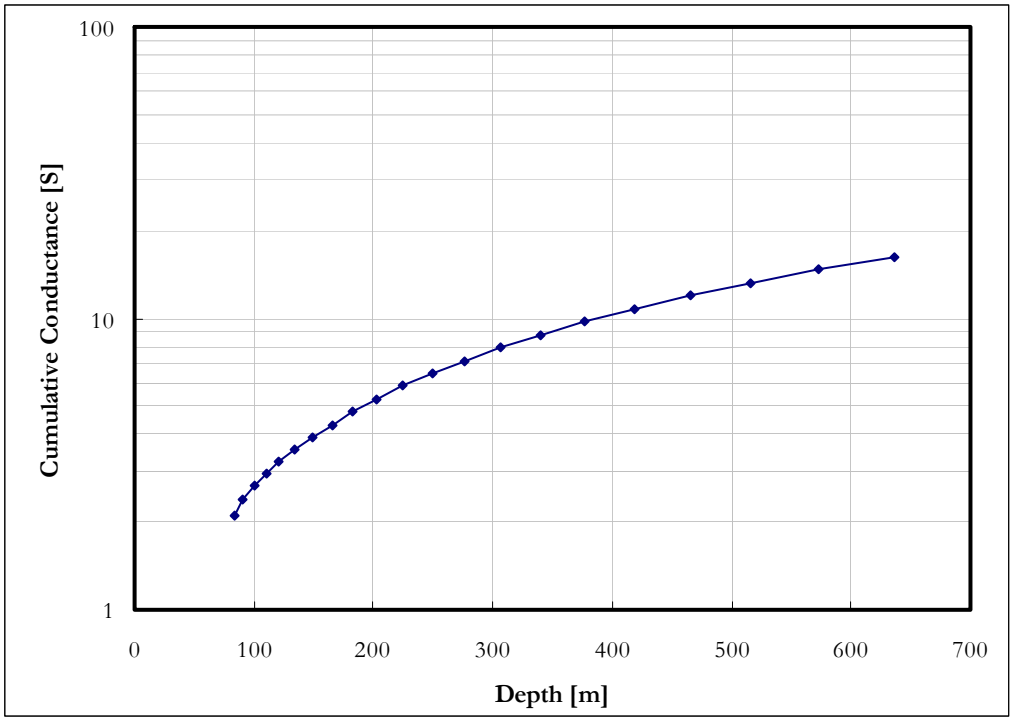

Figure 4-24 Cumulative conductance versus depth, 0.02 S/m (50 Ω.m) half space

.

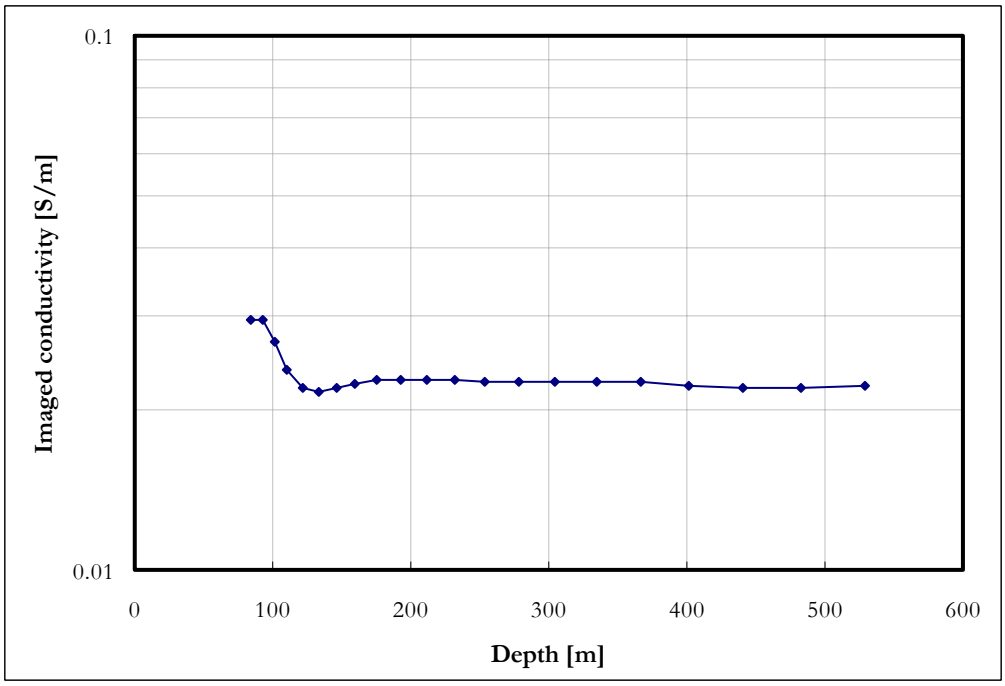

Figure 4-25 Conductivity versus depth, 0.02 S/m (50 Ω.m) half space.

4.5.3.2 Two layer earth with decreasing conductivity ($\sigma_1 > \sigma_2$)

Two models with different contrasts are presented in Figures 4-26 and 4-27. The first layer has a conductivity of 0.02 S/m and is 200 m thick in each instance while the second layer conductivity is changed from 0.002 S/m to 0.0002 S/m. The cumulative conductances rise smoothly with increasing depth and the conductivities approach the true values of the layers, although not a hundred percent accurate. However, the distinct nature of two layers with decreasing conductivity is clearly recognizable. The boundary (at 200 m) between the layers is not that easy to distinguish because of the gradual change in values on both curves, however it is easy to see that the different model curves start to diverge at this point when the second layer is starting to take effect.

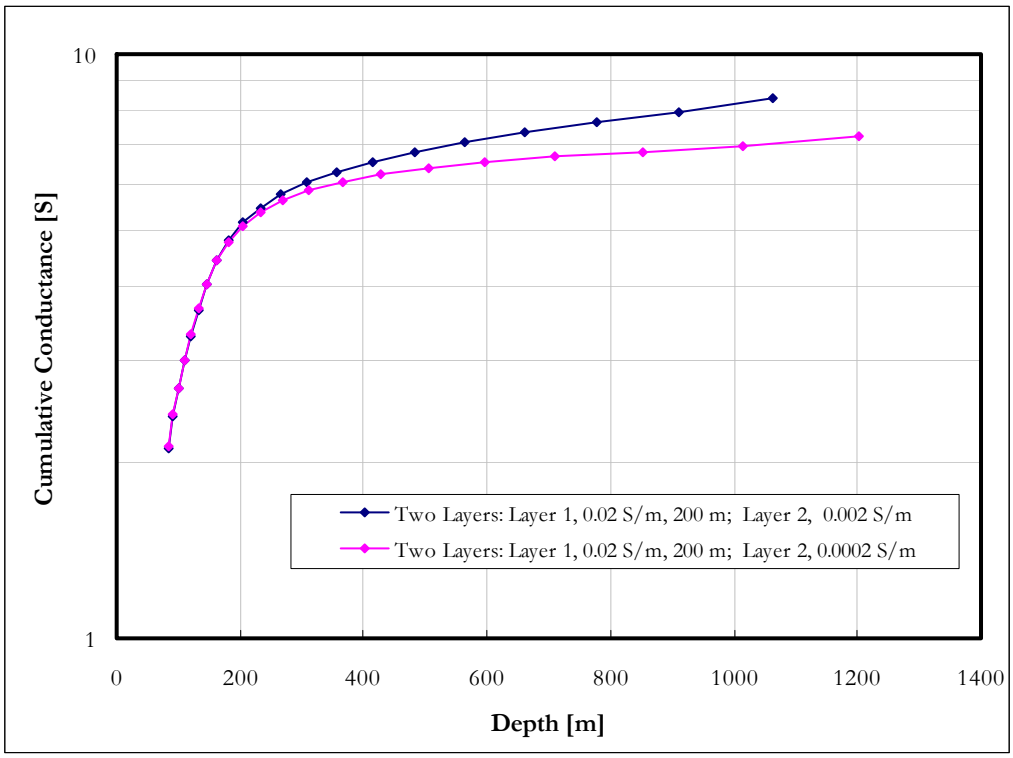

Figure 4-26: Cumulative conductance versus depth for two layers of decreasing conductivity; first layer thickness 200m.

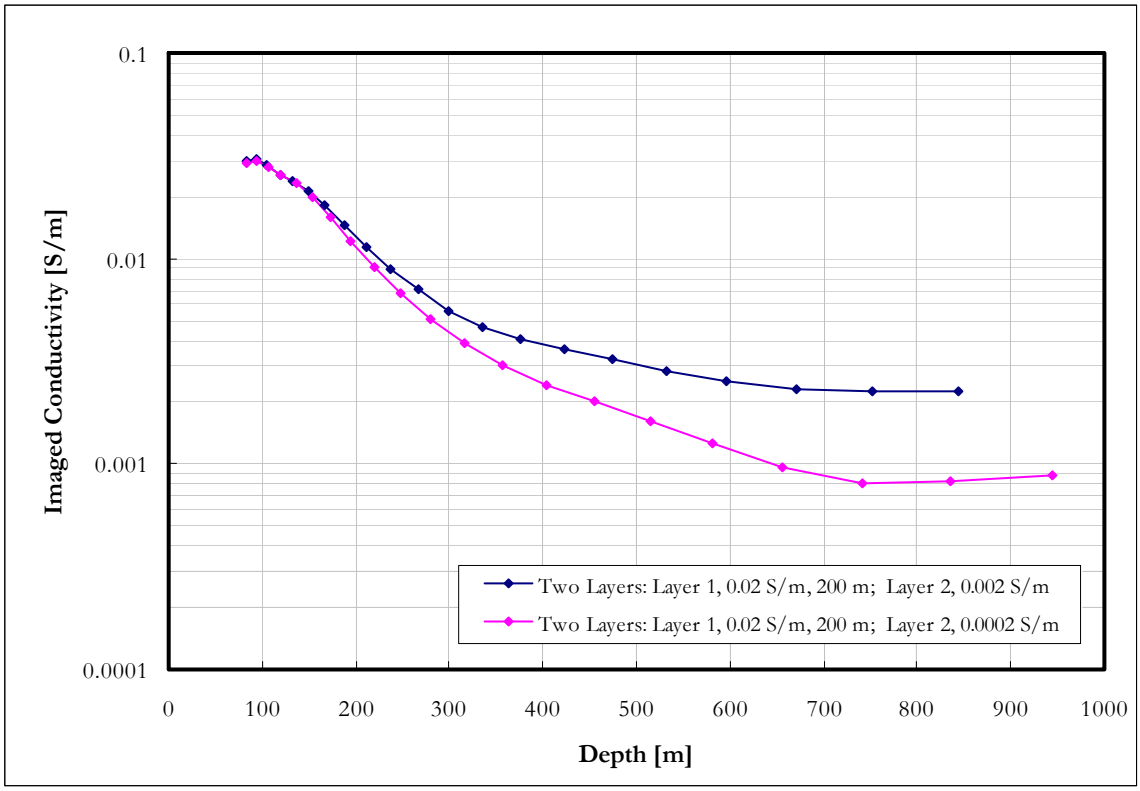

Figure 4-27: Imaged conductivity versus depth for two layers of decreasing conductivity; first layer thickness 200m.

4.5.3.3 Two layer earth with increasing conductivity ($\sigma_1 < \sigma_2$)

Once again two models with different contrasts are presented (Figures 4-28 to 4-30). The first layer still has the same parameters of 0.02 S/m and 200 m. The second layer conductivity is now changed from 0.2 S/m to 2 S/m. In this case the effect of the second layer is already visible before the 200 m mark. This method approximates a set of current distributions with one single filament and it can be expected that the transition would not be sharp and also that more conductive layers will influence the single filament even if its position is not indicated as inside the conductive layer itself. For the low contrast case (second layer conductivity = 0.2 S/m) the behaviour of the cumulative conductance and conductivity curves follow the expected pattern of increasing smoothly with depth and approximating the second layer conductivity ever closer after an initial overshoot. However, the high contrast case produces a very interesting phenomenon. Instead of yielding cumulative conductance and conductivity values at increasing depths with increasing time, a turning point is reached at some stage (300m depth for this case) after which time the equivalent S-layer filament is mapped with drastically increasing conductivity but decreasing depths. This type of unexpected behaviour contradicts the

assumption made in this method that cumulative conductance will always increase with increasing depth and the standard algorithm only calculates the derivatives for points until the depths start decreasing. For this specific case the slope of the curve was calculated in an alternate manner to investigate the conductivity behaviour.

The negative "conductivity" values and dramatic overshoot of the last positive slopes (Figure 4-28) show no relation to the true conductivities and does not add much value to the process. At first sight this might seem as a failure of the S-layer method, but the very distinctive pattern can easily be recognised on the cumulative conductance curves and will indicate the existence of a very conductive layer. The exact position of the boundary is not well defined, but can best be described from the conductivity curves as the first rise in conductivity. This transition is easier distinguished on graphs with linear scale (Figure 4-30).

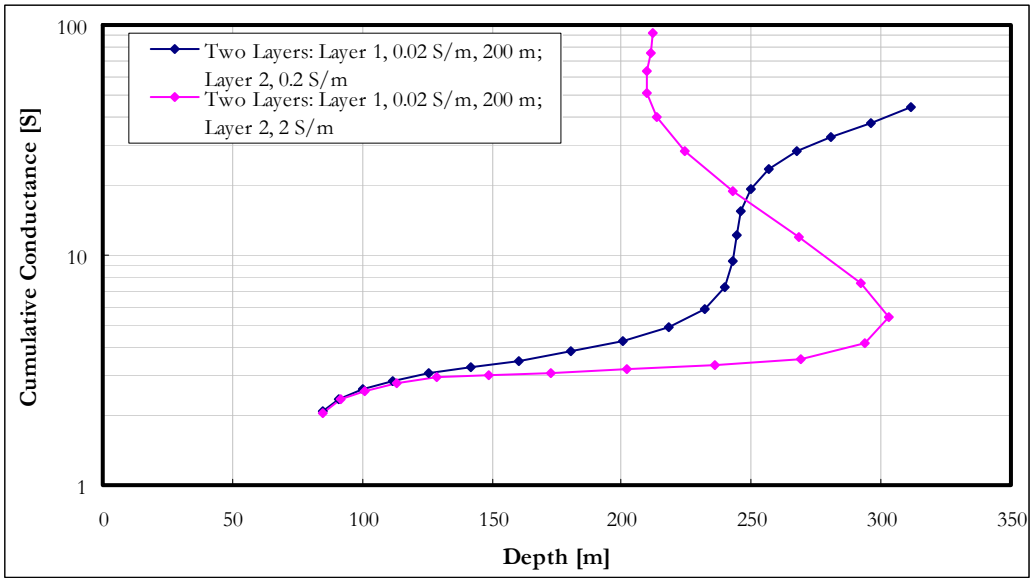

Figure 4-28: Cumulative conductance versus depth for two layers of increasing conductivity; first layer thickness 200m.

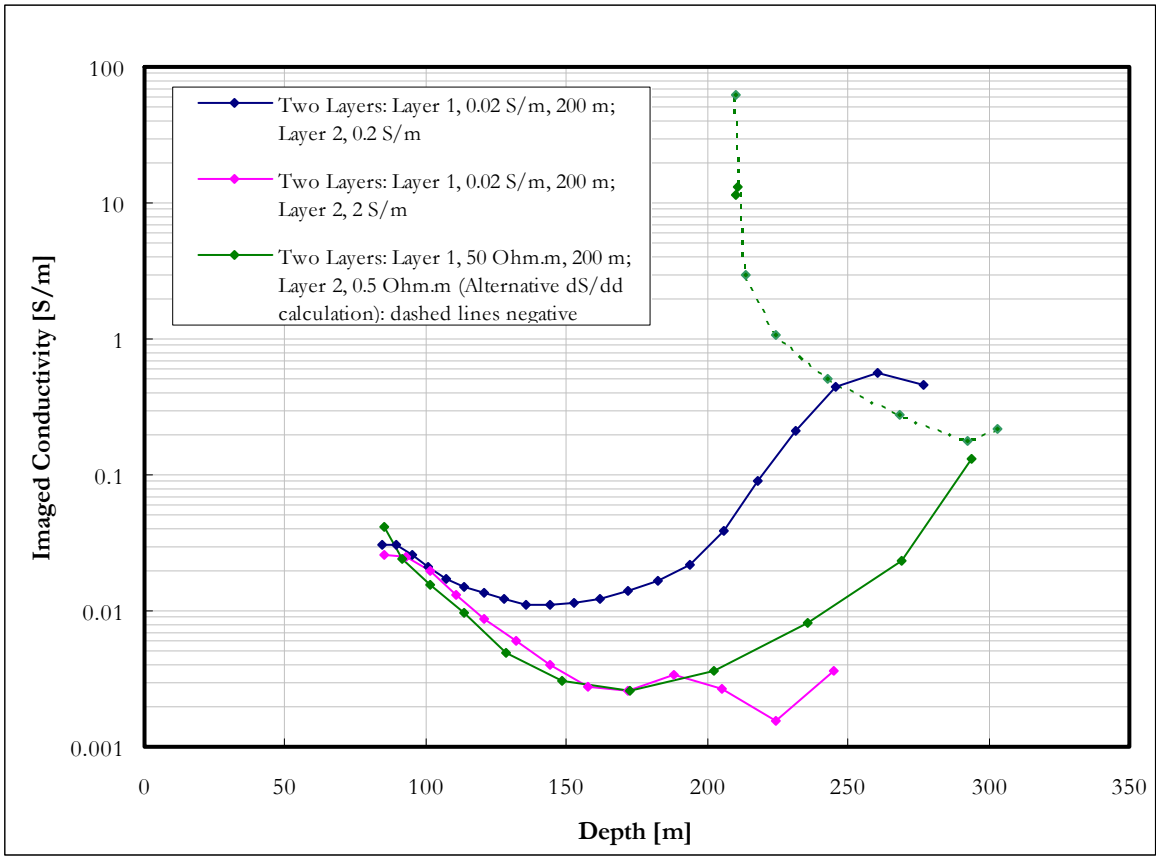

Figure 4-29: Imaged conductivity versus depth for two layers of increasing conductivity; first layer thickness 200m.

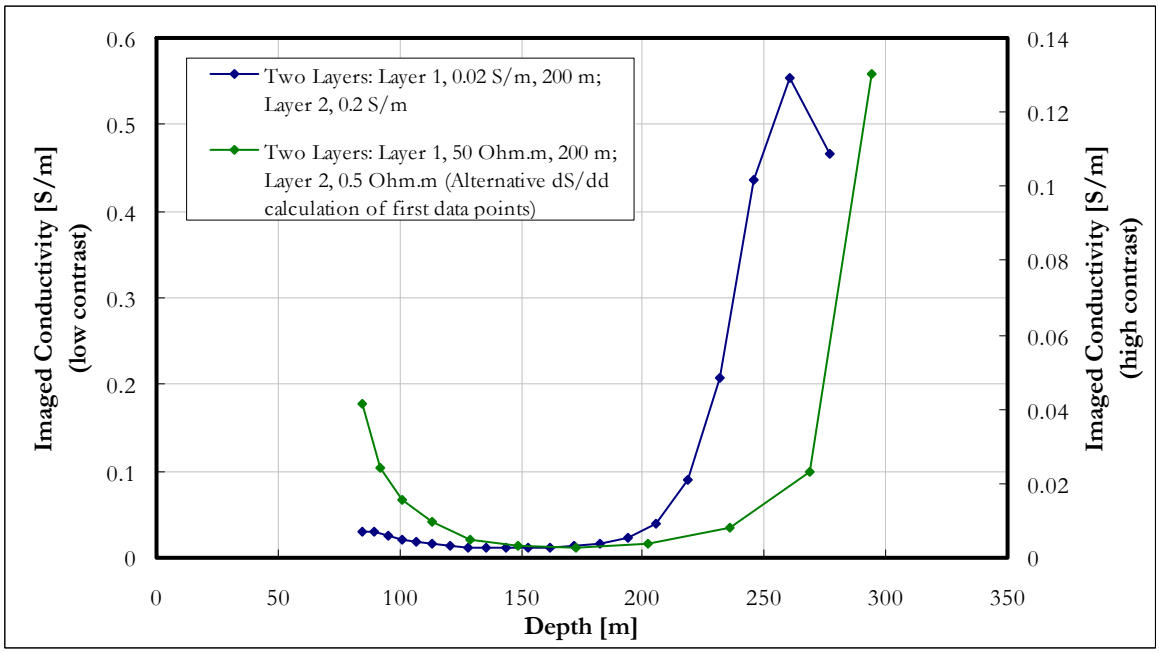

Figure 4-30: Imaged conductivity versus depth for two layers of increasing conductivity; first layer thickness 200m – linear scale.

The physical implication of this phenomenon can possibly be explained by a reflection of the equivalent S-layer filament at the very conductive high contrast boundary. As currents are induced into the second layer it can act as a secondary source and induce currents in the first layer again, diffusing away from this source, i.e. upwards. These currents are closer to the receiver than the ones in the second layer itself, diffuse quickly in the more resistive layer (implying large $\partial B_z/\partial t$) and will therefore dominate the measured signal for a certain time. At this point the assumptions made in developing the S-layer transform are clearly not valid anymore and the calculated conductivities and depths have to be filtered out from any future presentation of data.

4.5.3.4 Conductive layer in half space

Firstly, the influence of contrast in conductivity is investigated and secondly the thickness of the layer is changed. Four different contrasts and thicknesses were modelled and analysed for a conductive layer 150m deep in a 0.02 S/m half space. The results for conductivity contrasts are shown in Figures 4.31-4.33.

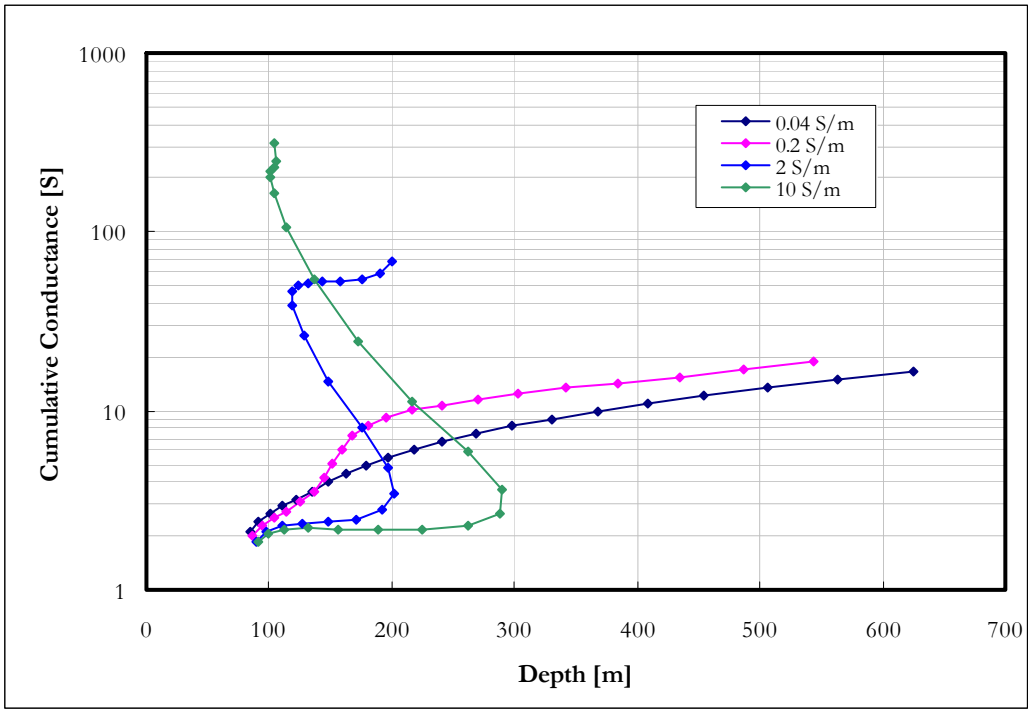

Figure 4-31: Cumulative conductance for a 15m thick layer of varying conductivity at 150m depth in a 0.02 S/m half space.

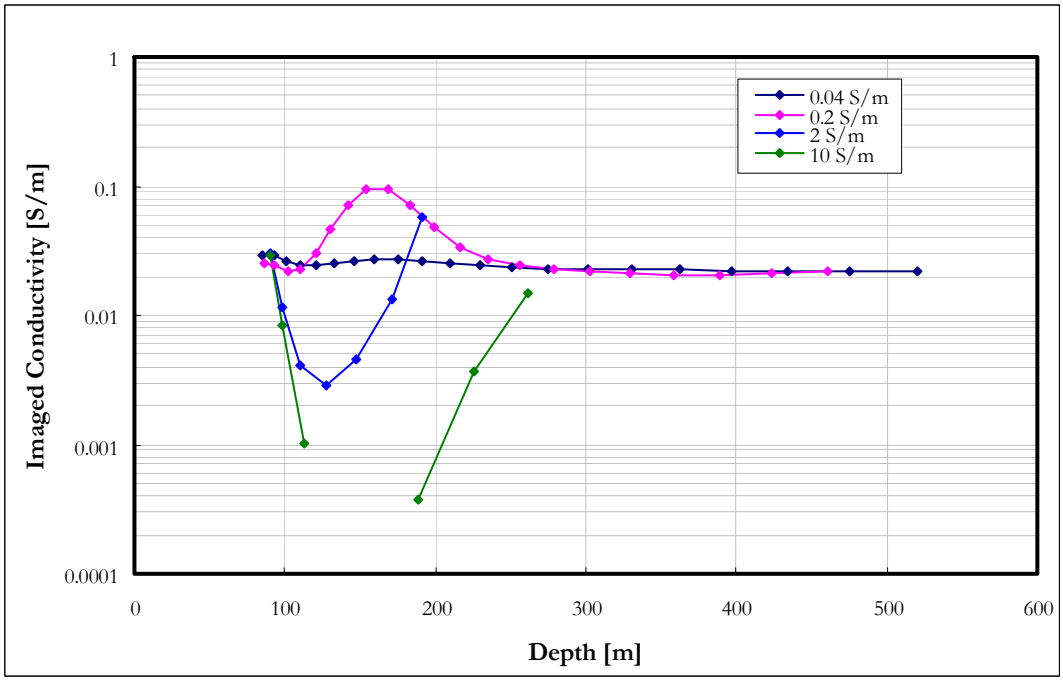

Figure 4-32: Imaged conductivity versus depth for a 15m thick layer of varying conductivity at 150m depth in a 0.02 S/m half space.

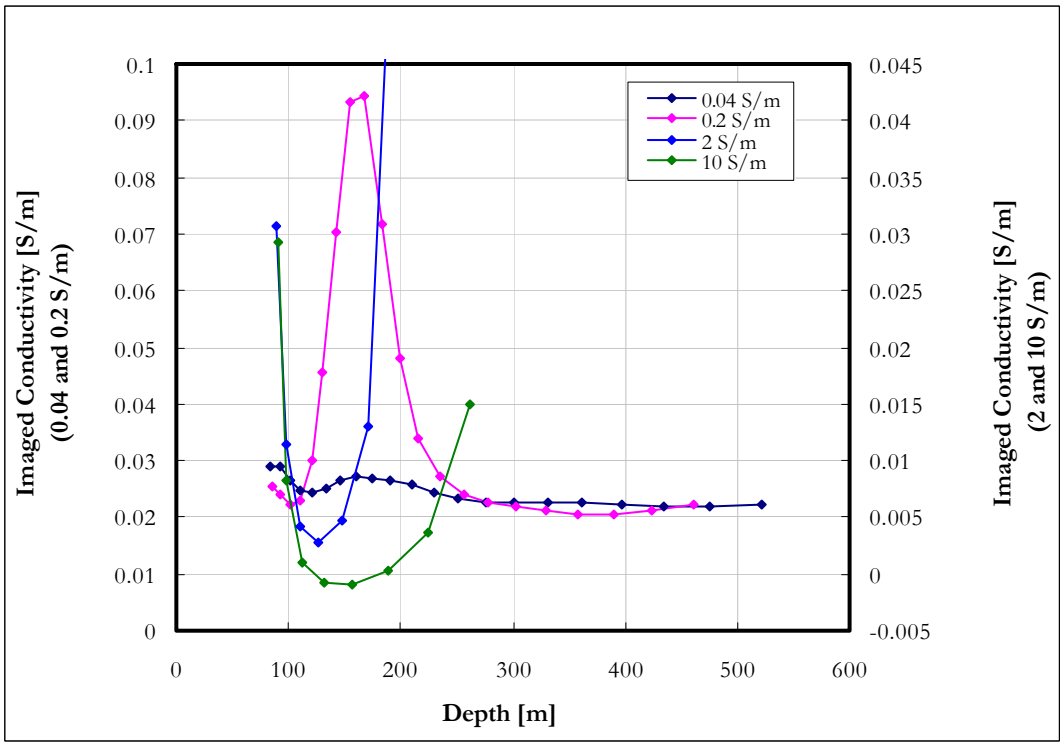

Figure 4-33: Imaged conductivity versus depth for a 15m thick layer of varying conductivity at 150m depth in a 0.02 S/m half space; linear scale.

The S-layer transform is clearly very sensitive to conductive layers and even with a conductivity contrast of 1:2 (0.02:0.04) is still able to resolve the layer. Depths for the low

contrast cases are predicted accurately although the high contrasts are not accurately mapped. The two most conductive layers generate underestimated values for conductivity (Figures 4-32 and 4-33) and might be interpreted to be more resistive than the half space if the conductivity sections are consulted without reference to the distinctive cumulative conductance signature.

Next, the effect of layer thickness for the low conductivity contrast scenario is investigated. Thicknesses of 2 m, 5 m, 10 m, 15 m, 20 m, 50 m and 100m are used (Figures 4-34 to 4-36). It is important to notice that the anomaly widths remain the same until a critical thickness is reached and only an increase in amplitude with increasing layer thickness is seen. Although the top of the layers are well defined, the true thickness and conductivity are not uniquely determined. Very important, though, is that the high contrast behaviour of decreasing depths with time is not seen here, no matter how large the conductivity-thickness product becomes.

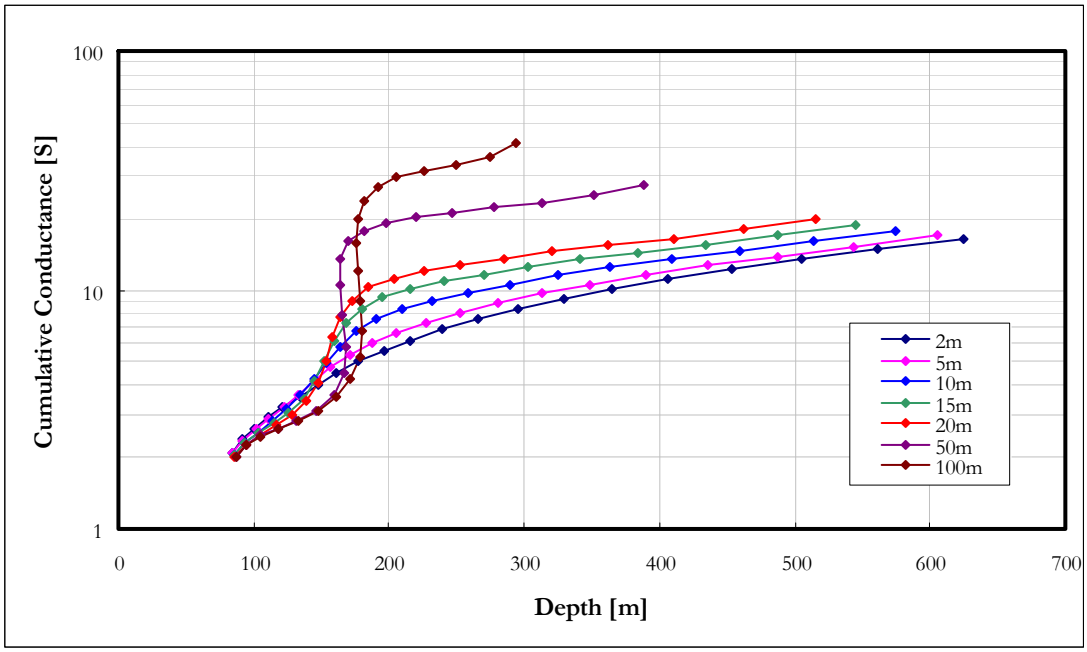

Figure 4-34: Cumulative conductance for a 0.2 S/m layer of varying thickness at 150m depth in a 0.02 S/m half space.

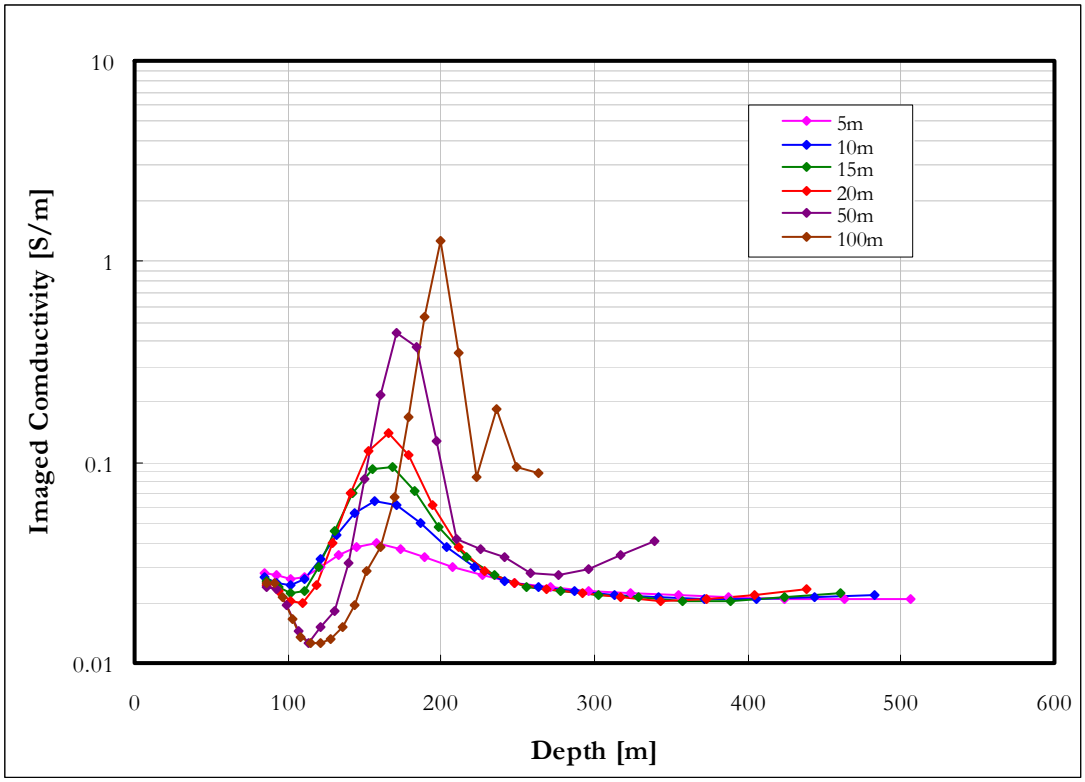

Figure 4-35: Imaged conductivity for a 0.2 S/m layer of varying thickness at 150m depth in a 0.02 S/m half space.

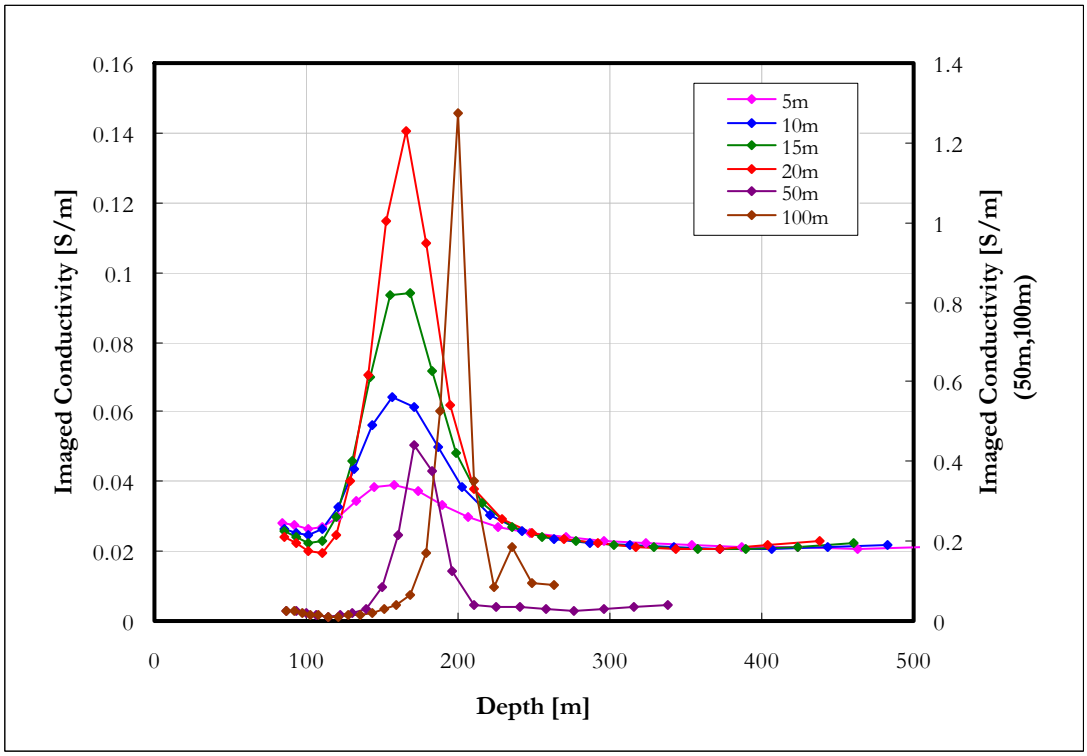

Figure 4-36: Imaged conductivity for a 0.2 S/m layer of varying thickness at 150m depth in a 0.02 S/m half space; linear scale.

The effect of layer thickness for the high contrast scenario is presented in figures 4-37 – 4-39.

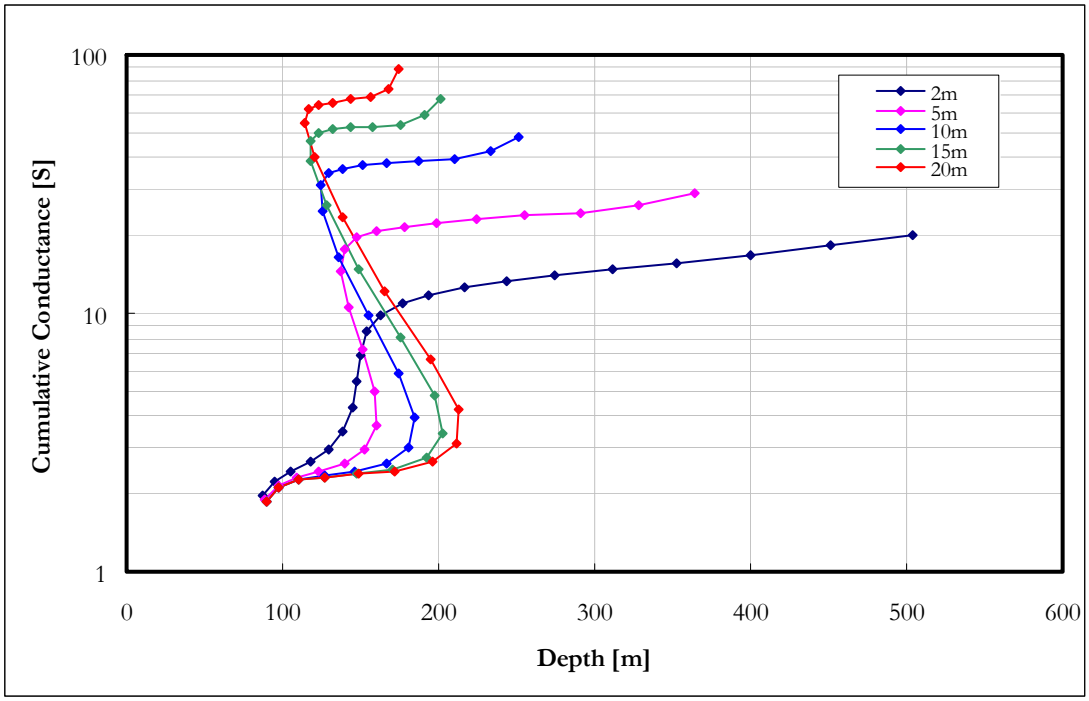

Figure 4-37: Cumulative conductance for a 2 S/m layer of varying thickness at 150m depth in a 0.02 S/m half space.

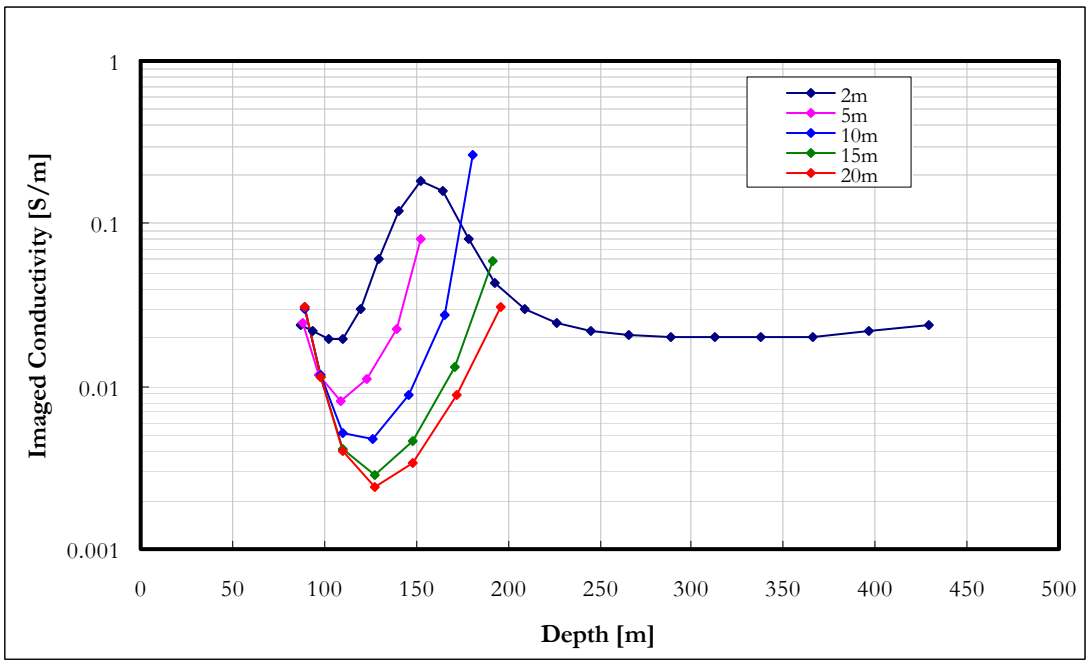

Figure 4-38: Imaged conductivity for a 2 S/m layer of varying thickness at 150m depth in a 0.02 S/m half space.

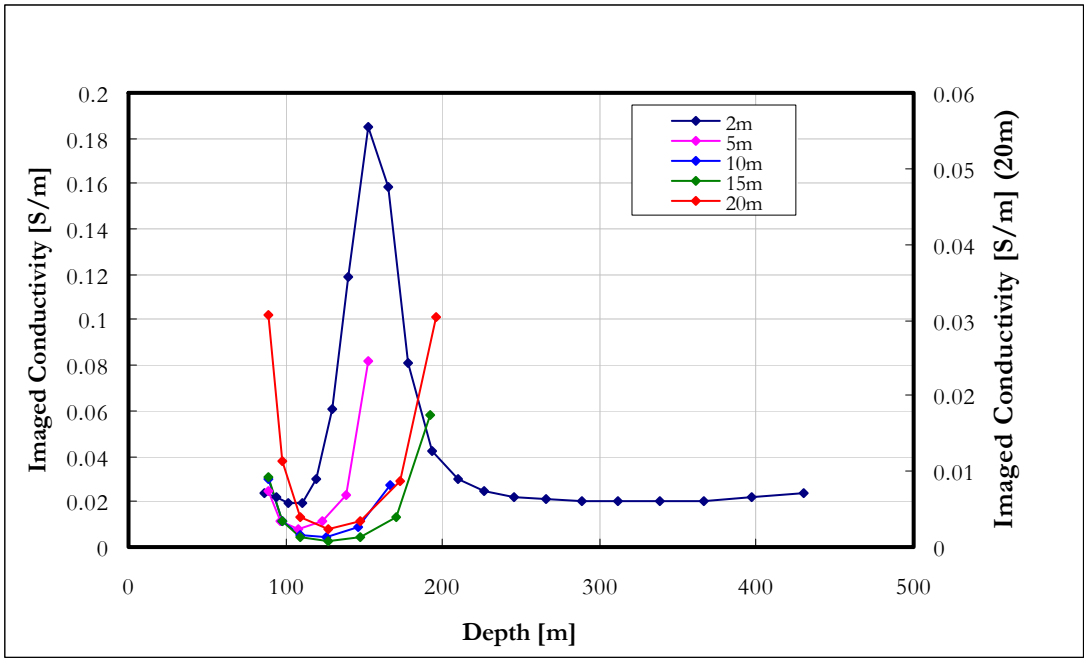

Figure 4-39: Imaged conductivity for a 2 S/m layer of varying thickness at 150m depth in a 0.02 S/m half space – linear scale.

Except for the 2 m layer, all the curves exhibit the high contrast behaviour. The thicker the layer becomes, the closer the curves resemble the two layer case with very little or no influence from the earth below the conductive layer contributing to the signal.

The effect of varying depth of a conductive layer is shown in Figures 4-40 – 4-42. The width of the anomaly increases with depth to top of the conductive layer while the amplitude decreases. One case of special interest is the layer at 50m depth. For the host rock conductivity of 0.02 S/m and the chosen system parameters, the shallowest depth of investigation is in the order of 100 m. However, if there is a conductive layer shallower than this, the depth of investigation is adapted to that. The curve is distorted compared to those of the deeper layers in the sense that there is no rise from the host rock response into the conductive layer. It actually takes a shape more indicative of a two layered earth.

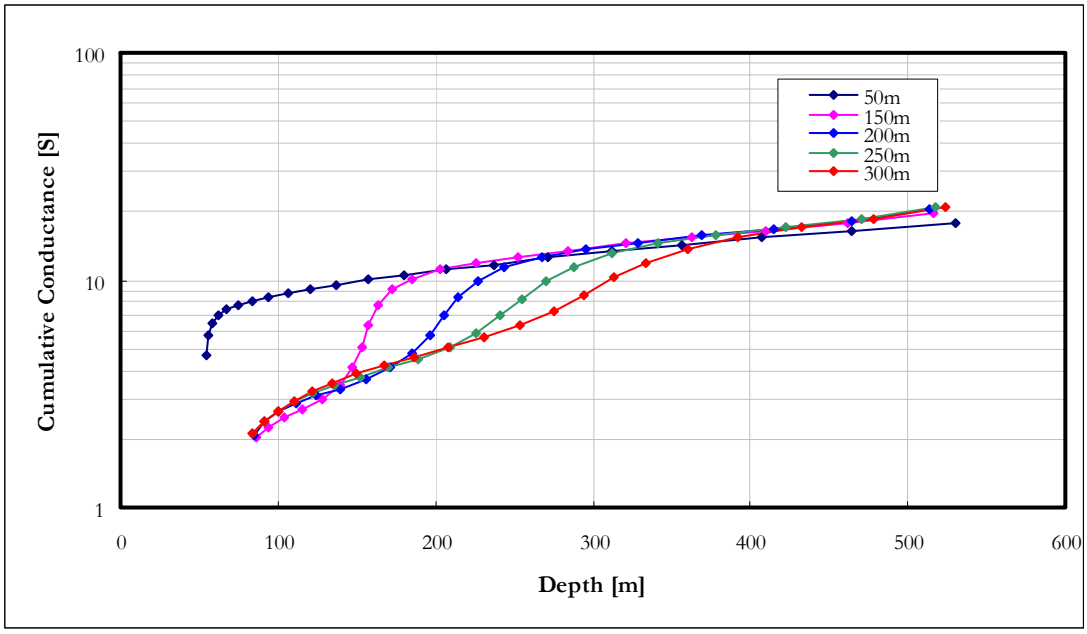

Figure 4-40: Cumulative conductance for a 0.2 S/m layer of 20 m thickness at various depths in a 0.02 S/m half space.

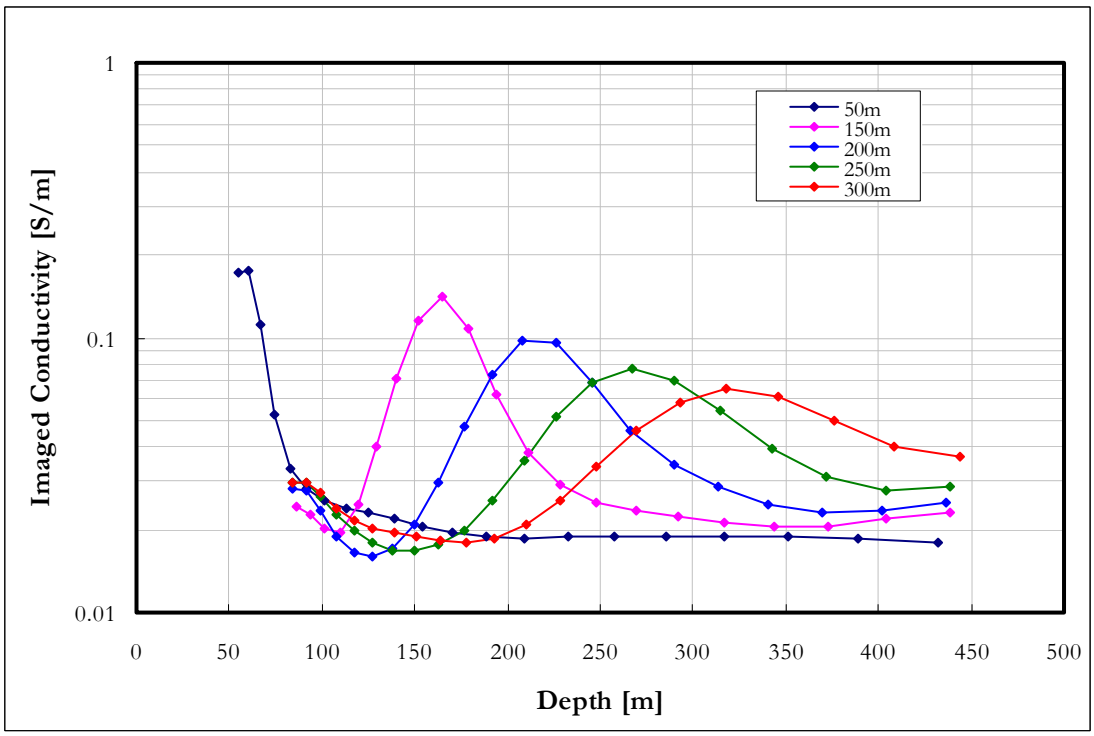

Figure 4-41: Imaged conductivity for a 0.2 S/m layer of 20 m thickness at various depths in a 0.02 S/m half space.

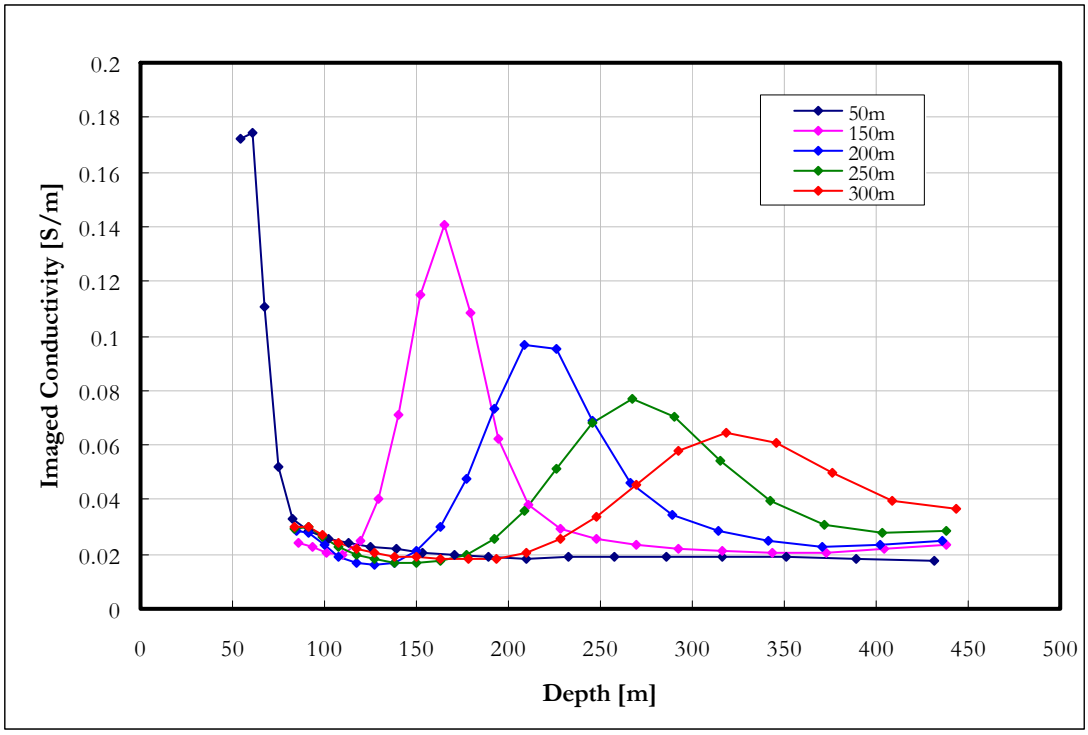

Figure 4-42: Imaged conductivity for a 0.2 S/m layer of 20 m thickness at various depths in a 0.02 S/m half space – linear scale.

The last factor contributing to the thin layer anomaly investigated is the host rock conductivity. A 20 m thick plate having conductivity of 0.2 S/m is modelled at 150 m depth in different host rock environments (Figures 4-43 – 4-45). The behaviour of all the curves is as expected from the previous experiments. High host rock conductivities (resulting in low contrasts) give the bell shaped conductivity function of depth while the high contrast (low host rock conductivity) results in the depth reversal of cumulative conductance plots, although the extent of this reversal is less than for the same contrast in a more conductive host rock. The depth of investigation decrease with increase in host rock conductivity, except for when a conductive layer is situated shallower than the "first channel depth" at which point the depth of investigation is governed by the depth of the conductor (0.01 S/m and less in this case). The imaged conductivities in these examples were calculated after the high contrast effects dissipated, yielding the correct host rock response.

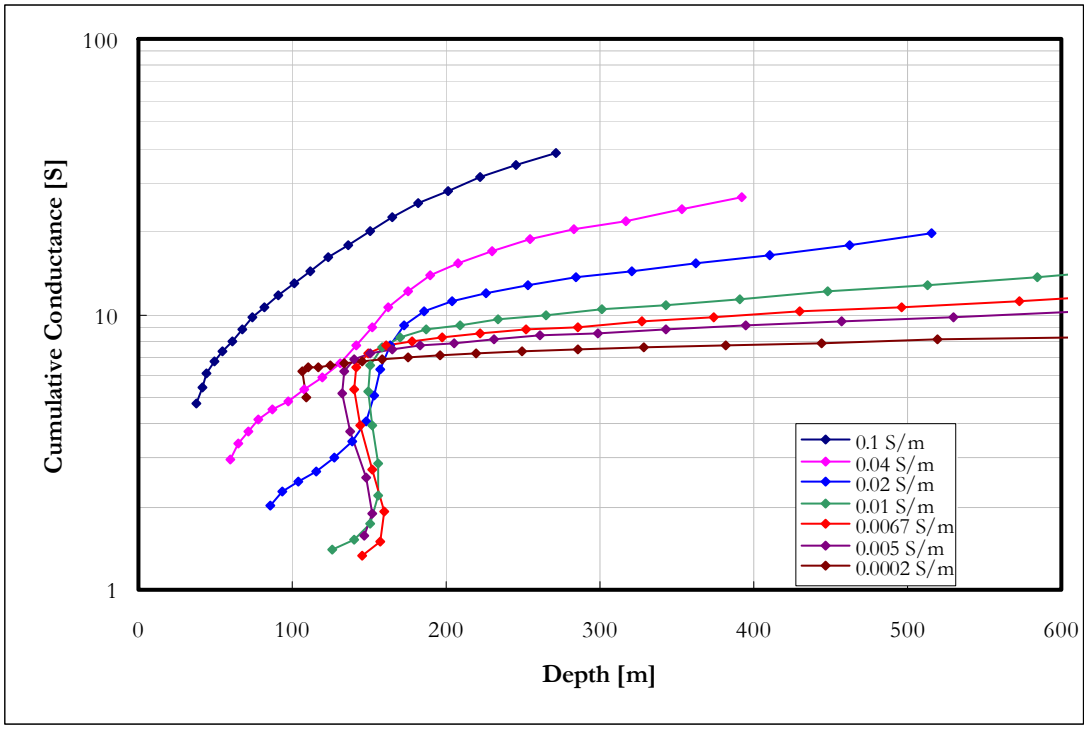

Figure 4-43: Cumulative conductance for a 0.2 S/m layer of 20 m thickness at 150 m depth in various host rock conductivities.

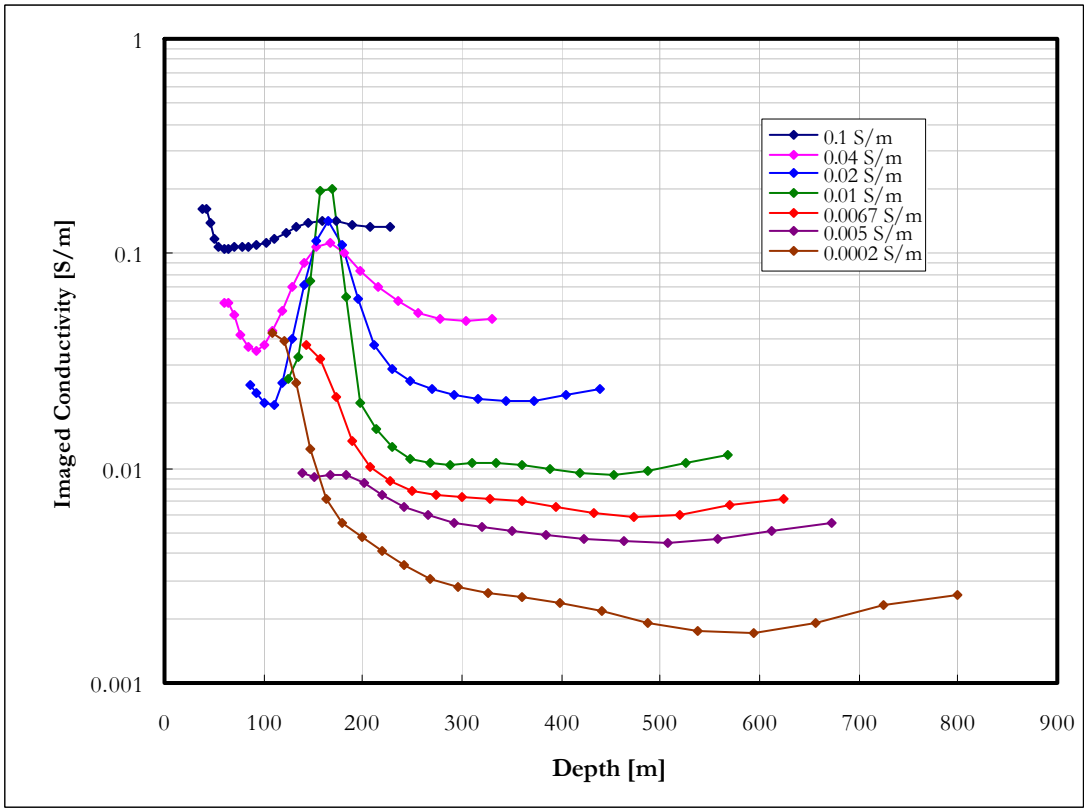

Figure 4-44: Imaged conductivity for a 0.2 S/m layer of 20 m thickness at 150 m depth in various host rock conductivities.

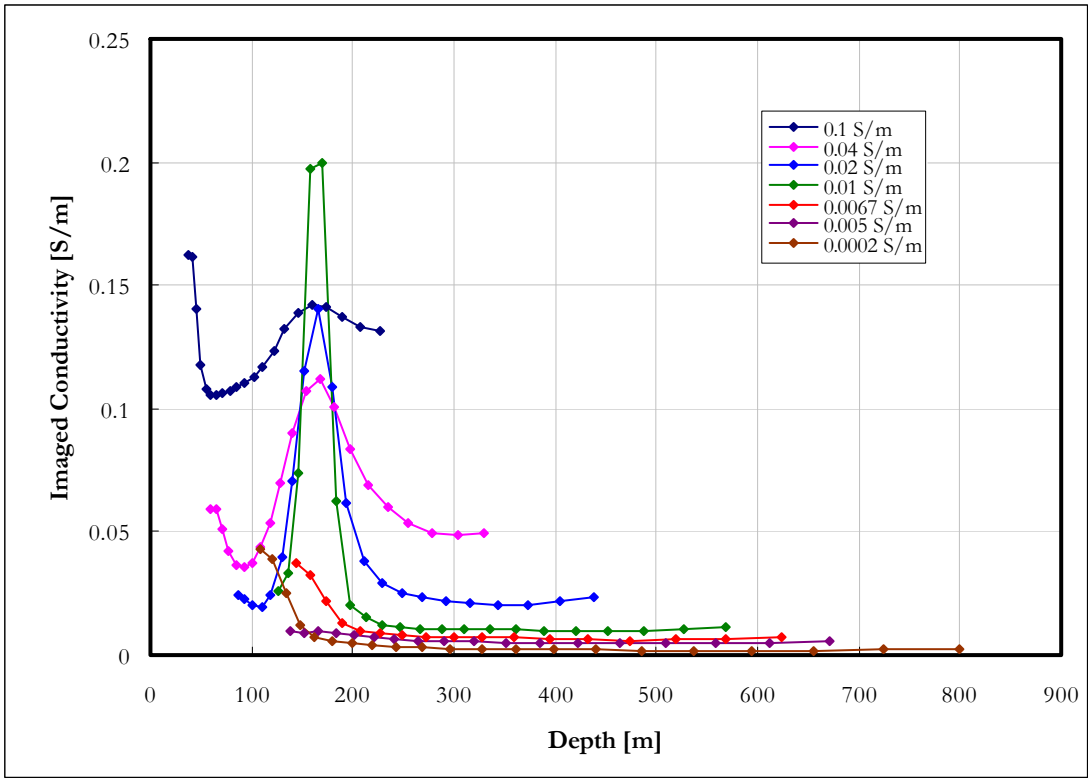

Figure 4-45: Imaged conductivity for a 0.2 S/m layer of 20 m thickness at 150 m depth in various host rock conductivities - linear scale.

Examining the S-layer transform performance in delineating a layered earth provides important insights into the characteristic behaviour and effectiveness of the technique. However, in order to map the subsurface accurately the study has to be extended to bodies with finite dimensions. Conductive, horizontal plates and prisms are modelled and their S-layer transform responses analysed in the following two sections.

4.5.3.5 Conductive, horizontal plates in a half space

The S-layer transform response of conductive horizontal plates with a thickness of 20 m and varying horizontal dimensions are compared to that of the infinite layer. This is done for both the low and high contrast scenarios. The side lengths of the square plates were chosen as 100 m, 200 m, 300 m and 400 m respectively and conductivities of 0.2 S/m and 2 S/m were used in a 0.02 S/m host rock. The low contrast results are shown in Figures 4-46 to 4-48 and the high contrast results in Figures 4-49 to 4-51.

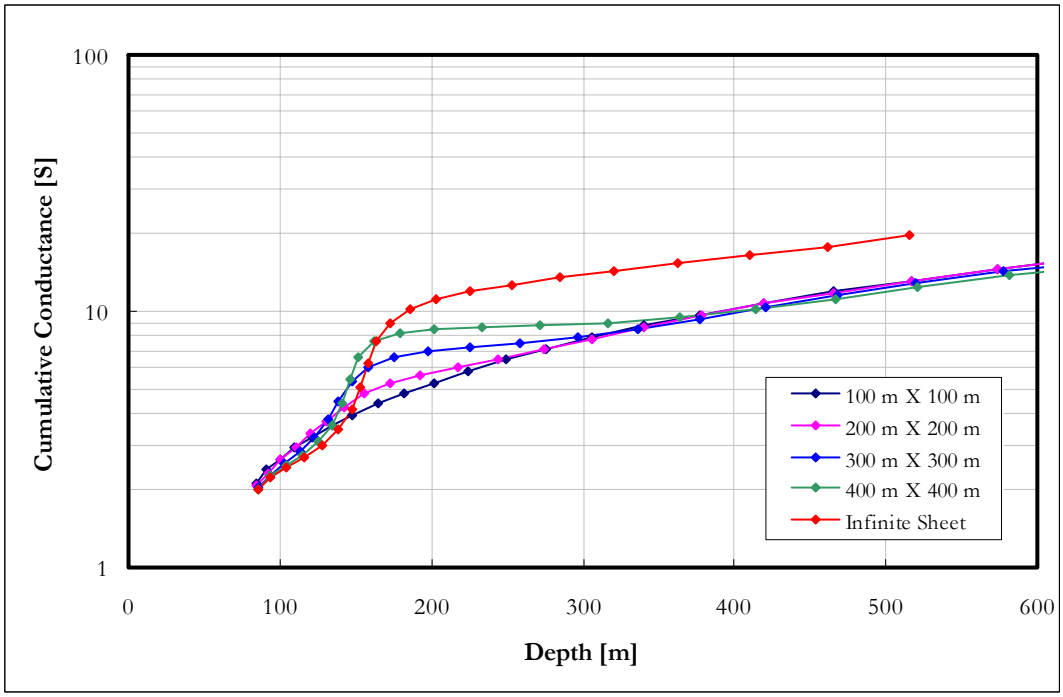

Figure 4-46: Cumulative conductance for a 0.2 S/m plate of 20 m thickness at 150 m depth in 0.02 S/m host rock. The horizontal dimensions vary from 100 m to infinite.

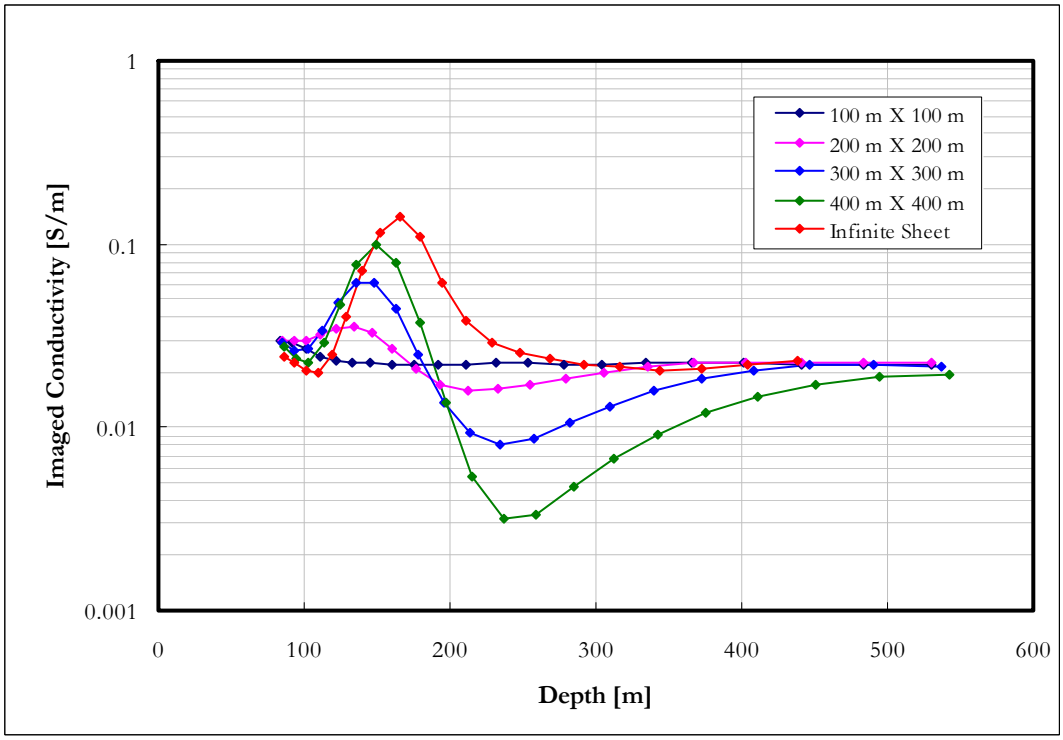

Figure 4-47: Imaged conductivity for a 0.2 S/m plate of 20 m thickness at 150 m depth in 0.02 S/m host rock. The horizontal dimensions vary from 100 m to infinite.

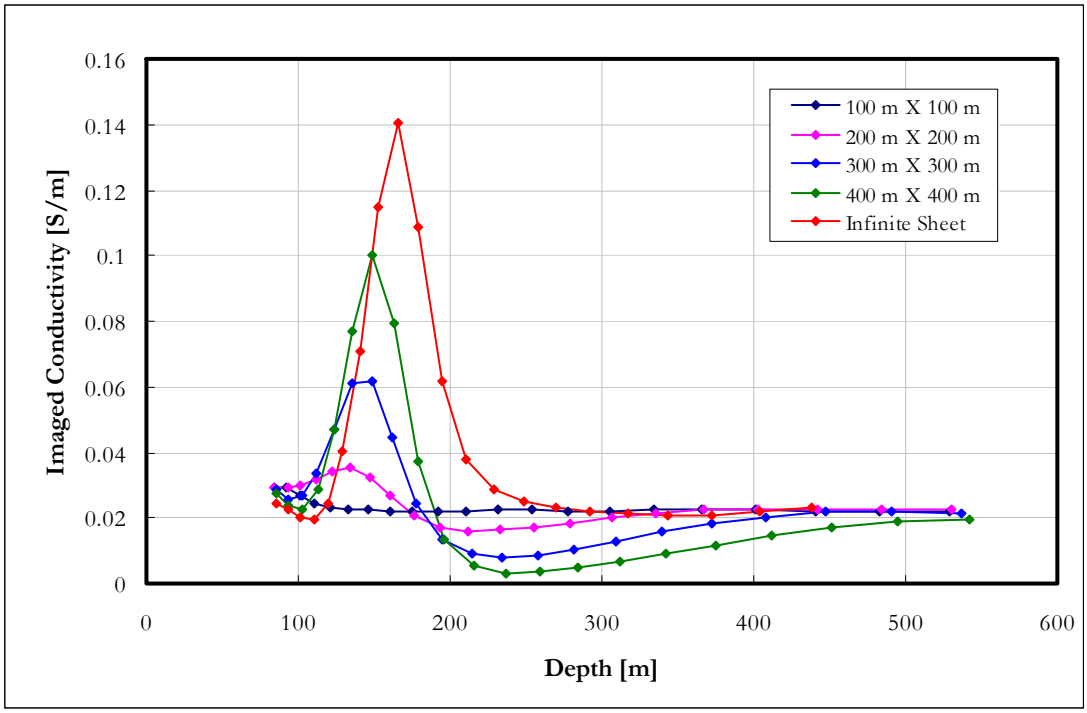

Figure 4-48: Imaged conductivity for a 0.2 S/m plate of 20 m thickness at 150 m depth in 0.02 S/m host rock. The horizontal dimensions vary from 100 m to infinite; linear scale.

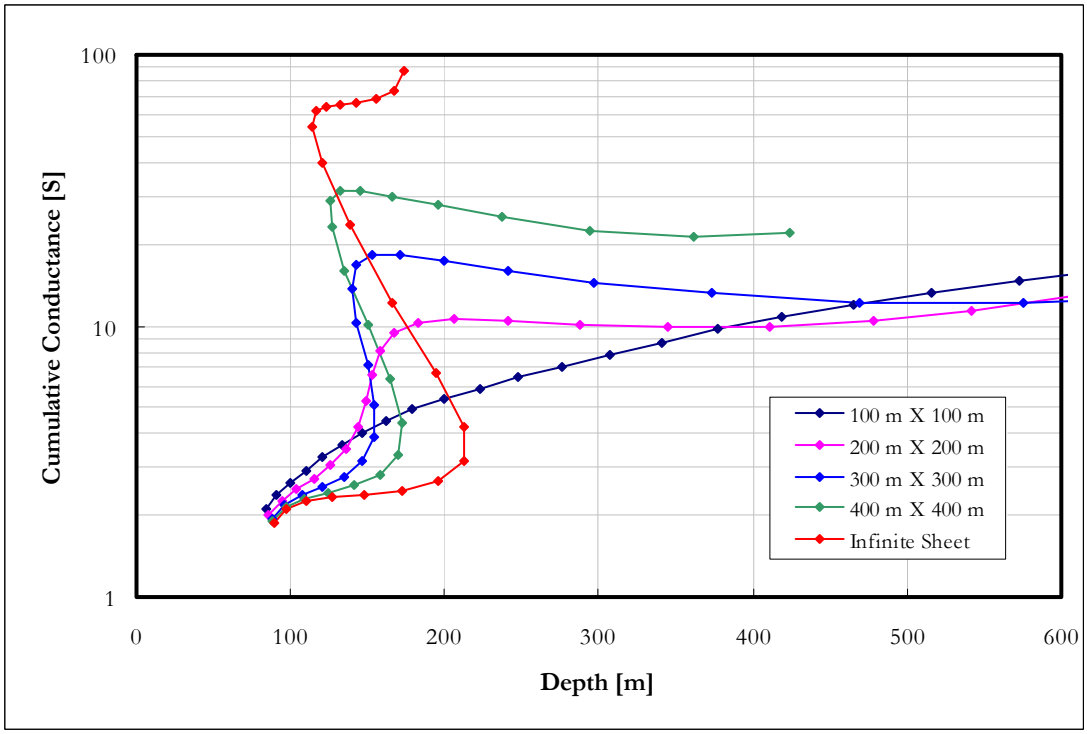

Figure 4-49: Cumulative conductance for a 2 S/m plate of 20 m thickness at 150 m depth in 0.02 S/m host rock. The horizontal dimensions vary from 100 m to infinite.

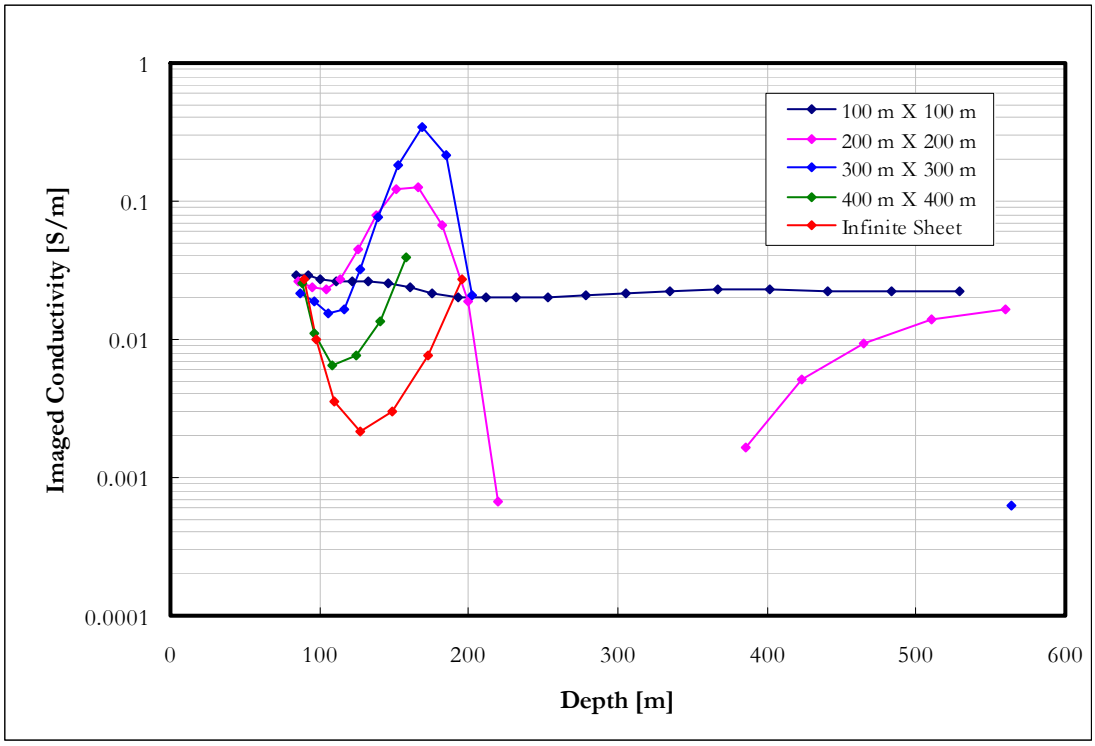

Figure 4-50: Imaged conductivity for a 2 S/m plate of 20 m thickness at 150 m depth in 0.02 S/m host rock. The horizontal dimensions vary from 100 m to infinite.

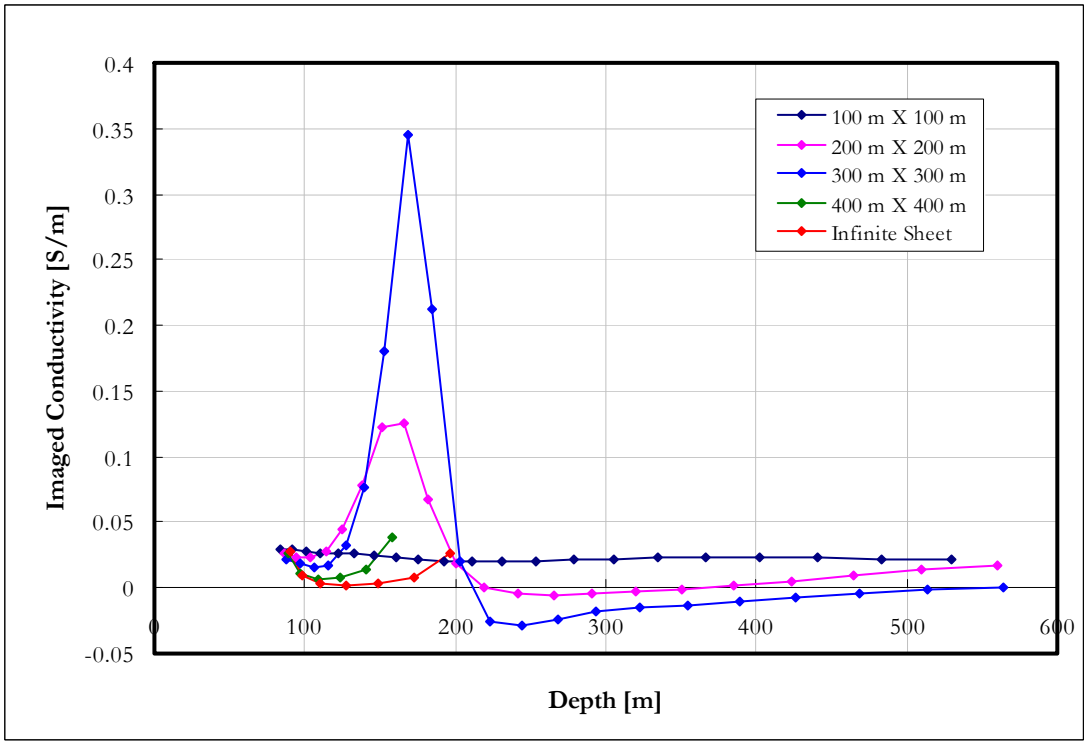

Figure 4-51: Imaged conductivity for a 2 S/m plate of 20 m thickness at 150 m depth in 0.02 S/m host rock. The horizontal dimensions vary from 100 m to infinite; linear scale.

The plates show very similar responses compared to that of the infinite layer. The main differences are that the depths would be underestimated slightly for the smaller plates if the same criteria are used as for the infinite layer and that the finite plates cause "lower than background" imaged conductivity anomalies after the peak values, reaching negative values in the high contrast cases. This behaviour is due to a reduction in cumulative conductance values and not a reduction in depth as was found for high contrast boundaries. It is therefore important to distinguish between the reasons causing negative imaged conductivities as these contain important information on the subsurface conductivity structure.

4.5.3.6 Conductive prisms in a half space

The effect of thicknesses in the same order as horizontal dimensions is investigated in this section. The same sizes and conductivities are used as for the horizontal plates. Results for the low contrast models are shown in Figures 4-52 to 4-54.

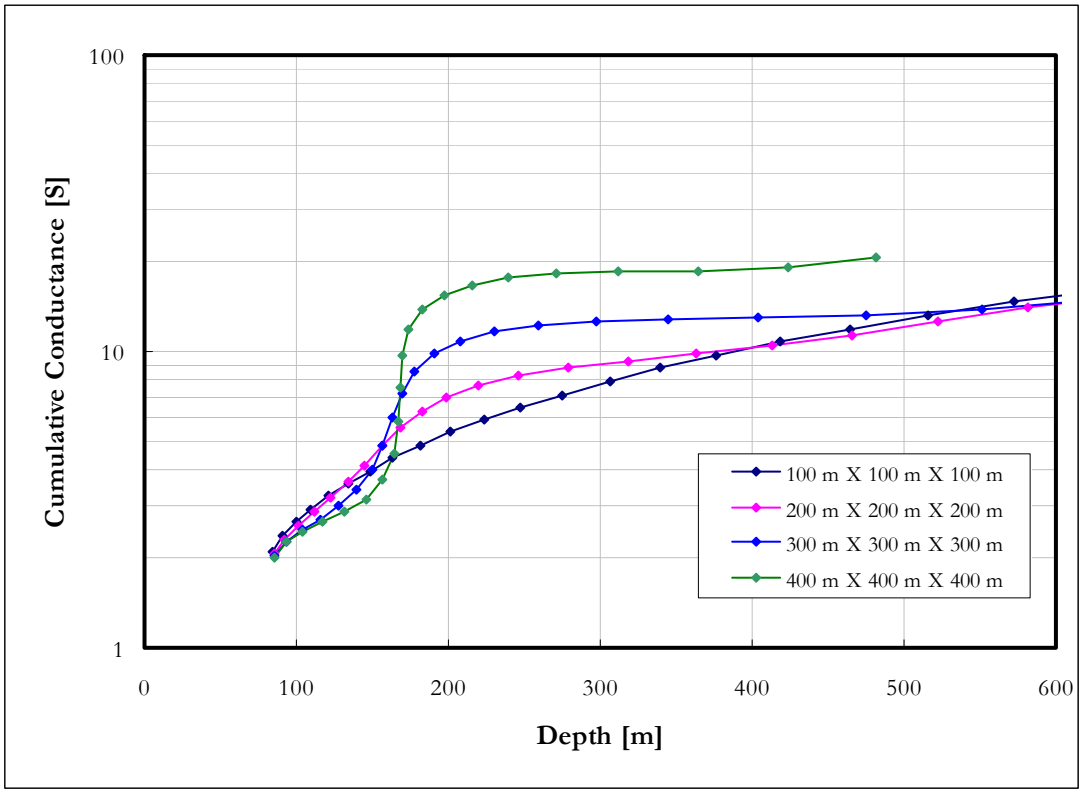

Figure 4-52: Cumulative conductance for a 0.2 S/m prism at 150 m depth in a 0.02 S/m host rock. The prism dimensions vary from 100 m to 400 m.

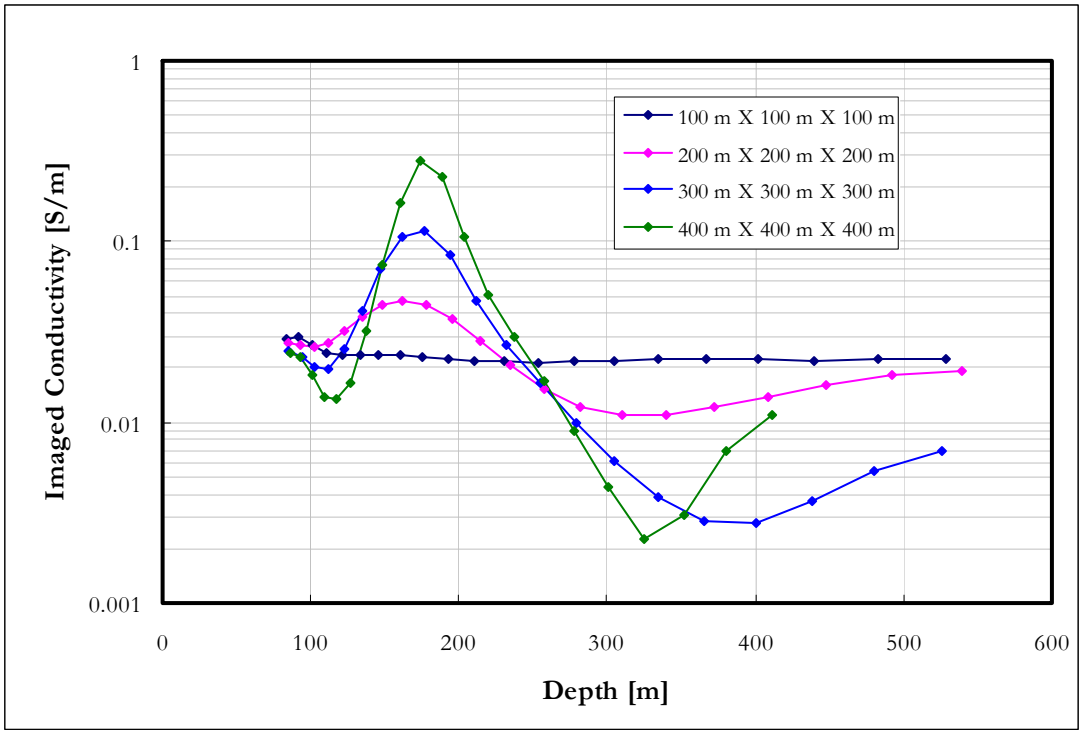

Figure 4-53: Imaged conductivity for a 0.2 S/m prism at 150 m depth in a 0.02 S/m host rock. The prism dimensions vary from 100 m to 400 m.

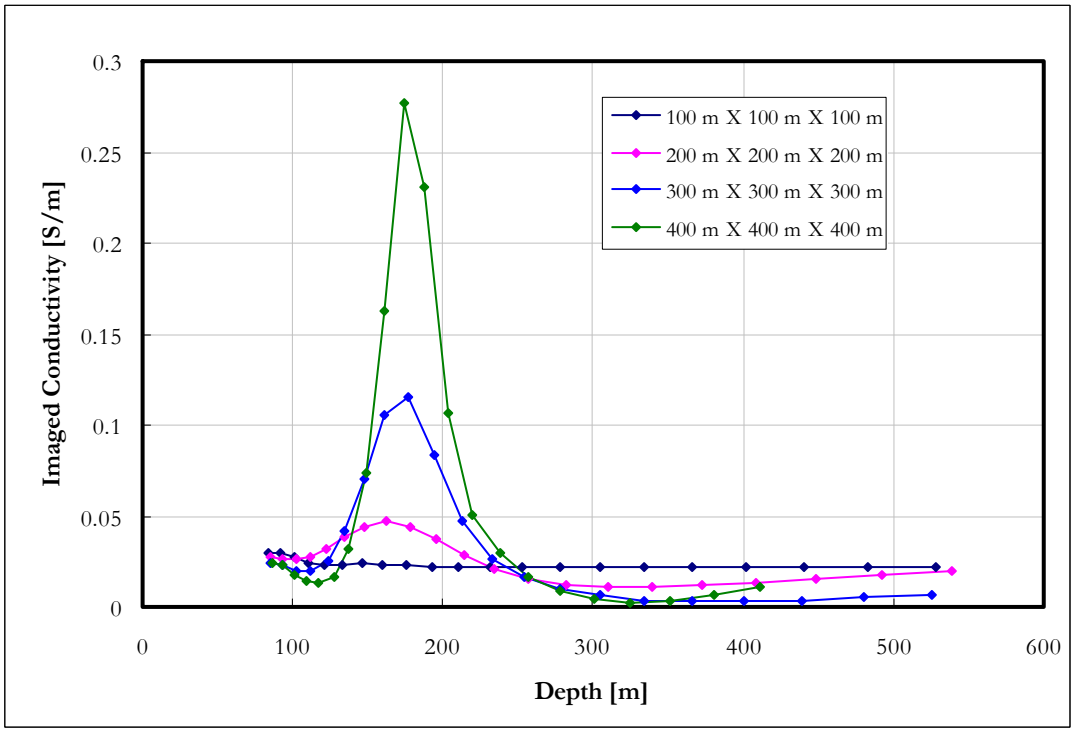

Figure 4-54: Imaged conductivity for a 0.2 S/m prism at 150 m depth in a 0.02 S/m host rock. The prism dimensions vary from 100 m to 400 m; linear scale.

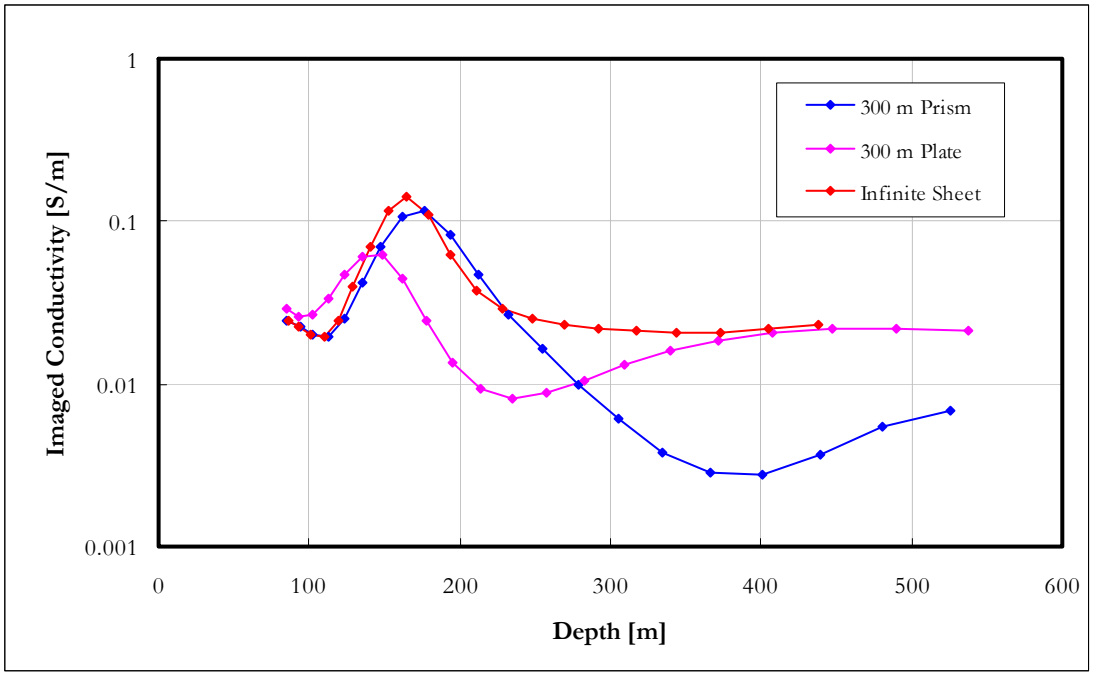

Figure 4-55: Comparison between imaged conductivities of a 0.2 S/m prism, 20 m thick plate and infinite sheet of 20 m thickness at 150 m depth in a 0.02 S/m host rock. Both the plate and prism have horizontal dimensions of 300 m.

Figure 4-55 shows a comparison of the infinite sheet, thin plate and prism responses. Compared to the plates, the prisms are imaged with higher conductivity values and depths and actually come very close to the infinite sheet model except for the lower conductivity values following the main positive peak. Responses obtained from prisms with a high conductivity contrast to the host rock are presented in Figures 4-56 to 4-59. Similar patterns are observed as with the low contrast case. However, the decreasing depth associated with high contrasts is visible on the 300 m prism but not the 300 m plate. Also, the high contrast prisms do not match the high contrast infinite sheet as closely as with the low contrast models.

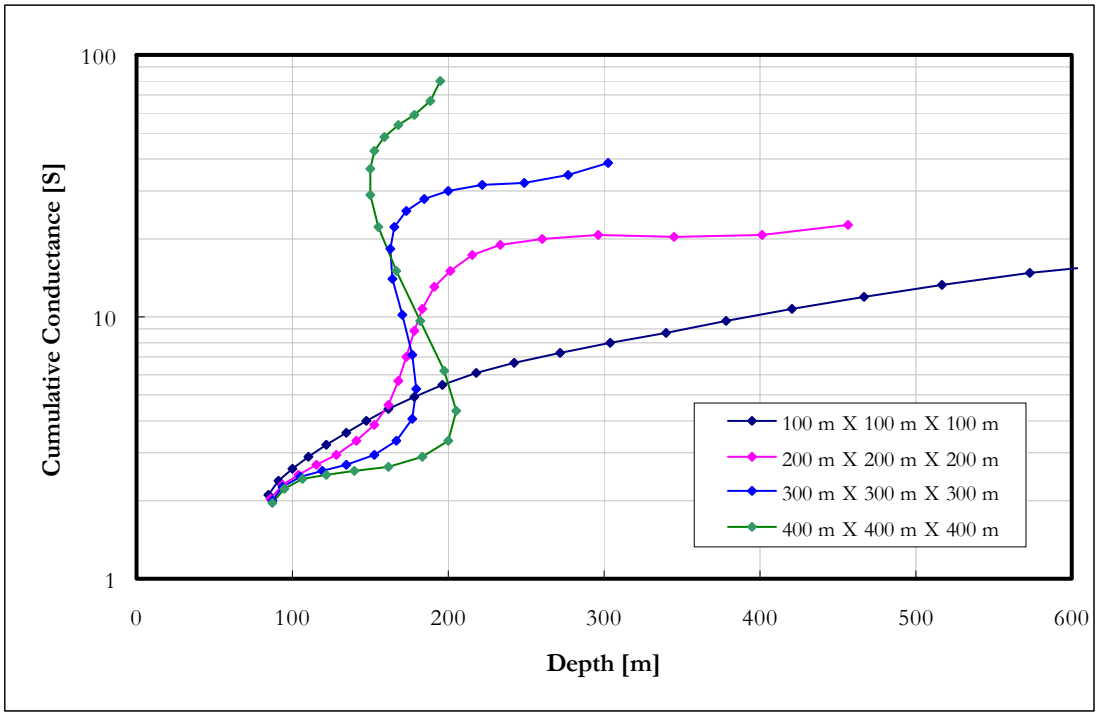

Figure 4-56: Cumulative conductance for 2 S/m prisms at 150 m depth in a 0.02 S/m host rock. The prism dimensions vary from 100 m to 400 m.

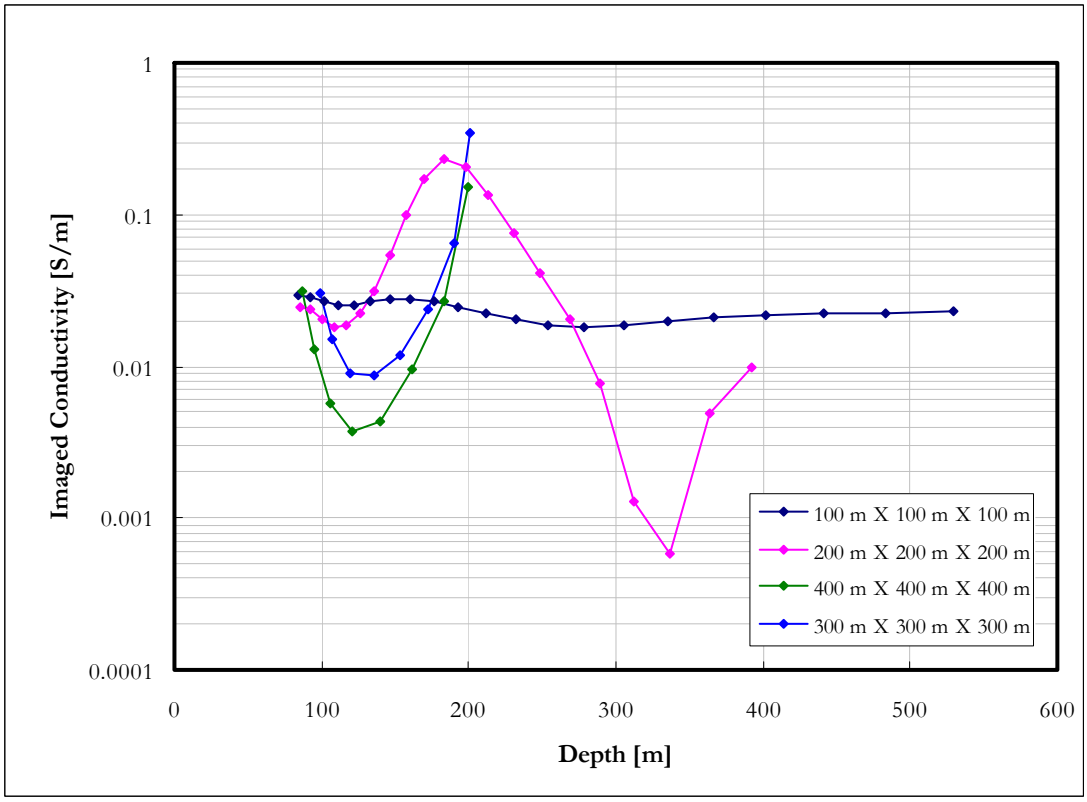

Figure 4-57: Imaged conductivity for 2 S/m prisms at 150 m depth in a 0.02 S/m host rock. The prism dimensions vary from 100 m to 400 m.

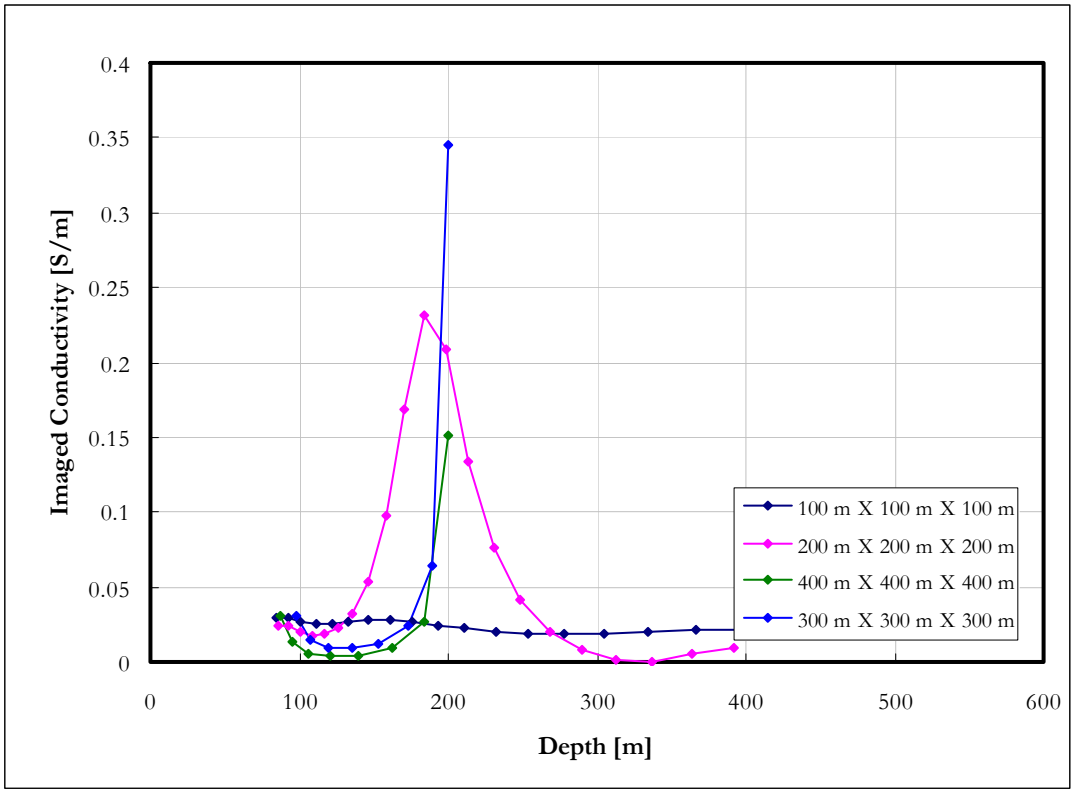

Figure 4-58: Imaged conductivity for 2 S/m prisms at 150 m depth in a 0.02 S/m host rock. The prism dimensions vary from 100 m to 400 m; linear scale.

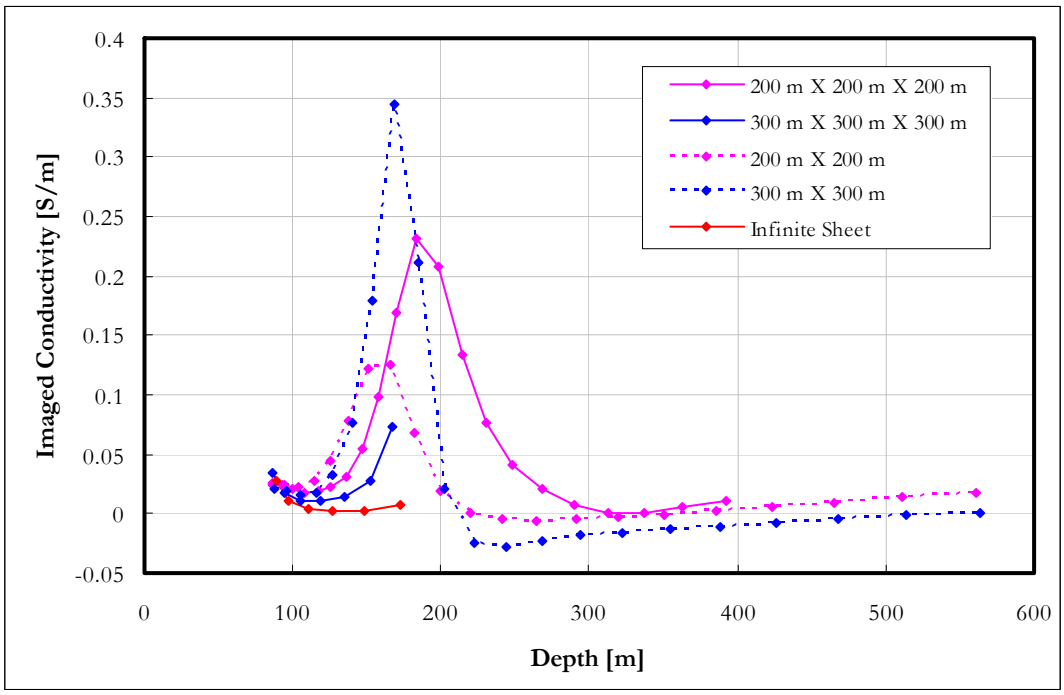

Figure 4-59 : Comparison between imaged conductivities of 2 S/m prisms, 20 m thick plates and infinite sheet of 20 m thickness at 150 m depth in a 0.02 S/m host rock. Plates and prisms with horizontal dimensions of 200 m and 300 m are shown.

4.5.4 S-layer differential transform compatibility filter

The "returning smoke ring" behaviour illustrated in high conductivity contrast scenarios in 1.3 can also be observed in field data (Figure 4-60).

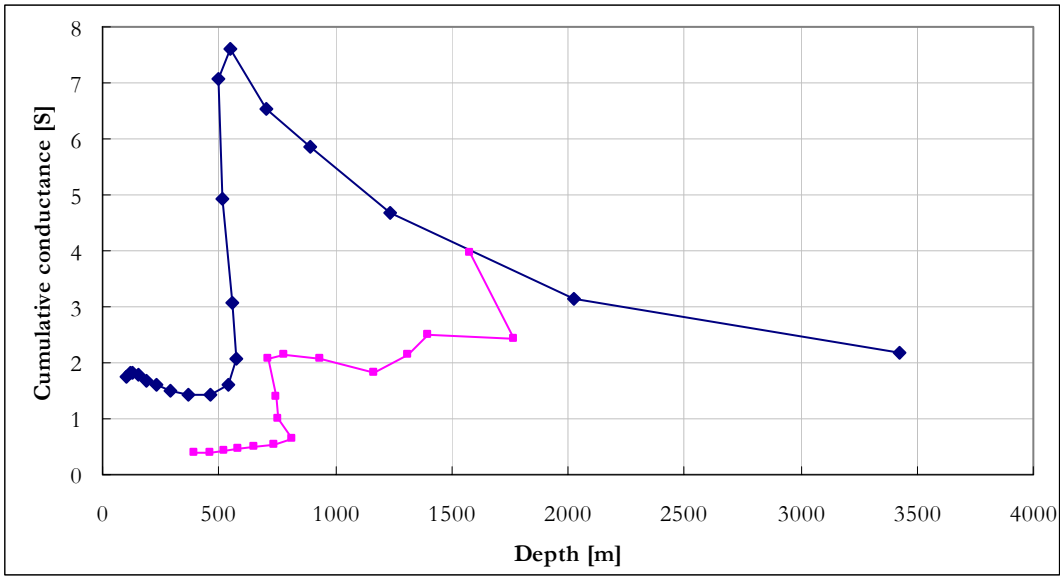

Figure 4-60: Examples of field data showing "returning smoke ring" behaviour (stations -1200 and -150 from line 4950, Rosh Pinah data set).

Only data conforming to the S-layer differential transform assumption of a monotonously increasing cumulative conductance curve can successfully be processed with this algorithm. A filter is therefore designed to only allow data compatible with the transform assumptions to be processed. This filter discards all data after the first point where a decrease in depth with an increase in channel number is observed. It also tests for unrealistic increases in conductance values which sometimes precedes the decreasing depth behaviour. Specifically, this is implemented as follows.

Step 1: Find the first data point conforming to S-layer late time behaviour.

For each sounding data values are analysed until the first three data points are found which conform to:

d[i-1]<d[i]<d[i+1] AND

abs((S[i]-S[i-1])/S[i])<1 AND

abs((S[i]-S[i+1])/S[i])<1.

The first data point passed through the filter is (d[i-1], S[i-1]).

Step 2: Find the first following data point not conforming to S-layer late time behaviour.

Apply the same conditions as in step 1, but look for the first point NOT satisfying these. The last point passed through the filter is then (d[i], S[i]).

The value of "1" chosen in conditions (b) and (c) is chosen based on empirical analysis of the case history 1 data set consisting of 1500 soundings over both resistive and conductive terrain. It is chosen to rather pass values that may be too high (resulting in excessively high conductivities) because these can always be filtered out at a later stage in the conductivity grids. Following this approach means that conductors will not be filtered out, and at worst will be assigned exaggerated conductivities. It has already been shown in the previous section that conductivities are normally underestimated by the algorithm and that the actual numeric values of conductivity should not be taken as the absolute truth especially for confined conductors. The value of this algorithm is in the identification and location of subsurface conductors and is not promoted as a complete and final interpretation tool.

4.5.5 Imaged conductivity depth sections generated from synthetic data

The final product of the algorithm as described in this chapter is illustrated in Figures 4-61and 4-62 for six synthetic models. In Figure 4-61 it is important to note the migration effects similar to seismic data for vertical plates and low contrast conductors. It is produced for the same reason of applying one-dimensional assumptions to three-dimensional data; i.e. plotting all data below the point where it was measured. Migration routines similar to those found in seismic processing can be developed to correct for this but falls outside the scope of this study. High conductivity contrasts of the horizontal plate and prism result in data not conforming to the S-layer differential transform assumptions and are filtered out – resulting in white areas underneath these conductors. It is clear from the low contrast data as well that the lower boundaries of confined conductors are not resolved by this algorithm and that the apparent loss of data underneath conductors is in fact a useful tool indicating high conductivity contrasts.

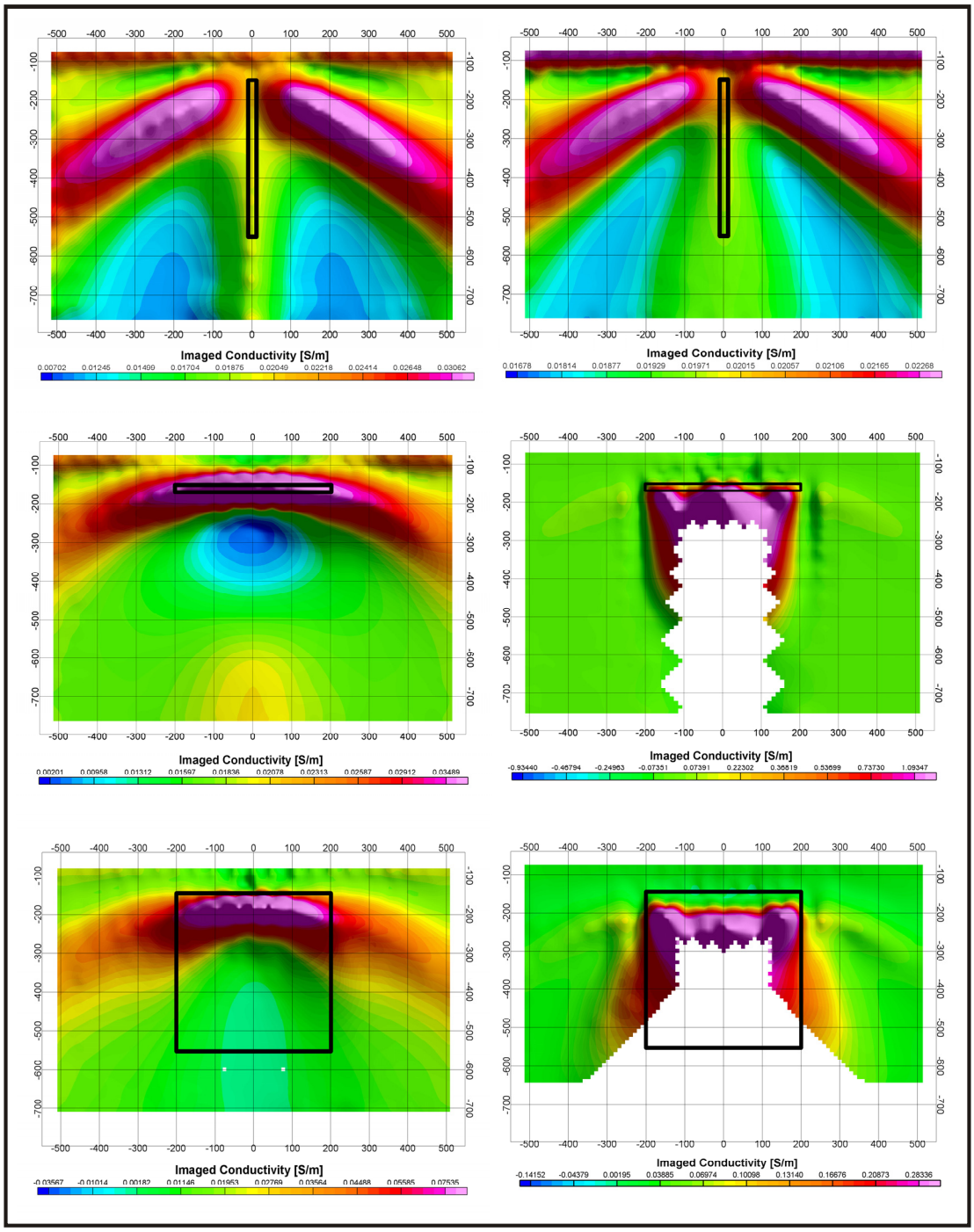

Figure 4-61: S-layer differential transform results (conductivity depth section) on synthetic data.
Top: Thin vertical plate (400mX 400m X 20m)
Middle: Thin horizontal plate (400m X 400m X 20m)
Bottom: Prism (400m X 400m X 400m).
Left hand side are low contrast scenarios (0.2 S.m^{-1} conductor in 0.02 S.m^{-1} half space). Right hand side are high contrast scenarios (2 S.m^{-1} conductor in 0.02 S.m^{-1} half space).

In Figure 4-62 the decay curve analyses are superimposed on the conductivity-depth sections. Each dot represents a channel which shows the indicated decay behaviour.

Channels are scaled so that channel 1 corresponds with the top of the section and channel 20 to the bottom. Note the half space (-2.5) decay that is observed on all models at some stage. Although conductors are present the conductive nature of the half space itself causes the dominant decay to be that of -2.5 as mentioned by Singh (1973) and discussed in 2.3.4. Only the high contrast horizontal plate shows finite conductor decay in the late time. Automated decay constant analyses should be applied with great care if the half space response has not been removed from data in a conductive host rock environment. It is clear that under these conditions the S-layer differential transform is a more effective way of determining the presence and locality of conductive bodies

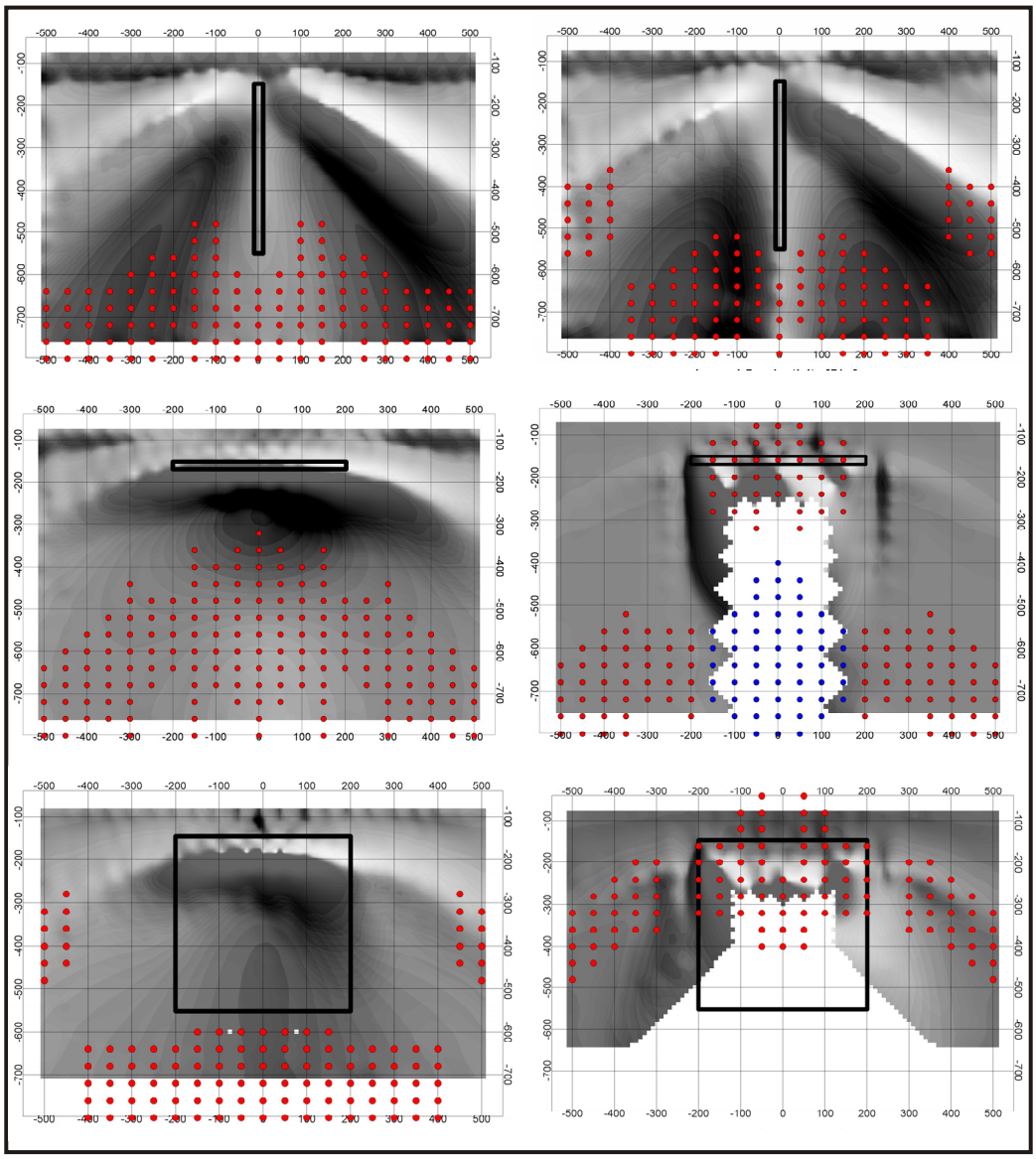

Figure 4-62: Same models as in Figure 4-63. Red dots indicate half space decay behaviour and blue dots indicate conductor in "free air" decay.

Table 2: Summary of S-layer differential transform performance on synthetic models. (h = thickness, d =depth, l= side length of square plate and prisms)

Model	Cumulative Conductance vs depth	Imaged Conductivity vs depth	Comments
Half space σ = 0.02 S/m	Smoothly increasing with depth	Good approximation (12% error) to true conductivity in "late time"	
Two Layers σ_1= 0.02 S/m σ_2 = 0.002 S/m h_1 = 200 m	Smoothly increasing with depth, layer boundary clearly defined	Show decreasing trend with depth; values close to true conductivity; layer boundary not clearly defined	Decreasing conductivity, low contrast
Two Layers σ_1= 0.02 S/m σ_2 = 0.0002 S/m h_1 = 200 m	Smoothly increasing with depth, layer boundary clearly defined	Show decreasing trend with depth; second layer values not close to true conductivity; layer boundary not clearly defined	Decreasing conductivity, high contrast
Two Layers σ_1= 0.02 S/m σ_2 = 0.2 S/m h_1 = 200 m	Smoothly increasing with depth, layer boundary not clearly defined	Show increasing trend with depth (except for early time); values close to true conductivity for first layer only; layer boundary defined as "first increase" in conductivity, especially on linear scale	Increasing conductivity, low contrast
Two Layers σ_1= 0.02 S/m σ_2 = 2 S/m h_1 = 200 m	Decreasing depths with increasing times, layer boundary not clearly defined	Show increasing trend with depth (except for early time); values close to true conductivity for first layer only; layer boundary defined as "first increase" in conductivity, especially on linear scale; negative conductivities calculated	Increasing conductivity, high contrast "Reflecting smoke-ring" behaviour
Conductive layer in half space (varying σ contrast) σ_{HS}= 0.02 S/m σ_{Layer} = 0.04 S/m and	Smoothly increasing with depth	Resolve layer position well but with underestimation of conductivity values.	Low contrast

σ_{Layer} = 0.2 S/m d_{Layer} = 150 m h_{Layer} = 15 m			
Conductive layer in half space (varying σ contrast) σ_{HS}= 0.02 S/m σ_{Layer} = 2 S/m and σ_{Layer} = 10 S/m d_{Layer} = 150 m h_{Layer} = 15 m	Decreasing depths with increasing times	Layer depth overestimated proportional to contrast; initial decrease of conductivity before increasing to sometimes erroneously high values.	High contrast
Conductive layer in half space (varying thickness) σ_{HS}= 0.02 S/m σ_{Layer} =0. 2 S/m d_{Layer} = 150 m h_{Layer} = 2 m, 5 m, 10 m, 15 m, 20 m, 50 m and 100 m	Change in curve characteristic for 50m and 100m thickness.	2m to 20m see similar graphs except for increase in maximum conductivity values with well defined top of layer; 50m and 100m thickness gives overestimation of depth proportional to thickness.	Low contrast behaviour (increasing depths mapped with increasing time) remains even if conductivity-thickness product becomes very large
Conductive layer in half space (varying thickness) σ_{HS}= 0.02 S/m σ_{Layer} = 2 S/m d_{Layer} = 150 m h_{Layer} = 2 m, 5 m, 10 m, 15 m, 20 m	Thicknesses more than 2m exhibit decreasing depths with increasing time.	Overestimation of depths for 10m and thicker proportional to thickness.	High contrast. The thicker the layer becomes, the closer the curves resemble the two layer case with very little or no influence from the earth below the conductive layer contributing to the signal.
Conductive layer in half space (varying depth) σ_{HS}= 0.02 S/m σ_{Layer} = 0.2 S/m d_{Layer} = 50 m, 150 m,	Smoothly increasing with depth. 50m shows anomalous behaviour (see comment)	Width of the anomaly increases proportional to depth while the amplitude decreases. Maxima slightly deeper than layer top boundary.	Low contrast. Conductive layers shallower than "first channel expected depth for host rock" maps at correct depth but with slightly distorted curves –

200 m, 250 m, 300 m h_{Layer} = 20 m			can be mistaken for two layer earth.
Conductive layer in half space (varying host rock cond.) σ_{HS}= 0.0002 S/m, 0.005 S/m, 0.0067 S/m, 0.01 S/m, 0.02 S/m, 0.04 S/m and 0.1 S/m. σ_{Layer} = 0.2 S/m d_{Layer} = 150 m h_{Layer} = 20 m	Host rock conductivities < 0.01S/m results in the depths decreasing with time of cumulative conductance plots, although the extent of this reversal is less than for the same contrast in a more conductive host rock.	Depth of investigation determined by host rock conductivity or shallower-than-first-channel-depth conductive layer.	Higher host rock conductivities cause more severe "non-late-time" distortions in early channels.
Conductive horizontal plate in half space (varying hor. dimensions) σ_{HS}= 0.02 S/m σ_{Plate} = 0.2 S/m l_{Plate} = 100 m, 200 m, 300 m, 400 m d_{Plate} = 150 m h_{Plate} = 20 m	Smoothly increasing with depth. 100m too small to resolve with current parameters.	Depths are slightly underestimated proportional to side length of plates; underestimation of conductivities just below plates.	Low contrast.
Conductive horizontal plate in half space (varying hor. dimensions) σ_{HS}= 0.02 S/m σ_{Plate} = 2 S/m l_{Plate} = 100 m, 200 m, 300 m, 400 m d_{Plate} = 150 m h_{Plate} = 20 m	300m and larger side lengths produce decreasing depths with increasing times. 100m too small to resolve.	100m and 200m side lengths give negative conductivities below plates.	High contrast. Second instance when negative conductivities can be calculated.
Conductive prism in half space (varying dimensions) σ_{HS}= 0.02 S/m	Smoothly increasing with depth. 100m too small to resolve.	Depth to top and conductivity values resolved better than thin plates.	Low contrast. 300m and larger dimensions resemble infinite layer apart from underestimation of

σ_{Plate} = 0.2 S/m l_{Plate} = 100 m, 200 m, 300 m, 400 m d_{Plate} = 150 m			conductivities below prism.
Conductive prism in half space (varying hor. dimensions) σ_{HS}= 0.02 S/m σ_{Plate} = 2 S/m l_{Plate} = 100 m, 200 m, 300 m, 400 m d_{Plate} = 150 m	100m still not resolved. Decreasing depth with increasing time for 300m and 400m prisms.	Behaviour similar to infinite high contrast plates with overestimation of depths and negative conductivities below prisms.	High contrast.

In general the S-layer differential transform performs more reliably in low contrast environments although the "decreasing depth with increasing time" behaviour serves as a very important indicator of high contrast conductors. Keeping in mind that depths will be overestimated in this event (and underestimated for conductors with dimensions less than 300m) still allows the results to be interpreted accurately for the presence of a conductor even if there are constraints on the accuracy of depth to top in some cases. The depth to bottom cannot be determined from this algorithm. Imaged conductivities approach true conductivities for very thick layers (half space and two layer case) but this is not the case for confined conductors. However, the imaged conductivity behaviour can be used successfully to indicate "lower", "higher" and "much higher" conductivities. Negative conductivities should not be just be discarded as invalid as it can be indicative of small confined conductors at shallower depths as well as the presence of high contrast conductors. In fact, the exact cause of negative conductivities for every instance can be found by inspection of the cumulative conductance curves if needed.